January 2019

High Frequency Percussive Ventilation For Tumor Motion Immobilization

Ina Marina Sala
Wayne State University, inasala@gmail.com

HIGH FREQUENCY PERCUSSIVE VENTILATION FOR TUMOR MOTION IMMOBILIZATION

by

INA MARINA SALA

DISSERTATION

Submitted to the Graduate School

of Wayne State University,

Detroit, Michigan

in partial fulfillment of the requirements

for the degree of

DOCTOR OF PHILOSOPHY

2019

MAJOR: MEDICAL PHYSICS

Approved by:

_____

Advisor Date

_____

_____

_____

_____

_____

DEDICATION

To my parents, family and patients

ACKNOWLEDGMENTS

I would like to sincerely thank the following individuals that have helped and guided me along the way:

- My advisor, Dr. Thomas Guerrero, MD, PhD who has guided me through this with grace, thoughtfulness and determinism. I'm grateful for his knowledge, leadership and the opportunities that he has created for me. It has been a true privilege and will forever be thankful.
- Dr. Jay Burmeister, PhD, as the Co-Advisor of my committee, for his guidance, honest feedback, creativeness, and sedulous patience. He has been a true inspiration.
- Dr. Rakowski, Dr. Nalichowski and Dr. Pankuch for their continued support and indispensable feedback in making me a better person. It has been a truly wonderful experience and I feel privileged to have had all of them as my mentors. I have become a better professional as a result of their teaching and valuable feedback throughout the years.
- My friend and colleague, Ms. Hazel Ramirez, MS, DABR for her continued support in all data collection at Northwestern Medicine Proton Center. Her expertise, inspiration and determinism has truly made this a memorable journey.

- Dr. Tanya Powell, MD, Dr. Diana Chung, MD, Dr. Vinai Gondi, MD and all of the other Radiation Oncology Consultants, LLC that have inspired and helped me along the way.
- Dr. Christian Hyde, MD and Dr. Girish Nair, MD that have tirelessly guided me through every publication and humbly taught me valuable qualities.
- My respiratory therapist, Ms. Beverly Maurer has been a pillar in this. Her guidance, time, determinism and feedback throughout all volunteer/patient data collection is indispensable.
- Sincere appreciation to all the research members (Evan, Afua, Nick and Carl) at Beaumont Health, Royal Oak, MI, Karmanos Cancer Institute, Detroit, MI and Northwestern Medicine, Warrenville, IL for their continued support in providing me with the tools and knowledge to succeed.

TABLE OF CONTENTS

LIST OF TABLES

LIST OF FIGURES

CHAPTER 1: INTRODUCTION OF PROTON AND PHOTON RADIOTHERAPY WITH MOTION MANAGEMENT

1.1 General Overview of Radiotherapy

Radiation was first discovered by Wilhelm Conrad Roentgen at the end of the 19th century. While performing experiments using positive and negative charged electrodes, he noticed a green fluorescence color upon the application of high voltage. Intrigued by such light and unable to identify it, Wilhelm called them unknown rays or "X"-rays. Furthermore, in late 1895, he discovered that such unknown "rays" were capable of penetrating through some objects, but not the other. This phenomenon was observed when he first photographed his wife Bertha's hand. It was clear from the photograph that denser materials, like Bertha's ring, created a much darker image, resulting in less penetration of the unknown "X"-rays.

Just after the discovery of the unknown "X"-rays, Becquerel, a French scientist, noticed that storing a sample of uranium under a photographic plate, in a cloudy day, the plate still appeared to have been exposed to light (Reed & Pa, 2011). Like Roentgen, Becquerel was also able to deduce that uranium was emitting natural radiation. This remarkable work was further researched by Mme. Curie who was recognized as a Nobel Prize winner, together with Becquerel in 1903.

Although the above discoveries drastically changed the field for decades thereafter, the initial consequences on human health were still unknown despite the initial theorization by Mme. Curie that radiation could indeed become

dangerous by indicating in her Nobel Prize notes that: “…if one leaves a small glass ampulla with several centigrams of radium salt in one’s pocket for a few hours, one will feel absolutely nothing. But the 15 days afterwards redness will appear on the epidermis…”. Although, her statement was not backed up by broad scientific data or massive trials like those performed today, it was certainly an observation that Mme. and her husband Pierre Curie noticed accidentally (Curie, 1967). Consequently, radiation was often used as a tool by the general public to create “cool toys” for the kids, measure show sizes**,** and design glowing watches for the adults. As further research was performed, the scientific community began to understand more about the unknown **“**rays**”** and the implications to human health since the broad and uncontrolled use of radiation led health implications (Reed & Pa, 2011).

Today, we know more about radiation (“X”-ray) itself and its interaction with matter. We define radiation as emission and propagation of energy in space or medium. Most textbooks will define radiation as particle or wave. Particle radiation is propagation of energy by traveling corpuscles that have a defined rest mass and within limits have a defined momentum and defined position at any instant” (Faiz Khan, Structure of Matter, 2003). Consequently, the wave model, also known as the electromagnetic model, is described as the oscillating electric and magnetic field. An electromagnetic wave can be represented by the spatial variations in the intensities of an electric field and the magnetic field, the fields being at right angles to each other at any given instant (Faiz Khan, Structure of Matter, 2003).

Furthermore, electromagnetic radiation can be divided into several modes like: light waves, heat waves, radio waves, microwaves, ultraviolet rays, X-rays and Γ -rays (in order of increasing energy). All of these modes can be further explained by the following equation:

$$E = \hbar\boldsymbol{\nu} \quad \textbf{(1)}$$

Where E is the energy carried by the photon, $\hbar$ is the Planks constant and $\boldsymbol{\nu}$ is the frequency. With frequency being defined as:

$$\nu = \frac{c}{\lambda} \quad \textbf{(2)}$$

where c is the speed of light and λ is the wavelength. It is obvious from equations (**1**) and (**2**) that the shorter the wavelength the higher the energy. As a result, the X- and Γ-ray of the spectrum mentioned above would exhibit a much higher energy than that of visible light.

There are two different ways of producing X-rays. The first method is bremsstrahlung and the second is characteristic. Bremsstrahlung X-ray comes from the German word “to break”. In this method, the interaction of high energy electrons to the Coulomb field of a nucleus deaccelerates the incoming electron leading to loss of energy that is emitted as X-ray. The mechanics of this method are well known and widely used in both diagnostic and therapy setting. The second method, characteristic X-ray, constitutes of an incoming electron interacting with an orbital electron of an atom, leading to a vacant spot, which is known as an ionized atom. When this vacancy is created, another electron from an outer orbital will drop down and fill the vacancy, releasing characteristic

energy in the process. This characteristic X-ray is ‘characteristic’ of the binding energy difference of the orbital shells involved.

The main difference between X- and Γ- rays is their origin, but their interaction with medium is described by three different techniques:

- Photoelectric effect: this phenomenon occurs when the incoming photon is completely absorbed by an atom in the medium, resulting in one of the orbital electrons to be ejected. Such interaction will occur with a tightly bound electron, like those in the inner most shells. Essentially, all of the energy from the incoming photon ($E = h\boldsymbol{\nu}$) is transferred to the ejected electron. The resulting energy of the ejected electron is $\mathrm{T} = \mathrm{h}\,\nu\ - E_b$ where $\mathrm{h}\cup$ the energy of the incoming photon is and $E_b$is the binding energy of the bound electron. The probability of this interaction to occur depends on the photon energy and the atomic number of the absorbing material (medium). This relation is often denoted as: $\frac{Z^3}{E^3}$ where Z is the atomic number of the medium and E is the energy of the incoming photon. Therefore, photoelectric interaction will be more prominent for high Z and low E.
- Compton effect: this phenomenon occurs when the incoming photon interacts with a free bound atomic electron in the medium, resulting in the scatter of the electron and photon. There are special cases that one can apply, together with the laws of conservation of energy and momentum,

to determine the final energy of the ejected electron and photon. The energy of the ejected electron is denoted as:

$$T = h\nu_0 - \frac{h\nu'}{1 + \frac{h\upsilon_0}{mc_0}(1 - cos\phi)} \quad \textbf{(3)}$$

And the energy of the ejected photon is:

$$h\upsilon' = \frac{h\nu_0}{1 + \frac{h\upsilon_0}{mc_0}(1 - cos\phi)} \quad \textbf{(4)}$$

Where $h\nu_0$ is the energy of the incoming photon, $h\nu'$ is the energy of the ejected photon, T is the energy of ejected electron, mc_0 is rest energy of the electron and ϕ is the angle of scattered photon. The probability of a photon going through a Compton interaction will depend on the electron density, which is the number of electrons per unit mass. This is described in literature as Z/A. Therefore, unlike photoelectric, Compton interaction is independent of Z and proportional to Z/A. The probability of Compton decreases with increasing photon energy.

- Pair production: this phenomenon occurs when an incoming photon is completely absorbed in the Coulomb field of an atomic nucleus to create an electron and positron pair. The average energy received by the electron and positron is:

$$T = \frac{h\nu_0 - 1.022MeV}{2} \quad \textbf{(5)}$$

Where $h\nu_0$ is the energy of the incoming photon and 1.022 MeV is the rest energy of the electron and positron. The probability of this interaction

to occur increases with increase in photon energy and increases with atomic number by approximately Z^2.

Until now, we've discussed the production of x-ray (photon), their three main interactions with matter, and the probability of the interaction to occur. However, as described in literature (Kogel, 2009), it is the charged particles that would eventually create the most biological effects that clinicians aim to deliver to a target. Joiner et al. states that almost all of the photons produced by linear accelerators have sufficient energy to cause ionizations, but most biological damage is done by the ejected electrons themselves, which go on to cause further ionizations in the molecules they collide with, progressively slowing down as they go (Kogel, 2009). The charged particles (electrons, protons etc.) are called directly ionizing and the uncharged particles (photons) are characterized as indirect. Unlike the three main interactions of photons (indirectly ionizing) discussed above, the electrons (directly ionizing) will interact with matter in three ways.

Soft collision: this type of interaction is denoted in ***Figure 0-1****:* (b>>a) will occur when the charged particle passes an atom in matter at a considerable distance. The net effect is the transfer of a very small amount of energy to an atom of the absorbing medium (Frank Herbert Attix, Charged-Particle Interactions in Matter, 1986). *b* in the figure denotes the impact parameter and *a* is the radius of the atom.

Hard Knock-on collision: this type of interaction occurs when the impact parameter b is approximately equal to the radius a. The incidence charged

particle will interact primarily with a single atomic electron, which is then ejected from the atom with a considerable kinetic energy (Frank Herbert Attix, Charged-Particle Interactions in Matter, 1986). These types of collisions occur far less than the soft collision (***Figure 0-1***:).

Coulomb-force interaction: this type of interaction occurs when the impact parameter b<<a (***Figure 0-1***:). This would occur when the incoming charged particle interacts with the Coulomb force of the nucleus. The electron is scattered elastically and does not emit an x-ray photon or excite the nucleus (Frank Herbert Attix, Charged-Particle Interactions in Matter, 1986). Because the electron loses a very small (often insignificant) kinetic energy, this mechanism is not for the transfer of energy to the absorbing medium, but it is an important means of deflecting electrons (***Figure 0-1***:) (Frank Herbert Attix, Charged-Particle Interactions in Matter, 1986).

As charged particles traverse a medium, the expected value of the rate of energy loss per unit length is defined as stopping power. To be more specific: collisional or radiative stopping power. Where collisional stopping power is the sum of all energies lost due to soft and hard knock-on collisions, and radiative stopping power is simply the energy lost due to radiative interaction (b<<a). The collisional stopping power will depend on $\frac{Z}{A}$, the velocity of the particle itself, and the charge of the particle. In short, the collisional stopping power will decrease with increase Z of the medium (in clinical setting this would be tissue, bone etc.). Consequently, the collisional stopping power will increase when the velocity is

small. Lastly, an increase in particle charge will quadruple the collisional stopping power.

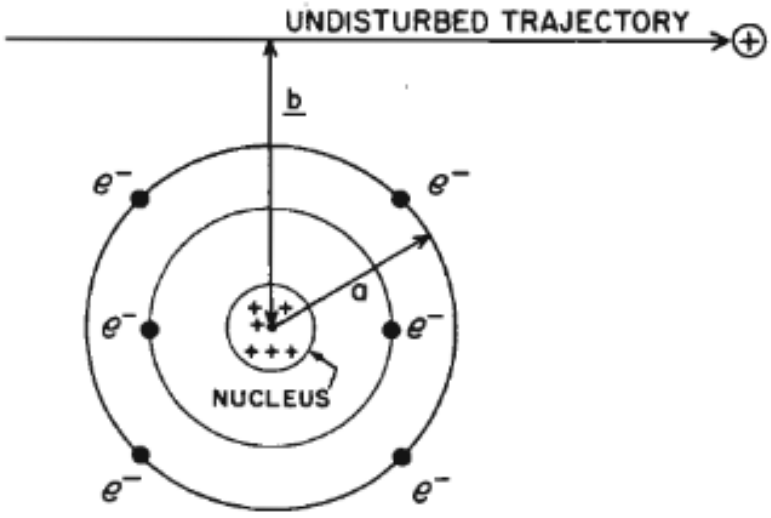

Figure 0-1: Charge particle collisions- *(Attix, 1986)*

Radiotherapy in medicine has evolved extensively starting from the basic X-ray generators that were used for superficial treatments to our current Linear Accelerators used for deep seated targets. For this dissertation, I will focus on linear accelerator radiotherapy. A linear accelerator often referred to as a “linac” is a sophisticated device that accelerates charged particles to treat with electrons or gamma rays. Today, tumors are mainly treated with three types of particles: electrons, protons and photons. As described above, these types of directly or indirectly ionizing particles will interact with matter differently, but for this dissertation, I will focus on external beam photon and proton radiotherapy.

1.2 Photon and Proton Radiotherapy

Prior to discussing radiotherapy techniques, let us first discuss how photons and protons are produced.

Although there are several types of linear accelerators that are capable of producing photons, the most relevant and extensively used in clinical radiotherapy utilizes waves of 3GHz frequency, also known as S band.

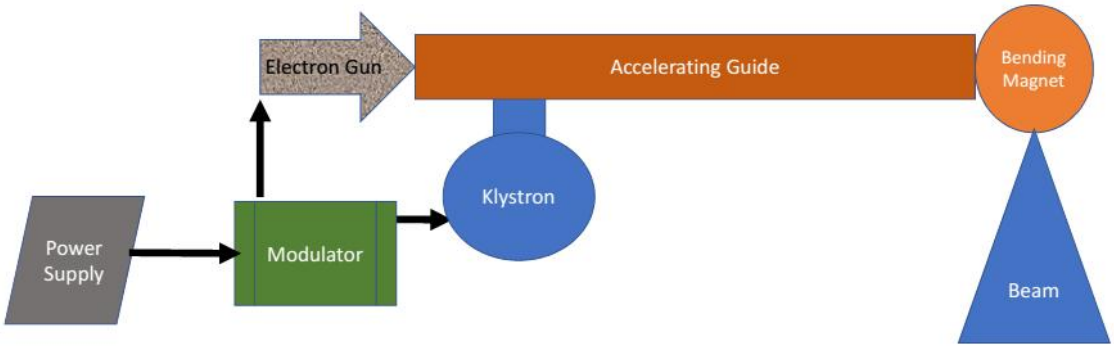

Figure 0-2: Typical radiotherapy linear accelerator

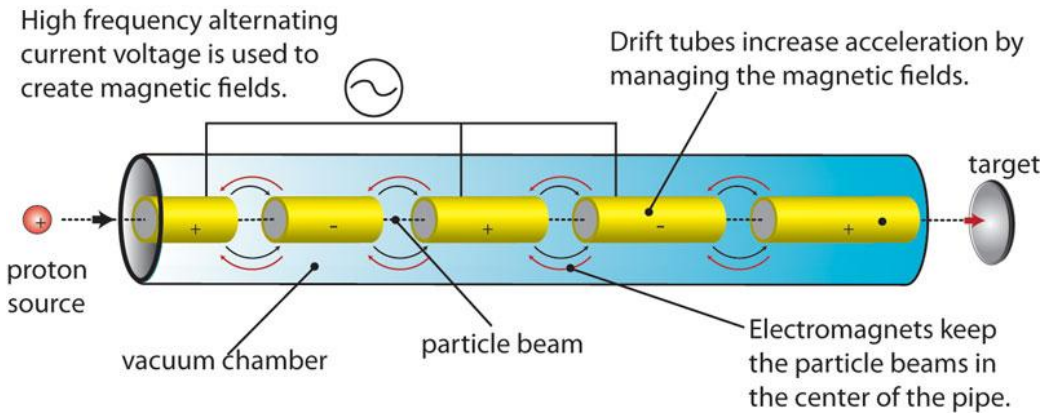

Figure 0-3: Typical Accelerator tube

The main components of a linear accelerator include (***Figure 0-2:***): power supply, modulator, Magnetron/Klystron, accelerating structure, electron gun, and

treatment head (Faiz Khan, Clinical radiation Generators, 2003) (Williams, 1997):

- The power supply is used to provide direct power to the modulator
- The modulator's main function is to supply negative-going high-voltage pulses to the cathode of the microwave generator valve (klystron/magnetron) and the electron gun.
- The magnetron is a microwave generator that is fed into the accelerating guide with a set frequency. Most magnetrons operate at a peak power of 5MW.
- The Klystron is a microwave amplifier. Unlike magnetron, linacs that utilize a klystron have a low power oscillator that drives the klystron itself. In short, klystron utilizes a hot wire cathode (negatively charge) that produces electrons which are accelerated by a negative pulse of voltage into the first cavity, called the buncher cavity, which is energize by low-power microwaves. The microwaves set up an alternating electric field across the cavity. The velocity of the electrons is altered by the action of this electric field to a varying degree by a process known as a velocity modulation. Because some electrons are sped up while some are slowed down, it results in bunches of electrons. As these electrons arrive at the anode (positive charged) side of the klystron, they will induce charges therefore generate a retarding electric field. The electrons suffer deceleration and by the principal of conservation of energy, the kinetic energy of the electrons is converted into high-power microwave that will

make its way to the accelerating structure (Faiz Khan, Clinical radiation Generators, 2003).

- Accelerating structure is an evacuated copper made tube with unequally spaced disks. Electrons are injected into this structure from the electron gun. They will interact with the electromagnetic field of the microwaves, which will allow them to gain energy as they traverse along the structure and out into the exit window of the structure (***Figure 0-3:***).
- The electron gun can be separated as diode or triode. Its main purpose is to create electrons that will be accelerated into the accelerating structure.
- The treatment head is comprised of several bending magnets and energy selection slits that would ensure the electron pencil beam to be well focused as it exits. Additionally, another main component in the treatment head is the target. The target is utilized for photon production. Further beam shaping devices like flattening filters, scattering foils, multi leaf collimators (MLC), metallic jaws etc. are used to further collimate the beam for clinical treatments. Other important components in this particular section of the linear accelerator are the ion chambers. The ion chambers allow for continual output verification of the beam and other parameters like flatness and symmetry.

The linear accelerators used in most clinics across the United States have the option to deliver either photons or electrons to the patients. Photons are predominantly used for deep seated tumors, whereas electrons are mostly for superficial targets. The photons in the linear accelerator are created by

accelerating electrons in the manner described above and then “smashing” them into a high Z target. This will allow the electrons to go through the bremsstrahlung interaction (Section 1.1) and consequently generate photons. For the electron beam, the target is moved away from the beam path.

For proton radiotherapy most clinics, will use a cyclotron. A typical design of the cyclotron is depicted in ***Figure 0-4:***. The cyclotron utilizes a proton source (H+) that is confined into a spiral shape by two D shaped electrodes, one positively charged and the other is negatively charged. A physical gap is created in between the two Ds. A magnetic field is applied perpendicular to the “Ds”, and as protons travel through one D and into the other the electric field is switched leading to an increase in velocity and consequently the path trajectory will increase as described in (***Figure 0-4:***). The final velocity at the exit window is directly correlated to the radius of the double Ds by the following equation:

$$v_{max} = \frac{qBr}{m} \quad \textbf{(6)}$$

Where q is charge, m is particle mass, B is magnetic field applied and r is the radius.

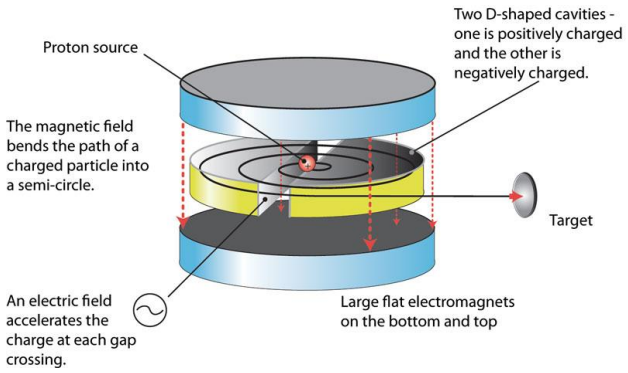

Figure 0-4: Typical Cyclotron (https://atomic.lindahall.org/what-is-an-atom-smasher.html)

As the proton particles exit the cyclotron window, they are magnetically guided into a final exit window. Contrary to the electron particles, protons are heavy charged particles which result in minimal scatter and therefore they exhibit a low entry dose, an increase of dose near the end of their range and a sharp exit dose. Such unique property allows protons to play an important role in radiotherapy and uniquely compliment electrons and photons. Depth dose curves that figuratively represent these unique properties of photons, electrons and protons are denoted in (***Figure 0-5:***).

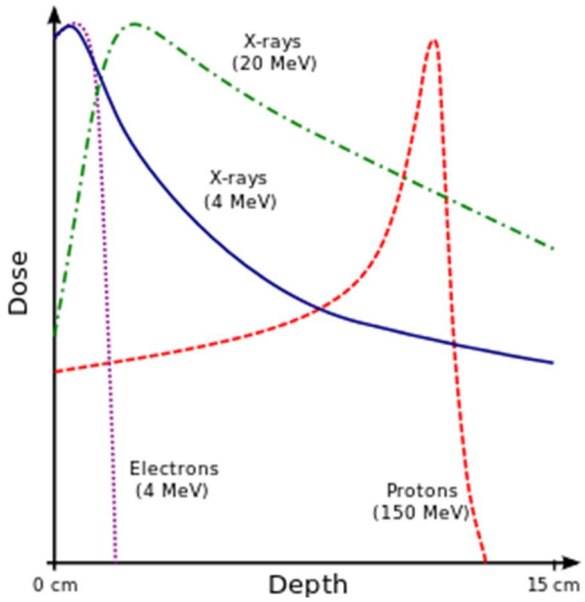

Figure 0-5: Depth Dose curves for photons, protons and electrons

The sharp increase of dose at the end of the proton range is defined as the Bragg peak. The width of the Bragg peak is often too narrow, as indicated in (***Figure 0-5:***), for most clinically observed targets in radiotherapy, as a result its modulation, also known as SOBP (spread out Bragg peak) is often necessary. Bragg peak modulation can be achieved by either switching beam energies or by introducing a modulator in the beam path. In either case, the weighted combination of all the peaks results in a flat dose distribution that is practical for uniformly treating deep seated targets.

1.3 Thoracic Radiotherapy Treatment Techniques

Thoracic targets are currently being treated with either photons or protons. Photon radiotherapy techniques consist of: Three Dimensional Conformal Radiotherapy (3DCRT), Intensity Modulated Radiotherapy (IMRT) and/or

Stereotactich Body Radiotherapy (SBRT) and for proton: pencil beam scanning (PBS) and passive scattering proton therapy (PSPT).

3DCRT techniques utilizes a CT (computed tomography) and a limited uniform photon beams that are delivered with static gantry and MLC shapes (or blocks).

IMRT utilizes the MLCs for beam shaping and modulation. The MLCs produce intensity maps with dozens of beamlets within one field whose intensities are independent of one another. IMRT plans are usually identified as static or VMAT/RapidArc IMRT. For a static IMRT, the gantry is stationary, but the MLC leaves will move while the radiation beam is ON to create the intensity modulated beam. For VMAT/RapidArc, the gantry is simultaneously rotating around the patient as the MLCs modulate the beam around the patient.

SBRT, unlike conventional radiotherapy, is a treatment technique that delivers fewer fractions of radiation (usually less than 5), but in a much higher dose. SBRT can be delivered either with 3DCRT or IMRT/RapidArc/VMAT, however clinicians tent to choose the latter, due to its ability to modulate the beam and conform the dose around the target better than 3DCRT.

PBS utilizes a few-millimeter (1 to 4 mm) pencil beam that is raster scanned across an area one spot at a time. Once the scanning is complete, the beam energy is changed to scan the next layer (depth). The most distal layer of the target is scanned first. PSPT relies on primary and secondary scattering material to create a 3D conformal dose distribution in the target. PSPT

technique is limited to a predesignated SOBP modulation, which must cover the full motion range of mobile targets.

For any of the above modalities, the patients with thoracic tumors will undergo an initial simulation. This entails placing the patient on the flat CT couch with an upper body immobilization and arms above their head. They are subsequently imaged via the CT scanner and the 3-dimensional images are used to create a computerized treatment plan with one of the three modalities previously described. The CT scanner uses a fixed X-ray and detector panel that rotates around the patient, and the detector panel records the X-ray that exits the patients' body. As the X-ray unit rotates around the patient, it will collect static images for each angle before it moves to a different section of the body. This is defined as a "slice" which runs along the superior to inferior direction of the body. Once all the desired slices are imaged, a mathematical algorithm is applied to create a 3-dimensional image with the appropriate electron density values, which is consequently used for treatment planning. For thoracic targets that are mobile, 4DCT is utilized. 4DCT introduces time as its fourth component. Like conventional CT, patients are scanned slice by slice utilizing the same X-ray source and detector, but each location is scanned for at least one breathing cycle. A mathematical algorithm is then used to bin all the slices based on the respiratory phases (or amplitude).

In any thoracic radiotherapy plan, the critical structures and targets are defined (contoured) by the planner and Radiation Oncologist respectively. Contours allow the treatment planning algorithm to optimize gantry angles, MLC

intensity modulation and other parameters such as desired dose to the target and OAR (organs at risk). CT imaging, as previously described, is simply a snapshot of the patient, at a particular time; as a result, organ motion is not well quantified, therefore 4DCT is often the imaging technique of choice. Due to spatial limitations of the scanner, limited information on target motion as well as setup uncertainties, several standard target definitions have been established by the International Commission on Radiation Units and Measurements (ICRU) Report 62, a supplement of ICRU 50 (***Figure 0-6:***) (ICRU 50, 1993; ICRU 60, 1999).

The initial target will be contoured as GTV (gross tumor volume) which implies that the target was defined by the physician through visualization or palpation. Subsequently an expansion margin is applied to create a CTV (clinical target volume). This expansion accounts for any subclinical involvement that is too small to see due to the limited spatial resolution of the CT scanner. Additionally, an internal margin (IM) is applied to the CTV to create ITV (internal target volume). This expansion allows for possible mobility of the target itself and often directly identified by the 4DCT. Lastly, a setup margin is applied to the ITV to create PTV (planning target volume). This margin will account for any setup errors that may occur during daily treatments. The PTV is often the final definition of a target that the planner will use to create the computerized treatment plan, in addition to contouring all of the organs at risk that are next to the PTV or in the beam path.

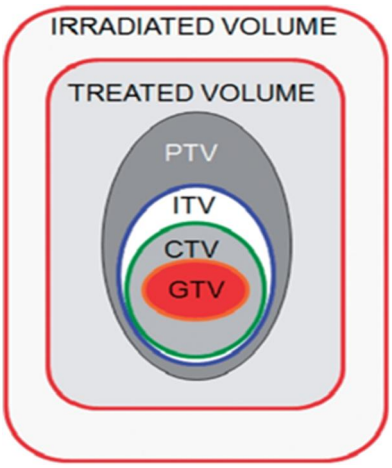

Figure 0-6: ICRU 50/62 target definition *(ICRU 60, 1999)*

1.4 Management of Respiratory Induced Tumor Motion

Improvements in radiation delivery techniques (Armstrong, 1993) of thoracic targets enable clinicians to achieve conformal dose delivery, while limiting dose to the OARs. However, the motion of a target continues to be a challenging parameter. The International Commission on Radiation Units and measurements (ICRU) Report 50 (ICRU 50, 1993) and the Supplement Report 62 (ICRU 60, 1999) describe the current recommendation for incorporation of tumor motion into radiation therapy planning. In the thorax, targeting is complicated by respiratory motion, which can cause tumor displacements as large as 2 cm during treatment (Shimizu, et al., 2001) (Seppenwoolde, et al., 2002).

Accurate targeting is critical, particularly for mobile tumors that are treated with SBRT. The American Association of Physicist in Medicine (AAPM) Task Group 76a report on the management of respiratory motion in radiation oncology (Keall, et al., 2006), recommends margins around the treatment target

be sufficient to ensure coverage of the target. In a landmark SBRT trial for early stage inoperable lung cancer, Timmerman, et al. used planning target volume (PTV) expansions from the gross tumor volume (GTV) of up to 5 mm in the axial dimension and 10 mm in the cranial-caudal (CC) direction (Timmerman, et al., 2010). This relatively large PTV expansion in the CC direction results in a larger volume of healthy tissue being irradiated.

For thoracic malignancies 4DCT provides a snapshot of the respiratory induced tumor motion which is used to individualize the internal target volume (ITV) (Pan, 2004), yielding smaller treatment margins than fluoroscopy. As 4DCT scanning and image-guided radiotherapy (IGRT) became more readily available, recent studies have reduced the PTV margins to a 5 mm uniform expansion around an ITV that accounts for respiratory motion (Liang) (Li X. e.) (Kilburn, 2016).

1.5 Respiratory Management Techniques

There are several motion management techniques that are utilized in the clinic to track or reduce tumor motion to meet the national recommendations and guidelines mentioned above. They include, but not limited to: abdominal compression, respiratory gating, respiratory tracking, breath hold, active breathing coordinator (ABC) and jet ventilation.

External abdominal compression technique is one way to control (compress) tumor motion. This technique utilizes a full or partial vac-lock body bag for

external patient immobilization and an abdominal compression plate (***Figure 0-7***).

Figure 0-7: Example of Full Body Vac-Lock with abdominal compression plate

The patients' abdomen is compressed with an external plate for both imaging and treatment. The downside of this technique for lung cancers continues to be its inconsistency and minimal dosimetric gain for lung sparing (Bouilhol, et al., 2013).

Respiratory gating (Keall , Kini, Vedam , & Mohan, 2002) (Kubo, 1996) and tracking (Shirato H. e., 2000) (Keall e. a., 2006) (Hospital, 2015) (Shirato H. e.) have been used to reduce the uncertainty in tumor targeting thereby reducing the free tissues irradiated. Both techniques have been previously used to lower the uncertainty in tumor targeting, therefore reducing the PTV margins. Such margin reduction benefits were presented by (Keall , Kini, Vedam , & Mohan, 2002). They investigated gating for treatment margins, image artifacts and volume for a spherical moving object. In that study, during the CT imaging of dynamically moving spheres, gating reproduced the static volume to within 1% whereas errors of over 20% were observed where gating was not used (Keall ,

Kini, Vedam , & Mohan, 2002). Furthermore, Keall et al., (Keall e. a., 2006) noted that gating can reduce margins from CTV to PTV by as much as 2 to11 mm. However, the downfall of these methods can often be associated with low Duty Cycle (DC) (Eq. 7), also known as the beam ON time, and accuracy of predictive filters.

Breath-hold gating techniques have been widely used in radiotherapy (Wong, 1999). One such technique is voluntary breath hold. The patient is coached to inhale and hold their breath. This technique has its limitations and therefore has not received widespread adoption due to the breath-holding capacity limitation of patient (10 – 20 sec). The second technique is ABC, a device and treatment method developed at William Beaumont Hospital which provides non-invasive internal immobilization of anatomies affected by respiratory motion, such as the breast and lung [20]. This is achieved through comfortable, simple and efficient assisted breath-hold techniques. Patient breath volumes are monitored, and the airway is closed as a fixed inspiratory volume for the duration that the patients holds the breath-hold button (***Figure 0-8:***). The ABC has been widely used for stereotactic treatment in the lung and has been proven effective in clinical practice for more than 15 years (Boda-Heggemann, 2016). The intra-fraction reproducibility for repeat breath-holds has been reported to be ≤ 2 mm (Glide-Hurst, Gopan, & Hugo, 2010). However, like breath holds, its use is limited to patients who are physiologically capable of breath-holds. Many lung cancer patients can not tolerate breath-holds.

Figure 0-8: A simulated patient demonstration of the ABC breath-hold. The machine allows reproducible assisted breath-holds at similar volumes between breath-holds by use of spirometer to measure tidal volumes.

Lastly, jet ventilation was reported for respiratory motion immobilization for use in *intubated* patients who received general anesthesia (Herfarth, 2000). This technique was limited to patients who were treated in a single fraction. Robotic tumor motion tracking using external surrogate markers has been reported for SBRT treatment of lung tumors (Schweikard). This technique treats continuously while the patient breathes freely (Seppenwoolde Y. e., 0094-2405), however is limited to the CyberKnife and now Radixact robotic treatment device. An ideal respiratory motion compensation method that has a high duty cycle (Eq. 7), will provide the patient comfort of free breathing, while not requiring special radiotherapy equipment.

1.6 Motivation for the Project

High frequency percussive ventilation (HFPV) is a novel immobilization technique that has gained little attention in radiotherapy. It utilizes high frequency low tidal volume ventilation to produce endotracheal percussion (Salim A. a., 2005) (Allan, Osborn, Chung, & Wanek, 2010). The device is an

adaptation of a pneumatic high frequency ventilator in which high flow jets of gas are delivered to the airways by a flow interrupter called a Phasitron. Activation of the venturi system within the Phasitron creates bursts of gas at frequencies of 100 to 400 bursts per minute within a tightly controlled ratio of gas delivery and passive exhalation. The device is used for mobilization and clearance of pulmonary secretions. HFPV improves oxygenation versus conventional ventilation, with no barotrauma, in patients with acute respiratory distress syndrome (Spapen, 2014) (Gallagher, 1989).

HFPV is designed to treat active pulmonary disease and to prevent the development of disease caused by secretion retention in either intubated sedated patients or spontaneously breathing awake patients. For example, HFPV was found to prevent deterioration in patients with acute exacerbation of COPD [30]. It is tolerated well enough for use in the pediatric outpatient setting in cooperative alert patients (Reardon, 2005).

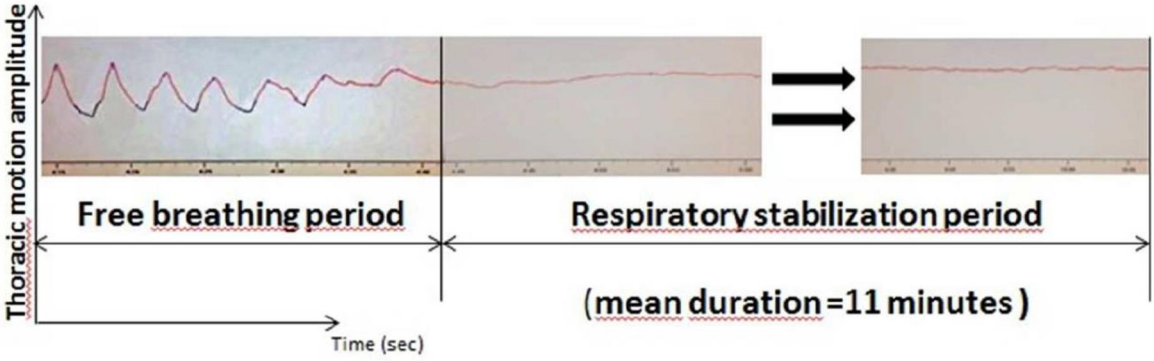

Figure 0-9: A graph of chest wall circumferential strain measured with an Anzai respiratory belt during free breathing period, onset of HFPV, and during the apneic-like HFPV period adapted from Peguret et al. *(Peguret N. a.-d., 2016)*

Recently, high frequency percussive ventilation (HFPV) was reported for immobilization of thoracic tumors for imaging (Prior J. e., 2016) and stereotactic body radiotherapy (SBRT) [33]. In Peguret's SBRT study, thoracic tumor respiratory motion was inferred from changes in the chest diameter measured by an Anzai respiratory belt (ANZAI Medical Co, Tokyo, Japan). A sample trace of the thoracic diameter from Peguret et al (Peguret N. e., 2016) is shown in ***Figure 0-9:***. There were patients who could not tolerate percussive ventilation assisted breath-holds for greater than 10 to 15 seconds. This preliminary study provided no direct evidence of tumor motion reduction and no evidence of intra-session reproducibility. Filling this gap in knowledge is an important consideration before moving HFPV into clinical practice for tumor immobilization for proton or photon therapy.

1.7 Hypothesis

- HFPV provides direct tumor immobilization of <5 mm for all targets exhibiting respiratory motion >10 mm
- HFPV provides reproducible thoracic immobilization with <5 mm residual motion, over 1-minutes intervals with rebreathing between each instance.
- Significantly reduces the interplay effects noticed in pencil beam scanning proton radiotherapy.
- HFPV can significantly reduce the PTV margin for thoracic targets and subsequently healthy tissue toxicity

1.8 Set Objectives

- The primary objective of this study is to test if HFPV can be a viable method for thoracic immobilization
- A second primary objective is to evaluate if HFPV can reduce lung tumor motion from ≥ 10 mm to < 5 mm. This will be the ***first*** study to directly measure tumor motion reduction using HFPV.
- A second objective is to evaluate the reproducibility of HFPV immobilization. Will the target return to the same location after re-breathing then repeat HFPV?
- Another secondary objective is to evaluate the interplay and dosimetric effects of HFPV motion.

CHAPTER 2: HIGH FREQUENCY PERCUSSIVE VENTILATION PROTOCOL

1.9 Introduction

This is a prospective trial of 15 volunteers and 10 patients with thoracic tumors that were utilized to develop our first experience with HFPV for thoracic tumor immobilization. The study was separated into two main cohorts. Cohort I entailed the recruitment of 15 healthy volunteers who underwent HFPV while monitoring for chest wall motion. Cohort II consisted of 10 patients with conspicuous thoracic tumor whose motion was identified to be greater than 10 mm.

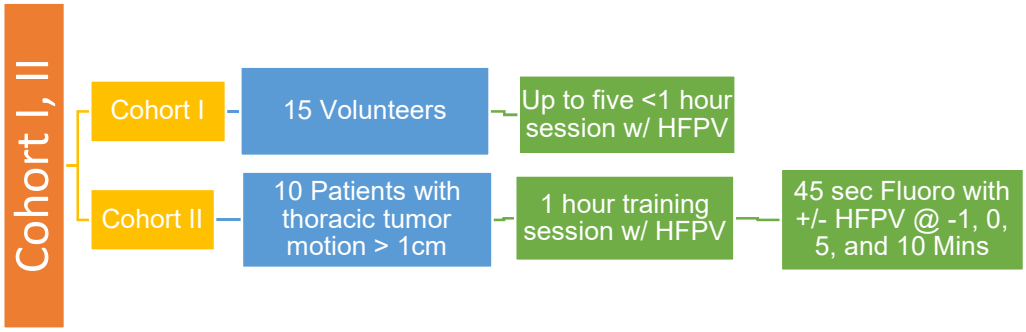

Figure 0-1: Study Cohorts & Scheme. Fifteen normal volunteers were recruited to gain familiarity with the HFPV device and monitoring equipment. Ten patients with conspicuous thoracic tumors that move ≥ 10 mm due to respiration on their treatment plan

All 10 patients would undergo fluoroscopic imaging while in free and HFPV breathing (***Figure 0-1***). Subsequent follow up studies were performed to validate the clinical and dosimetric impact of the data obtained from the above cohorts.

1.10 Methods

1.10.1 Cohort I: Eligibility, Recruitment and Selection

1.10.1.1.1 Inclusion Criteria

Volunteers must be older than 18 years of age and must be able to sign consent.

1.10.1.1.2 Exclusion Criteria

- Volunteers unable to tolerate the 1-hour sessions with HFPV.
- Volunteers with history of COPD or pneumothoraxes.
- Volunteers with hemoptysis.
- Volunteers requiring supplemental oxygen.
- Volunteers with fractured rib or unstable chest

- Volunteers with who report a known panic or anxiety disorder.
- Volunteers who are pregnant or who think they may be pregnant.
- Unable to sign informed consent due to cognitive impairment or health status.
- Patients who are <18 years old.

1.10.1.2 Study evaluation

The volunteers will be evaluated lying supine and flat on the treatment bed with their arms above their head. Their chest wall motion will be monitored using the Anzai Respiratory Monitor (Anzai Medical Co, Tokyo Japan). The device, which has FDA 510(k) clearance, makes no contact with the subject, using a laser and detector to monitor motion. Volunteers will undergo trial periods of HFPV using various interface devices – mouthpiece, face mask, nasal prongs, each evaluated for compliance and ease of use. The volunteer sessions will be completed within 1-hour time and may be repeated up to 5 times for a single volunteer. After each session, the volunteer will be asked to complete a feedback questionnaire

1.10.1.2.1 HFPV

The Percussionaire IPV-2C (Percussionaire Corp., Sagle, Idaho) is a pneumatic (air driven) device that delivers both continuous positive airway pressure (CPAP) and mini bursts of air. This combination allows air to enter behind mucus blockage, and vibration to dislodge mucus from the airway walls so it can be more easily coughed up. The Phasitron® uses a unique, patented

venturi as a “clutch” mechanism to protect the lung from over pressure. A biofilter is placed between the Phasitron and the patient. A video showing the home use of percussion ventilation in a cystic fibrosis pediatric patient is available on-line (https://www.youtube.com/watch?v=FpSicdEZOhw).

During this component we will compare use of various respiratory interfaces to volunteers (native Phasitron mouthpiece, ABC mouthpiece shown in ***Figure 0-8:***, face-masks, nasal prongs), respiratory settings, and chest wall motion. The nasal prongs and the active breathing control breathing tube (mouth piece) are used as one single unit during the administration of the percussive breathing. The face mask is a secondary testing piece that will be used on all volunteers as well. We will evaluate for ease of use, comfort, minimal motion, geometric interference, and compliance. We will seek to maximize comfort, minimize chest wall motion, maximize duration of apneic-like HFPV state, ease of use and reproducibility.

There are no reports of which, we or Percussionaire Corp., are aware that indicate an increased incidence of barotrauma or pneumothorax associated with high frequency percussive ventilation (HFPV). For example, one randomized trial comparing HFPV versus low tidal volume ventilation (LTV) in burn injury patients with acute lung injury found no HFPV patients developed barotrauma versus four who received LTV ($p = 0.04$) (Chung, 2010). There are reports on the use of percussive ventilation to treat pneumothorax in an infant with osteogenesis imperfect (Nino, 2009) and in adult post-surgical patients with persistent pneumothoraxes (Gatani, 2010). In order to be on the safe side, we

will consider risk factors for pneumothorax following CT-guided thoracic biopsy. The risk of pneumothorax requiring chest tube placement following CT-guided needle biopsy increases with emphysema present on CT (Laurent, 1999) and severe COPD (COPD stage GOLD 3 or greater (Vestbo, 2013). Severe COPD is identified with an FEV1 < 50% predicted value. In this study we exclude patients with history of pneumothoraxes, emphysema present on the RT planning CT, or FEV1 < 50% predicted value.

The duration of the HFPV administration depends on the comfort level of the individual subject. The goal of the session is to achieve greater than 5 minutes of lung immobilization under one hour of the training session. We will ask for feedback from the volunteer. This will assist us in developing the best tolerated and technical technique for the patient cohort. After this cohort, we will evaluate the data and the feedback to test in the patient setting of Cohort II.

1.10.1.2.2 Anzai Respiratory Motion

The Anzai AZ-733VI (Anzai Medical Co, Tokyo Japan) is an FDA approved device utilized in gated radiotherapy treatment and diagnostic PET/CT. The business card size laser/sensor measures the reflection of laser light (infrared) from the patient's skin, and the motion of the body surface (displacement of distance to the sensor) is recorded on the device computer. Volunteer and patient respiratory trace records will be anonymized and recorded using patient study number. IRB Both volunteers in cohort 1 and patients in cohort 2 will have their chest wall motion monitored for the duration of the training and experimental sessions (≤ 1 hours total each session).

1.10.1.2.3 Oxygen and Carbon Dioxide Supply

The SenTec Digital Monitoring System (SDMS) provides continuous and noninvasive real-time monitoring of transcutaneous CO_2 partial pressure (tc-PCO_2), functional oxygen saturation (SpO_2), pulse rate (PR), and pulsation index (PI) in adult and pediatric patients. A small dime size transducer is attached with a postage-stamp sized adhesive behind the subject's ear for monitoring. Both cohorts of patients will receive monitoring of tc-PCO_2, SpO_2, and PR during the training and experimental sessions.

1.10.2 Cohort II: Eligibility, Recruitment and Selection

1.10.2.1.1 Inclusion Criteria

- Patients with conspicuous lung tumor that exhibit greater than 10 mm motion on their radiotherapy planning 4DCT. Patient lung tumors must be visible on the AP CT projection scout.
- Patients must sign informed consent to enter this study.
- Documented not pregnant if child-bearing age woman.

1.10.2.1.2 Exclusion Criteria

- Patients unable to tolerate the 1-hour training and 20-minute imaging sessions (RT fluoroscopy).
- Patients with history of pneumothoraxes, emphysema present on RT planning CT, or FEV1 < 50% predicted value.
- Patients with hemoptysis.
- Patients requiring supplemental oxygen.

- Patient with fractured rib or unstable chest
- Patients with a known panic or anxiety disorder
- Unable to sign informed consent due to cognitive impairment.
- Patients who are <18 years old.

1.10.2.2 Study Evaluation

1.10.2.2.1 HFPV

The Percussionaire IPV-2C and Phasitron are described above. Patients in cohort 2 will receive a 1-hour training period with the HFPV device to minimize thoracic motion. They will then be brought to the RT treatment room where the on-board imaging device will be used to provide fluoroscopy. They will undergo 45 sec of fluoroscopy at 4 time points, one before with tidal breathing, one at the start of the HFPV, one after 5 minutes, and one after 10 minutes of using the IPV-2C. Patients will be allowed to rebreathe in between these fluoroscopy procedures.

1.10.2.2.2 Anzai Respiratory Monitor

Patients in cohort 2 will have their chest wall motion monitored for the duration of the training and experimental sessions (approximately 1 hour 15 minutes total). There is no direct contact with the patient, only a low power laser light is displayed and tracked on the patients' skin to measure chest wall skin motion.

1.10.2.2.3 SenTec

The SenTec Digital Monitoring System (SDMS) will provide continuous and noninvasive tc-PCO_2, SpO_2, and PR monitoring during the HFPV sessions. A small dime size transducer is attached with a postage-stamp sized adhesive behind the subject's ear for monitoring. A digital record is kept under the patient's study number.

1.10.2.2.4 RT Fluoroscopy

RT Fluoroscopy. The Elekta treatment machines have an on- board kV imaging system consisting of a low power diagnostic x-ray tube and a flat panel detector capable of imaging at 10 Hz. Patients will undergo one session of fluoroscopy before with tidal breathing, at onset of HFPV, at 5, and 10 minutes after onset. The patients will be allowed to rebreathe between the repeat fluoroscopy acquisitions. The tumor volume will be auto-segmented frame-by-frame using image intensity-based registration algorithm to ascertain the degree of the tumor motion

1.11 Analysis and Risks

1.11.1 Criteria for Study Removal

Healthy volunteers and patients unable to tolerate HFPV process due to discomfort or for any other reason. Subject (healthy volunteer or patients) choice (subjects can withdraw from the study at any time, for any reason). If subjects experience any of the following, shortness of breath, chest pain, increased oxygen requirement (pulse ox <88%), significant change in heart rate (>110bpm), fatigue, or vomiting, the patient will be evaluated by the radiation

oncologist. At this point, the study procedures will be stopped, and the subject participation will be completed. Data already acquired may evaluated within the study, including information related to the adverse event if attributed to the study. Study will be put on hold and evaluated by the ISMC if 2 of the first 5 subjects cannot complete the first 1-hour session. Evaluation will determine if a revision of study or the discontinuation of the study is necessary.

1.11.2 Registration procedure

Informed consent is required prior to participation in this study. The study coordinator will inform potential subjects about the study opportunity and ask if they would like to participate. If the patient is interested, they will be given an opportunity to read the informed consent and authorization document specific to the study and ask questions of the study coordinator. The patient will be informed about: 1) the rationale for the study; 2) the logistics of the study; 3) the risks of the study; 4) how the data will be used. Consent will be obtained by the study coordinator. The patient will be given a copy of the consent and asked to sign another copy for our records.

Patients will be registered for the study after pretreatment evaluation is completed and eligibly criteria are met. The principle investigator and all key personnel have completed NIH approved institutional and HIPAA training in the conduct of medical research studies.

1.11.3 Potential Risks

Two cohorts will be recruited for enrollment in this study, volunteers and patients with thoracic tumors that move ≥ 1 cm. The participation in this study for the cohort 1 volunteers will consist of no more than 5 sessions of HFPV while their chest wall motion is monitored. Their risk is solely due to HFPV. For cohort 2 patients their risk will be from HFPV and RT Fluoroscopy. The total dose per patient for this study is estimated at 28 mSv per patient in cohort 2. This dose is less than the Radiation Safety Committee guidelines of 50 mSv per year from research.

The volunteers and patients recruited to this study will receive HFPV while monitored for O_2 saturation and transcutaneous pCO_2. The HFPV is powered from the hospital supply O_2 and delivers a mixture of O_2 and room air. Patients may experience increased shortness of breath, chest pain, an increased O_2 requirement, change in heart rate or rhythm, blood pressure, fatigue, or emesis and panic. Risks also include under/over ventilation, under/over humidification, pneumothorax, pneumomediastinum, PIE, pneumoperitoneum, and hemoptysis. Volunteers or patients who experience any of these symptoms will be evaluated by a physician and discontinued from the study.

RT Fluoroscopy Cohort. The major risk from the RT fluoroscopy imaging is from the radiation. The dose equivalent for this device is estimated at 1 mSv/10 sec beam time. The RT fluoroscopy imaging will deliver approximately 28 mSv total dose to the patient.

CHAPTER 3: ESTIMATION OF CHEST WALL MOTION REDUCTION WITH HFPV – PROSPECTIVE STUDY

1.12 Abstract

Purpose: High frequency percussive ventilation (HFPV) employs high frequency low tidal volumes (100- 400 bursts/min) to provide respiration in awake patients while simultaneously reducing respiratory motion. The purpose of this study is to evaluate HFPV as a technique for respiratory motion immobilization in radiotherapy.

Methods: In this study fifteen healthy volunteers (age 30y-75y) underwent HFPV using three different oral interfaces. We evaluated each HFPV oral interface device for compliance, ease of use, comfort, geometric interference, minimal chest wall motion, duty cycle and prolonged percussive time. Their chest wall motion was monitored using an external respiratory motion laser system. The percussive ventilations were delivered via an air driven pneumatic system. All volunteers were monitored for PO_2 and tc-CO_2 with a pulse oximeter and CO_2 Monitoring System.

Results: A total of N=62 percussive sessions were analyzed from the external respiratory motion laser system. Chest-wall motion was well tolerated and drastically reduced using HFPV in each volunteer evaluated. The average peak-to-peak motion for free breathing was 8.14 mm (median: 6.90 mm, range: 2.70 mm – 18.6 mm) and for HFPV was 2.52 mm (median: 1.80 mm, range: 0.60 mm – 8.40 mm)

Conclusion: We believe HFPV may provide thoracic immobilization during radiotherapy, particularly for SBRT and pencil beam scanning proton therapy.

1.13 Introduction

Improving immobilization and delivery techniques for thoracic tumors continues to be essential in radiotherapy; particularly for patients undergoing stereotactic body radiotherapy (SBRT), hypo-fractionated regimens and pencil beam scanning proton therapy. Unlike photon radiotherapy, pencil beam scanning proton radiotherapy consists of a 2 to 3-millimeter spot that is “raster” scanned across the target one slice at a time. The pencil beam is moved across the field with the aid of fast and slow magnets. The depth is achieved by a range modulator that alters the proton beam energy, shifting the range and Bragg Peak (Newhauser, 2015).

For stationary targets, the pencil beam scanning proton therapy scans across each slice and creates a highly conformal dose deposition throughout the target. However, significant in-homogeneities have been noted for targets that move during pencil beam scanning proton therapy due to interplay effects (Langen K. a., 2001) (Shirato H. e.) (Bert C. a., 2008) (Seppenwoolde, et al., 2002). Bert et al. (Bert C. a., 2008), reported that the homogeneity on their radiographic films study was less than 80% for motion amplitudes of about 15 mm. The homogeneity for their treatment-planning study, based on patient data, was on an average 71% for 95% of the target volume. Such drastic interplay effects for targets that move during pencil beam scanning particle radiotherapy

have prompted institutions to employ techniques that would allow for reduction or monitor of target motion.

Undoubtedly the goal in radiotherapy planning continues to be its accurate delivery of radiation to the target while maintaining good sparing of nearby healthy tissue. However, acceptable distribution of absorbed dose within the target could become compromised when they are mobile. As a result, the International Commission on Radiation Units and measurements (ICRU) Report 50 (ICRU 50, 1993) and the Supplement Report 62 (ICRU 60, 1999) describe the current recommendation for incorporation of the tumor motion into radiation therapy planning. Subsequently, the American Association of Physicist in Medicine (AAPM) Task Group 76a report on the management of respiratory motion in radiation oncology (Keall, et al., 2006) recommends margins around the treatment target be sufficient to ensure coverage of the target. Lastly, in a landmark SBRT trial for early stage inoperable lung cancer, Timmerman, et al. (Timmerman, et al., 2010) used planning target volume (PTV) expansions from the gross tumor volume (GTV) of up to 5 mm in the axial dimension and 10 mm in cranial-caudal direction. Several papers have been published on ways to mitigate motion in order to achieve optimal dose distribution and comply with the above recommendations. Abdominal compression can be inconsistent and in cases increase target motion (Bouilhol G. a., 2013). Respiratory gating must rely on accurate predictive filters and has low duty cycle (Verellen, 2010) (Murphy M. J., 2004) (Keall, et al., 2006). Respiratory tracking can be invasive if fiducial markers are used, but most importantly the correlation of the external surrogate

(infrared tracking cubes or body surface tracking via stereo cameras) to internal tumor may not be accurate (Ionascu, 2007) (Seppenwoolde, et al., 2002). Breath hold relies on the ability of the patient to hold their breath during simulation and treatment. As a result, such technique is often reserved for patients who are physiological capable.

The obvious solution to the above challenges would be to immobilize the target itself. High Frequency Percussive Ventilation (HFPV) employs high frequency low tidal volume ventilation to generate endotracheal percussion. The patient is connected to the Intrapulmonary Percussive Ventilation/Impulsator (IPV) device (Percussionaire Corp., Sagle, Idaho) through the Phasitron and mouth piece interface (***Figure 0-1:***). Initiation of the IPV device will allow the Phasitron to deliver small bursts of air into the patients' trachea. The frequency of the air bursts can be 100 to 400 bursts per minute. The Phasitron is attached to a water reservoir which reduces dry throat, in addition to providing a path for carbon dioxide (CO_2) to escape the lungs while continually oxygenating (***Figure 0-2:*** and ***Figure 0-3:***).

Figure 0-1: Percussionator - Intrapulmonary Percussive Ventilation/Impulsator (IPV) 2C

Figure 0-2: Phasitron

Figure 0-3: Phasitron and tubing

While HFPV is often used in bronchial hygiene therapy and other acute respiratory diseases that allow for sustained improvement of oxygenation and ventilation for such patients (Spapen, 2014), recently it was reported as a technique to immobilize thoracic tumors for imaging purposes (Prior J. a., 2016) and stereotactic body radiotherapy (Peguret N. a.-d., 2016).

In this study, we recruited fifteen healthy volunteers (age 30y to 75y) and investigated various types of interfaces. The aim for this part of our study was to evaluate each interface device for compliance, ease of use, comfort, geometric interference, minimal chest wall motion, duty cycle and prolonged percussive time.

1.14 Methods and Materials

Fifteen healthy volunteers between October 2, 2017 and February 1, 2018 were enrolled in this Beaumont Research Institute Institutional Review Board approved observational study (IRB# 2017-046). Each volunteer signed an informed consent and were entered into the clinical research database prior to the study entry. Volunteers that were unable to tolerate HFPV or required supplemental oxygen, in addition to other medical concerns or pregnancy, were excluded from the study. All volunteers were evaluated lying supine with their arms above their head and a knee sponge for comfort.

Each volunteer was asked to undergo trial periods of HFPV using three different types of oral interface devices: Amici Tru-Fit Mouthpiece Kit with tubing, elbow and nose clips (***Figure 0-4:***), Fisher & Paykel Oracle 452 mask with straps and nose clips (***Figure 0-5:***) and Phillips Respironics Oro-Nasal mask with head gear (***Figure 0-6:***). Each interface connected to the Percussionaire IPV-2C via the Phasitron and single use tubing kit.

Figure 0-4: Amici Tru-Fit mouthpiece interface

Figure 0-5: Fischer & Paykel Oracle 452 interface

Figure 0-6: Phillips Respironics Oro-Nasal interface

The chest wall motion was monitored using Anzai respiratory monitor laser system (Anzai Medical Co., Tokyo, Japan). The Anzai, is an FDA approved system that utilizes a low power red laser which projects onto the patients' surface. Each volunteer underwent at least one HFPV session per interface, but multiple sessions were enabled. A typical example of two (Ns=2) HFPV sessions per interface is denoted in ***Figure 0-7:***

Python based code was developed to use Fourier transform for decomposition of the breathing curves from the time domain into frequency representation, as a validation to the manual IPV-2C dials. High peak indicates the frequency that dominates the signal. The peak frequency was validated by fitting on a cosine curve. The dominating frequency was validated against the Percussionaire's manual dial.

Another important parameter evaluated was the duty cycle. Duty cycle is the ratio of the amount of time that radiation delivery device is on T_{on} relative to the total treatment time $(T_{on} + T_{off})$ (Eq. **6**).

$$Duty\ Cycle = \frac{T_{on} + T_{off}}{T_{off}} \quad \textbf{(7)}$$

A threshold band (2 mm and 5 mm), highlighted in (***Figure 0-13:***) was created for each of the Ns=62 HFPV sessions and duty cycle were calculated for each threshold band.

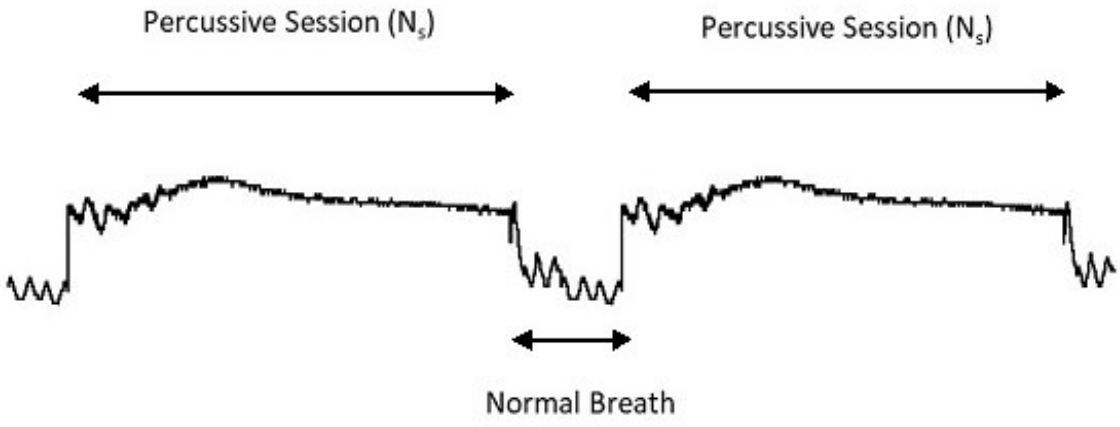

Figure 0-7: An example showing what a typical signal would look like for patient undergoing HFPV via one of the interfaces. Each volunteer undergoing HFPV could've resulted in multiple HFVP sessions as indicated in this figure (Ns=2)

A small tcCO_2 sensor from SenTec (SenTec AG, Therwil Switzerland) was placed onto the volunteers' forehead. It is a non-invasive, transcutaneous device that uses thin adhesive membrane attached onto the transducer to gather real time data CO_2, partial pressure (tc-PCO_2), functional oxygen saturation (SpO_2), pulse rate (PR) and pulsation index (PI). All volunteers in this study were monitored via SenTec device.

We utilized the Percussionaire IPV-2C (Percussionaire Corp., Sagle, Idaho) to provide HFPV bursts. The Percussionaire is pneumatic air driven device (***Figure 0-1:***) that delivers continues positive airway pressure (CPAP) and mini bursts of air (100 to 400 bursts/minute). The Phasitron is connected to the Percussionaire via single use tubing kit. Distilled water was used to provide moisturized air and prevent dry throat.

All volunteers (Nv=15) completed a Likert scale (1 strongly disagree - 5 strongly agree) subjective survey after each interface. Each subjective self-evaluating form consisted of eight linked questions separated into three main domains (***Table 1***). First domain (Q1,2,5) assessed for comfort, geometric interference and ease of use. Second domain (Q3,4,6,8) assessed for compliance. Third domain assessed for explanation of procedure. All volunteers were also allowed to provide written comments on each survey form. The duration and the number of HFPV sessions for each interface, was left at the discretion of the volunteer. Trained and authorized medical personnel operated all equipment.

Several statistical analyses were performed. A one-way Analysis of Variance (ANOVA) test was used to compare mask and different scores on the Likert scales. Additionally, a two-way ANOVA was performed to rule out interaction between questions and mask. A paired t test was used to compare the difference after. Kruskal Wallis test was performed to analyze duty cycle. A Friedman test was utilized to rank the prolonged time for each interface.

1.15 Results

All volunteers complied with the instructions and successfully completed multiple sessions of HFPV for each of the three interfaces. All fifteen subjects were able to participate for an hour-long session and hence were included in the analysis. The amount of time each person was under HFPV sessions using various masks were left to the discretion and tolerance of the subject. monitor shows a typical setup of the Fischer Paykel Oracle 452 interface. We evaluated the signals from the Anzai monitoring system for all fifteen volunteers. A total of Ns=62 of HFPV sessions were analyzed.

Figure 0-8: Typical HFPV setup for Fischer & Paykel Oracle 452 interface with nose clips and CO_2 skin monitor

Significant maturation effects were noted during the first five volunteers with both investigative team and patients learning the techniques involved in using the interface and HFPV. Ns=25 sessions were recorded for the first five volunteers, but fifteen of them were under sixty seconds. Subsequently, (Ns=37) sessions were recorded for the last ten volunteers and only four of them were

under sixty seconds. Due to these maturation effects in the first five volunteers, only sessions from the last 10 volunteers were used to analyze aim two and four. For aim two we analyzed one session per interface, per volunteer. Totaling Ns=30. However, one session was excluded as a deviance, which we believe was due to the geometrical fit of interface for the particular volunteer in neutral position. For aim four we elected all sessions from the last ten volunteers Ns=37.

The least square mean for Amici Tru-Fit, Fischer & Paykel Oracle 452 and Phillips Respironics Oro-Nasal were 3.81, 3.74 and 4.01 respectively. The second domain, represented by questions 3, 4, 6 & 8 on the survey, evaluated for compliance. The least square mean for Amici Tru-Fit, Fischer & Paykel Oracle 452 and Phillips Respironics Oro-Nasal were 2.48, 2.38 and 2.35 respectively. All three interfaces were reported favorably for comfort with Phillips Respironics Oro-Nasal interface average score higher than the other two. On the other hand, there was no statistical difference between the three interfaces for compliance. The third domain, represented by question 7 on the survey, evaluated for explanation of procedure. All three interfaces were scored very high (5 out of 5), therefore excluded from analysis.

	Amici TruFit	Fischer Paykel	Phillips Respronics
Domain 1 - Comfort (Least Square Mean)	3.81	3.74	4.01
1. Procedure was comfortable?	3.63	3.66	4.03
2. Procedure was easy?	4.09	4.09	4.44
5. Procedure was easy to tolerate?	3.72	3.47	3.56
Domain 2 - Compliance (Least Square Mean)	2.48	2.38	2.35
3. I felt shortness of breath?	2.75	2.63	2.53
4. I felt panicked?	1.63	1.44	1.38
6. Position was easy to hold?	4.53	4.44	4.38
8. I felt pain?	1.00	1.00	1.13
Domain 3 - Explenation (Least Square Mean)	5.00	5.00	5.00
7. Procedure thoroughly explained?	5.00	5.00	5.00
***1 Strongly Disagree and ***5 Strongly Agree (N_v=15)			

Table 1: Results from the subjective survey/questionnaire

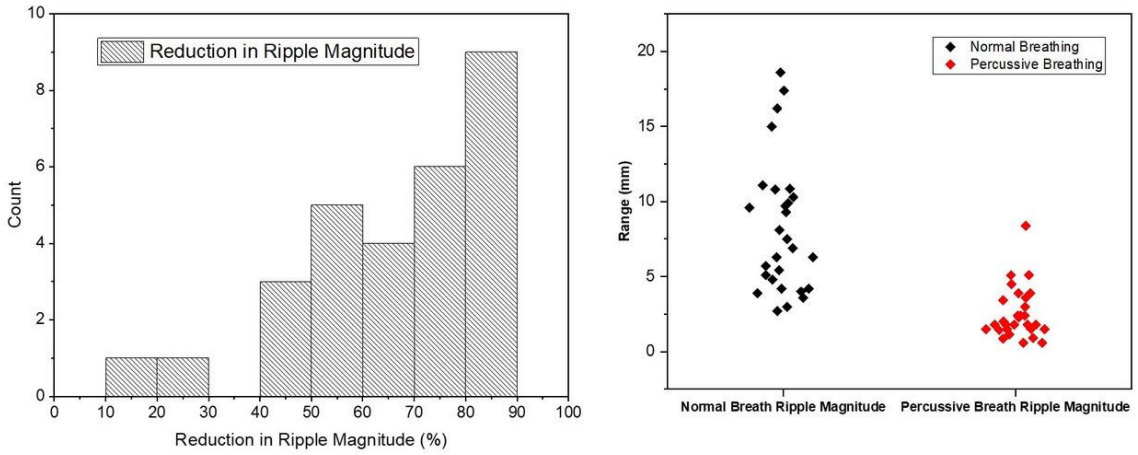

Figure 0-9: Amplitude Distribution a)Range of % Ripple (peak to peak) reduction while in HFPV b) Chest wall amplitude (peak to peak) for Free Breath vs. HFPV as measured by Anzai

Our next aim was to investigate the chest wall motion reduction while under HFPV for all Nv=10 volunteers. Ns=29 HFPV sessions were analyzed. A temporal local mean reduction of 65.97% (Ns=29, median: 71.43 %, range: 14.29 %-87.50 %) was observed for the ripple magnitude (peak to peak) between free breath vs. percussive (***Figure 0-9:***). A chest wall motion reduction

was observed from an average of 8.14 mm (median: 6.90 mm, range: 2.70 mm-18.6 mm) for free breathing to an average of 2.52 mm (median: 1.80 mm, range: 0.60 mm-8.40 mm) for percussive breathing. The mean difference before and after HFPV was 6.59 (95% CI 5.09-3.06, p< 0.001). A multi variance regression with significance for reduction in ripple percentage was significant for type of interfaces and baseline ripple value.

The mean frequency of all the breathing curves from the Fourier decomposition was 5.8839 cycles/second (353.03 cycles/min) for HFPV and 0.2252 cycles/second (13.51cycles/min) for free breathing ***Figure 0-10***. This was in agreement with the manual setting of the Percussionaire, which ranged from 340-360 cycles/min and average free breathing of all volunteers between 10-15 cycles/min. HFPV and free breathing pattern was validated by fitting a cosine curve, which was in agreement ***Figure 0-11***.

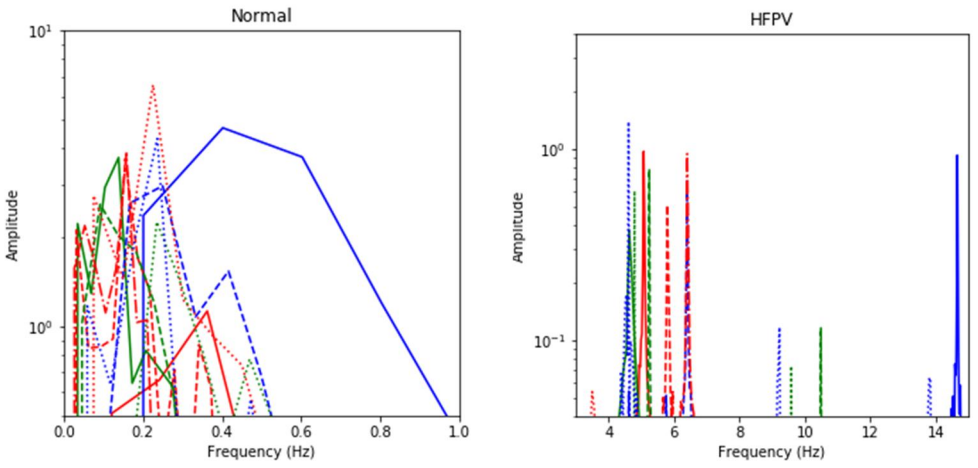

Figure 0-10: Fourier transformation from time domain to frequency domain of all chest wall curves obtained.

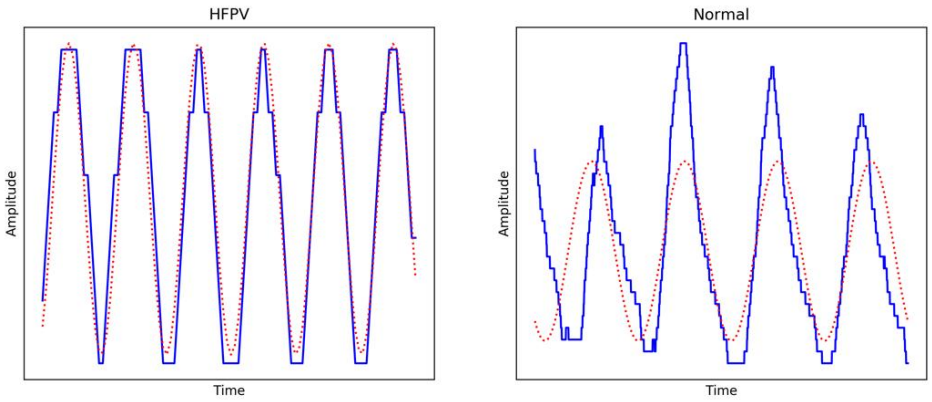

Figure 0-11: HFPV and Free breathing validation by fitting the peak frequency to a cosine curve

Out of Ns=62 HFPV sessions analyzed, the mean duty cycle for 2 mm threshold band was 55.67 % (range: 14.00 %-100.00 %, median: 52.09 %). Similarly, the mean duty cycle for 5 mm threshold band was 87.24 % (range: 31.85 %-100.00 %, median: 93.03 %). No statistical difference was noted between the interfaces with both ANOVA and Kruskal Wallis test. A histogram of both threshold bands is provided in (***Figure 0-12:***).

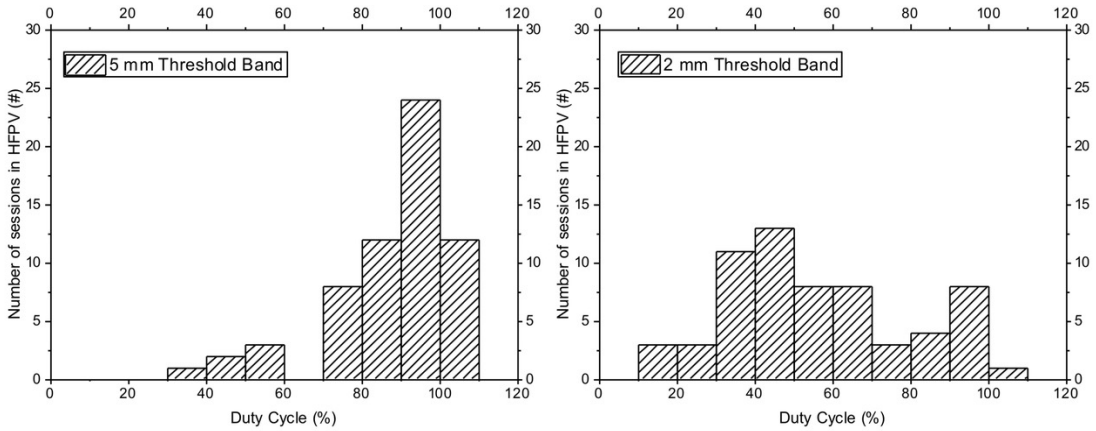

Figure 0-12: Duty Cycle distribution for each threshold band Ns=62 a) 5 mm b) 2 mm

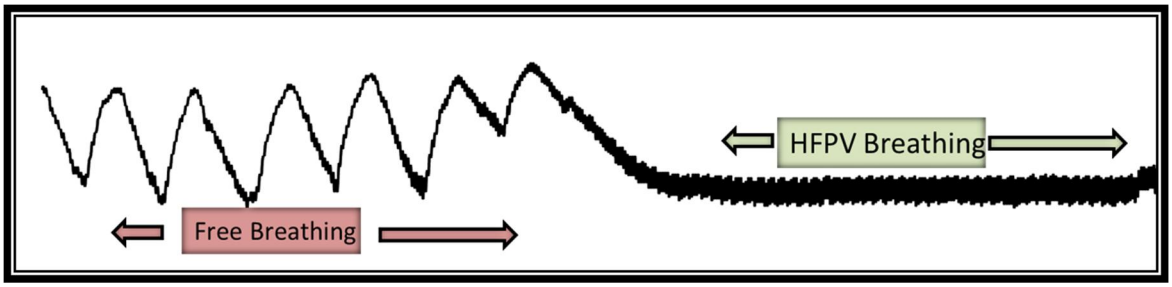

Figure 0-13: A typical chest wall motion recorded by Anzai detector. The initial section indicates free breathing followed by HFPV

Lastly, we investigated prolonged percussive time for each volunteer. Out of Ns=62, the average time in which the volunteers were under HFPV was 199.4 seconds (range: 9 sec-16.83 min, Upper 95% CI of mean: 258.8 sec, Lower 95 % CI of mean: 139.9 sec). Additionally, we investigated whether the prolonged percussive time was statistically significant between the three interfaces. A total of Ns=33 HFPV sessions from the last ten of the fifteen volunteers were analyzed, Ns=11 for Amici Tru-Fit, Ns=11 for Paykel Oracle 452 and Ns=11 for Phillips Respironics Oro-Nasal. Any percussive times less than sixty seconds were omitted from the set calculations. A Friedman test resulted in statistical significance between the three interfaces ($p< 0.001$). Mean for Amici Tru-Fit was 210.73 seconds (median: 174.00 sec, range: 60-570 sec, Upper 95%CI of mean: 311.78 sec), mean for Fischer Paykel Oracle 452 was 360.00 seconds (median: 273.00 sec, range: 107.00sec-897.00sec, upper 95%CI of mean: 524.05 sec), mean for Phillips Respironics Oro-Nasal was 400.73 seconds (median: 258.00sec, range: 68sec-1010.00sec, Upper 95%CI of mean: 629.29 sec) (***Table 2***)

Interface/#sessions in HFPV	Mean time in HFPV (sec)	Mean DC 5 mm band (%)	Mean DC 2 mm band (%)

Amici TruFit (Np=10, Ns=11)	210.73	82.20	43.93
Fischer Paykel (Np=10, Ns=11)	360.00	79.09	39.24
Phillips Respironics (Np=10, Ns=11)	400.73	78.96	48.75
Total mean time in HFVP for Np=15, Ns=62(sec)			199.37 sec

Table 2: Duty Cycle (DC) and prolonged HFPV time for all three interfaces

1.16 Discussion

All the results obtained during this study were performed on healthy volunteers. As a result, the reduction of chest wall motion and prolonged HFPV times may not reflect that of a compromised patient.

We selected three different types of oral interfaces that have been previously used in patients to mobilize and clear their pulmonary secretions. An average of all HFPV sessions (N_s=62 from all N_v=15), from all three interfaces, showed that the volunteers could tolerate percussions for an approximate average of 3 minutes to a maximum of 17 minutes. These times are promising and allow us to further investigate HFPV as a tool for motion reduction in a typical 15-minute radiotherapy appointment.

The CO_2 levels for the first five volunteers were within normal ranges therefore, we believe that providing detailed training to subjects and team will play an important role in maintaining long, consistent and comfortable HFPV sessions. Particularly for individuals that have no prior experience with aided breathing.

Our first aim for this study was whether or not volunteers would be able to comply with the procedure and subsequently provide feedback with regards to

ease of use, comfort and geometric interference. As reported, all three interfaces were favorable for comfort with Phillips Respironics Oro-nasal interface means score higher than the other two. No volunteer indicated pain or panic during the procedure. Almost all volunteers reported on the comment section of each subjective survey, that Amici tru-Fit mouthpiece was the hardest to hold in place during percussive ventilation due to lack of strap. Majority of the volunteers commented that Respironics Oro-nasal rested well on their face and introduced less dry throat than Fischer Paykel Oracle 452. However, they indicated that they felt higher leakage for Respironics Oro-nasal than Fischer Paykel.

Motion reduction while in HFPV breathing compared to that of free breathing, is an important parameter of this study. Particularly, if such technique is implemented for use in pencil beam scanning radiotherapy of mobile targets, which may result in drastic heterogeneous dose distributions (Shirato H. e.) (Ionascu, 2007) (Bert C. a., 2008) (Jiang, 2006) etc. Although, during this part of our study we only recorded chest wall motion, we report statistically significant reduction in ripple magnitude. These results are promising and require further research. We noticed that most volunteers experienced a drift in motion amplitude of the chest wall. We believe that such drifts were caused due to the air leaks around the interface, in addition to the wave pulses losing pressure in the buccal space/oral cavity as opposed to directly going into the oropharynx for proper ventilation.

Duty cycle for respiratory gated radiotherapy is typically 30-50 % for 3DCRT treatments (Guang-wen, 2011), less than 30% for IMRT treatments (Jiang, 2006) and of course 100 % for non-gated treatments. The ability to deliver the dose quickly after image verification is critical. Murphy et al (Murphy M. J., 2004) estimated that if the imaging interval was approximately 2 minutes, then the percentage of dose that is misdirected by more than 1 mm was in the order of 11 %, whereas 2 % of the dose was misdirected by more than 1.5 mm and less than 1 % was off target by more than 2 mm. Furthermore, they noticed that if the imaging interval was reduced by 1 minute, then the mis-targeting was halved. High frequency percussive ventilation allows us to keep the duty cycle considerably higher than the current means for IMRT and pencil beam scanning proton radiotherapy. A median of 93 % duty cycle was observed for 5 mm threshold band and a median of 52 % for 2 mm. Since no smoothing filters were applied when collecting the Anzai data (raw data) and the system, like many, is known to have an inherent noise component (Heinz, 2015) (McNamara, 2008), we believe that the duty cycle for the 2 mm and 5 mm threshold band could be slightly higher than reported here. Example of the noise peaks are reported in (***Figure 0-14:***).

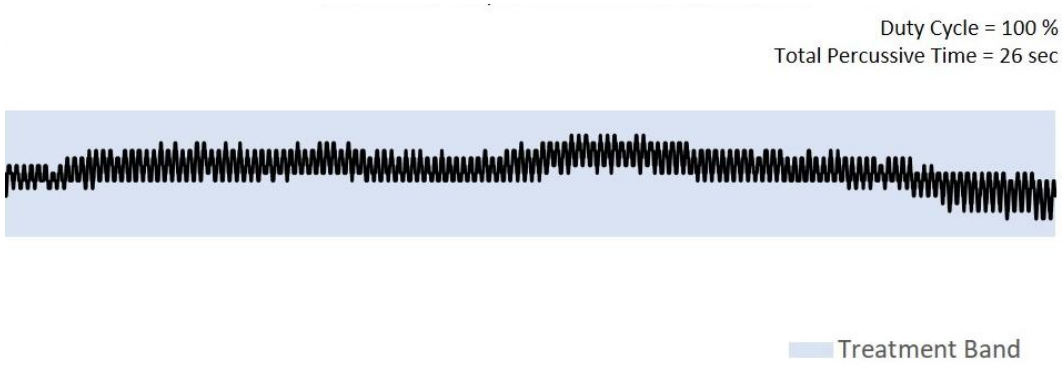

Figure 0-14: Sample signal of Amplitude drift & noise from Anzai laser

Additionally, it is believed that leakage around the interface allowed the volunteers to not be fully ventilated, resulting in the chest wall amplitude drifts noted above. Consequently, resulting in low duty cycle for both 2 mm and 5 mm threshold band.

Our last aim for this study was to examine the prolonged time under HFPV and whether one of the interfaces prolonged percussive time more than the other. Recalling that each volunteer underwent at least one percussive session [***Figure 0-7:***] per interface (number of sessions was left at the discretion of the volunteer), we recorded a total of Ns=33 (Nv=10), 11 sessions per interface that were greater than sixty seconds. Statistical differences were noted between the three interfaces ($p < 0.0001$). The mean prolonged time for Phillips Respironics oro-nasal was longer than the other two interfaces. We believe that this was due the straps around the neck/forehead and the ability of the interface to rest comfortably around the patients' oral space as indicated in the comment section of the subjective survey. However, it is important to note that the duty cycle for

the 5 mm threshold band was lower for Phillips Respironics than the other two interfaces. We believe that this was due to the indirect path of the percussive bursts, different from Fischer & Paykel Oracle 452. The Amici TruFit allowed for similar direct path; however, the lack of straps around the face made it difficult to keep the interface in place for long periods of time.

1.17 Conclusion

In this part of the study, we showed that the Fischer & Paykel Oracle 452 interface can prolong the percussive sessions when compared to the other two. Chest-wall motion was well tolerated and drastically reduced using HFPV in each volunteer evaluated. Average chest wall motion during free breathing and HFPV was measured at 8.14 mm and 2.52 mm respectively. Even though tumor motion may or may not correlate well with that of the chest wall, we expect that the reduction in motion, in addition to prolonged time under HFPV, may translate to tumor immobilization. As a result, we believe HFPV may provide thoracic immobilization during radiotherapy, particularly in the SBRT and scanning pencil beam proton therapy setting.

CHAPTER 4: DOSIMETRIC QUANTIFICATION OF INTERPLAY EFFECTS OF HFPV FOR PENCIL BEAM SCANNING PROTON AND GRADIENT EFFECTS FOR PHOTON RADIOTHERAPY: RETROSPECTIVE PHANTOM STUDY

1.18 Abstract

Purpose: High frequency percussive ventilation (HFPV) is an emerging technique to reduce respiratory motion. The purpose of this study is to evaluate

the interplay effects of free vs. HFPV breathing for pencil beam scanning proton radiotherapy as well as gradient effects for photon radiotherapy.

Methods: Healthy volunteers were previously recruited to undergo free and HFPV breathing while simultaneously measuring their chest wall respiratory motion from projecting a laser light on the patients' skin and measuring its displacement to the laser sensor. Ten respiratory wave forms obtained from the sensor were utilized to drive a dynamic thoracic phantom which held Gafchromic film at iso-center. Each film was irradiated with a proton pencil beam scanning plan of a known pattern while simultaneously moving with the pre-determined pattern. Same method was applied for photon films.

Results: Free vs. HFPV curves showed statistically significant differences in Gamma passing rates. Mean gamma passing rate was 77.03 % (SD: 4.11) and 99.20 % (SD: 0.55) for free- and HFPV breathing patterns respectively. The number of re-paintings necessary to achieve optimal interplay mitigation was drastically reduced from 10 to 1 for free vs. HFPV, respectively. HFPV resulted in consistent Gamma passing rates across several depths of a spread-out Bragg peak while free-breathing resulted in a significant decrease at the distal edge. Mean gamma rates for HFPV at 6, 9 and 12 cm depth were: 99.28, 98.24, 96.76% whereas for free-breathing 72.46, 71.58 and 54.21%.

Conclusion: Using HFPV as a thoracic immobilization technique may provide significant advantages in addressing motion mitigation of proton interplay effects as well as photon gradient effects.

Keywords: HFPV, motion reduction, interplay, respiratory motion, pencil beam scanning proton}

1.19 Introduction

Recent clinical trials in proton radiotherapy have led to promising results (Siegel, MillerKD, & Jemal, 2015), but motion management of mobile tumors remains a serious challenge (Allen A, et al., 2012) for both protons and photons.

Although, photon radiotherapy has been the standard of care for thoracic cancer for decades, the technological advances and clinical trials in proton radiotherapy have led to promising and effective results (Westover, et al., 2012). Data shows that proton radiotherapy can spare more healthy tissue, while maintaining a conformal dose distribution around the target, compared to photon radiotherapy (Chang, et al., 2016) (Gomez, et al., 2013) (Register, Zhang, Mohan, & Chang, 2011). The first proton facilities in the United States, utilized for clinical therapy, was in operation at Loma Linda University Center in California as well as Harvard University in Boston in the early 1950s. Since then, therapy proton treatment centers have increased to an astonishing 32 (PTCOG, 2019), with additional centers currently under construction.

Protons are considered to be heavy charged particles which result in minimal scatter, high cross sections and inversely proportional stopping power. The resulting effect is that they deposit low entry dose, higher energy at the end of their range, known as the Bragg peak, and essentially no dose beyond the peak. These properties result in extensive reduction of integral dose when compared to photon radiotherapy (Allen A, et al., 2012). The width of the Bragg peak is

often too narrow for most clinically observed targets in radiotherapy, as a result its modulation; also known as SOBP (spread out Bragg peak) is often necessary. Bragg peak modulation can be achieved by either switching beam energies or by introducing a modulator in the beam path. In either case, the weighted combination of all the peaks results in a flat dose distribution that is practical for uniformly treating deep seated targets (***Figure 0-5:***).

There are two main delivery techniques in proton radiotherapy: passive scattering proton therapy (PSPT) and pencil beam scanning (PBS). PSPT relies on primary and secondary scattering material in order to create a 3D conformal dose distribution in the target, whereas PBS utilizes a sub-centimeter pencil beam that is scanned across the target one spot at a time. Unlike PBS, PSPT technique is limited to a predesignated SOBP modulation, therefore not optimal for mobile targets. However, recent guidelines from PTCOG (Particle Therapy Co-Operative Group) suggest that PBS has resulted in clinically positive outcomes when treating thoracic tumors with minimal motion (Chang, et al., Consensus Guidelines for Implementing Pencil-Beam Scanning Proton Therapy for Thoracic Malignancies on Behalf of the PTCOG Thoracic and LYmphoma Subcommittee, 2017).

Despite the technological advancements which have substantially improved the beam delivery accuracy, mobility of the target and motion management remain an important variable that require attention. Target motion is often represented as two types: stochastic and systematic (Murphy M. J., 2004). Stochastic motion is random in both time and direction. Systematic motion can

consist of slow, quasi-static changes in position due to effects such as muscle fatigue as well as rapid, cyclic changes caused by respiration and heartbeat (Murphy M. J., 2004). These types of motions lead to target displacement in the thoracic region that can be as large as 2.47 cm during treatment (Seppenwoolde, et al., 2002) (Shimizu, et al., 2001). Such discrepancies in tumor motion have been widely discussed in the literature (Seco, Robertson, & Trofimov , 2009) (Torshabi, 2013) (Evans, Coolens, & Nioutsikou, Effects of averaging over motion and the resulting systematic errors in radiation therapy, 2006) (Harada, et al., 2016) (Jakobi, Perrin, Knopf, & Richter, 2018) (Liu, et al., 2007) (Mutaf, et al., 2011) (Hui, et al., 2008) (Zeng, et al., 2015) (Dasu, Flejmer, Edvardsson, & Nystrom, 2018), particularly when utilizing PSPT vs PBS (Langen & Zhu, 2018).

It is reported that 50 % of early-stage and 40 % of locally advanced non-small-cell lung carcinoma (NSCLC) move greater than 5 mm in the superior/inferior direction, respectively (Liu, et al., 2007) (yu, Lin, Balter, Zhang, & Dong , 2012), thus necessitating some form of motion management. National guidelines do not recommend treatment of tumors with motion greater than 5 mm (Keall, et al., 2006). Keall et al. (Keall, et al., 2006), recommends against focal treatment of tumors having greater than 5 mm of motion unless the radiation facility has no motion management techniques available or the patient is unable to tolerate them. The dosimetric impact of tumors whose motion is < 5 mm was demonstrated to be minimal by Li et al (Li X. e.), however for motion >5 mm, dose homogeneity and deterioration is significant, therefore, if motion

mitigation is not available, re-painting the tumor is recommended (Kang, et al., 2017).

Motion mitigation techniques for proton therapy have been extensively discussed by Chang et al. (Chang, et al., Consensus Guidelines for Implementing Pencil-Beam Scanning Proton Therapy for Thoracic Malignancies on Behalf of the PTCOG Thoracic and LYmphoma Subcommittee, 2017). Their recommendations include the following: motion analysis, 4D dose, robust optimization evaluation, re-scanning, breath hold, gating and tracking.

The first recommendation requires the analysis of target motion in all directions, proton beam path, patient anatomy, and the water equivalent thickness to select beam angles. This is accomplished by the use of iterative processes, while avoiding critical structures. The downside of this recommendation is that the greatest motion occurs in the superior to inferior direction (Sarudis, Karlsson-Hauer, Nyman, & Back, 2017). Therefore, orienting a beam in that direction would be challenging. Additionally, the challenges of mapping the correct density while the target is moving in and out of the field can be difficult to accomplish.

Second, 4D dose utilizes all 10 phases of a typical 4DCT scan to obtain an average dose of each individual phase without considering the time dependence of the fluence delivery. The disadvantage of this method lies in the uncertainties of 4DCT which can underestimate tumor volume (Shi, Chen, D'Souza, & Mistry, 2013) (Dou, et al., 2015).

Third, robust optimization evaluation is simply a method that allows the optimizer to create a worst-case scenario plan in the event of tumor motion for a target contoured using 3D or 4D CT. Although, such feature is used in some clinics, its downside is the decrease of motion sensitivity and certainly may not accurately predict tumor motion during treatment (Chang, et al., Consensus Guidelines for Implementing Pencil-Beam Scanning Proton Therapy for Thoracic Malignancies on Behalf of the PTCOG Thoracic and LYmphoma Subcommittee, 2017).

Fourth, re-scanning is a widely used method to mitigate motion interplay. This method allows for the dose to be delivered in several "layers" within a single daily fraction. It smears the dose by allowing the pencil beam to scan across the target several times, therefore potentially catching a different phase of the motion. The downside of this method is the time it takes to switch between layers, therefore re-scanning is not recommended for proton units with slow energy switching and has shown to be more sensitive to the starting phase (Bernatowicz, Lomax, & Knopf, 2013).

Lastly, PTCOG recommends the use of breath hold, gating and tracking as means to mitigate motion. Breath hold relies on the patients' ability to take the same volume of air and hold their breath longer than 10 to 20 seconds. This is often not reliable and only limited to patients who are physiological capable of breath holds. Gating treatments rely on the beam to turn on/off during a preset phase (or amplitude). The downside of this method is its low duty cycle and the accuracy of the predictive filters. Tracking uses either fiducial markers or skin

surface to track the tumor, however it can be invasive to the patient and superficial tracking may or may not correlate well with the tumor itself (Seppenwoolde, et al., 2002) (Ionascu, 2007).

One technique that has gained less attention as a tool for tumor motion immobilization is HFPV. HFPV continues to be widely used in mobilization and clearance of the pulmonary secretions for patients with acute chronic pulmonary disease (Allan, Osborn, Chung, & Wanek, 2010) (Salim & Martin, 2005). It provides high frequency bursts of oxygen into the patient's trachea, while allowing for CO_2 to escape through the same interface. The device is an adaptation of a pneumatic high frequency ventilator in which high flow jets of gas are delivered to the airways by a flow interrupter called a Phasitron. Activation of the venturi system within the Phasitron creates bursts of gas at frequencies of 100 to 400 bursts/minute within a tightly controlled ratio of gas delivery and passive exhalation. HFPV improves oxygenation versus conventional ventilation, with no barotrauma, in patients with acute respiratory distress syndrome (Gallagher, 1989) (Spapen, 2014). Such technique was recently used in imaging by (Peguret N. a.-d., 2016) and in radiotherapy by (Prior J. a., 2016).

On an IRB approved study (IRB# 2017-046), our institution recently recruited healthy volunteers who underwent HFPV (Sala I. , Maurer, Myziuk, Stevens, & Guerrero, 2018). The primary purpose of this follow up IRB approved study: is to investigate the relative interplay effects and the dosimetric impact of free vs. HFPV motion for PBS and photon radiotherapy. For PBS we aim to investigate:

the Gamma index Γ, mitigation of interplay effects by the use of re-painting, and the dosimetric consistency across the SOBP for free vs. HFPV breathing curves. For photon we aim to investigate: The gradient effects for free vs. HFPV breathing patterns by analyzing gamma Γ index and hot/cold spots for HFPV and free breathing patterns relative to and static.

1.20 Methods and Materials

1.20.1 Proton

Chest wall breathing curves from ten volunteers, who previously underwent free and HFPV (Sala I. , Maurer, Myziuk, Stevens, & Guerrero, 2018), were imported into our dynamic thorax motion management software (CIRS, Inc Norfolk, Virginia). A typical signal imported in the phantom's software is shown in (***Figure 0-1:***)

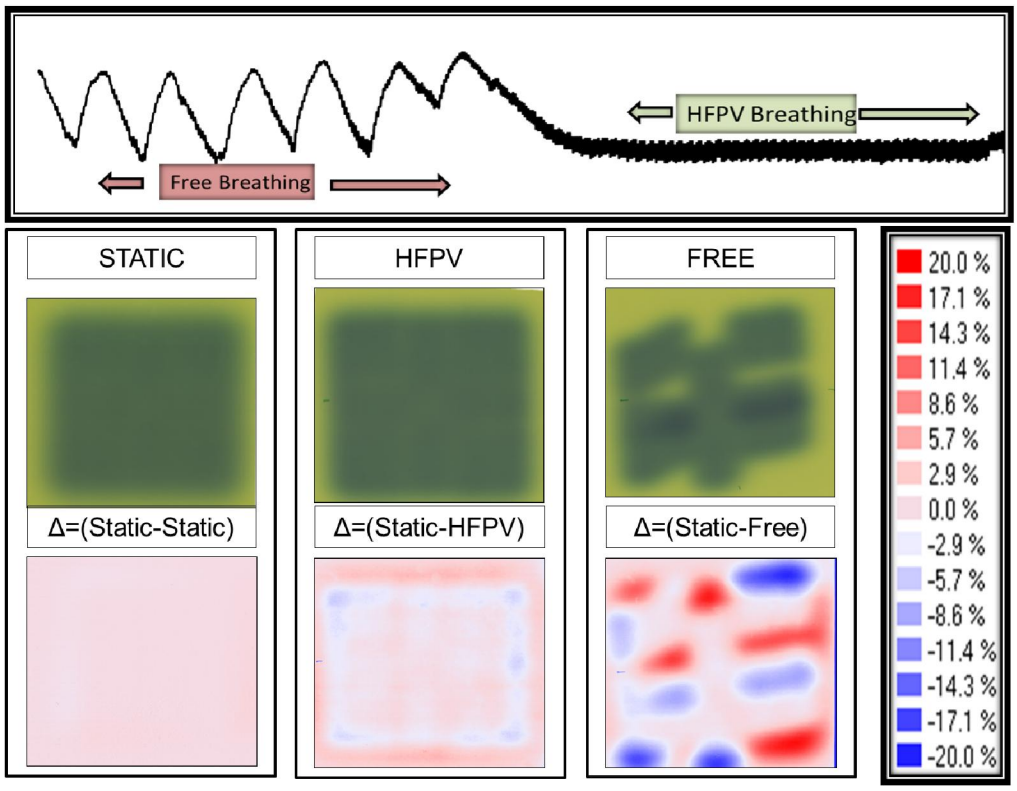

Figure 0-1: A typical chest wall motion signal recorded from volunteer A. First row represents the Gafchromic films at static, HFPV and free breathing patterns for volunteer A acquired at a random location in the free and HFPV curve. The second row represent a differential dose map

The dynamic thorax phantom is comprised of the main body phantom, a surrogate motion platform and a lung equivalent rod with interchangeable targets (***Figure 0-2:***). Both, the rod and the surrogate motion platform, are connected to an actuator. The surrogate motion platform is designed to simulate chest wall or diaphragmatic motion, whereas the rod (with target) is designed to simulate target motion. Both are controlled by the CIRS software. The main body of the phantom has similar densities to tissue and lung. The rod with replaceable target sizes is located in the right lung. For the purpose of this study, all twenty of our motion curves were imported into the surrogate platform, whereas the rest of the motion axis from the rod/target were set to zero.

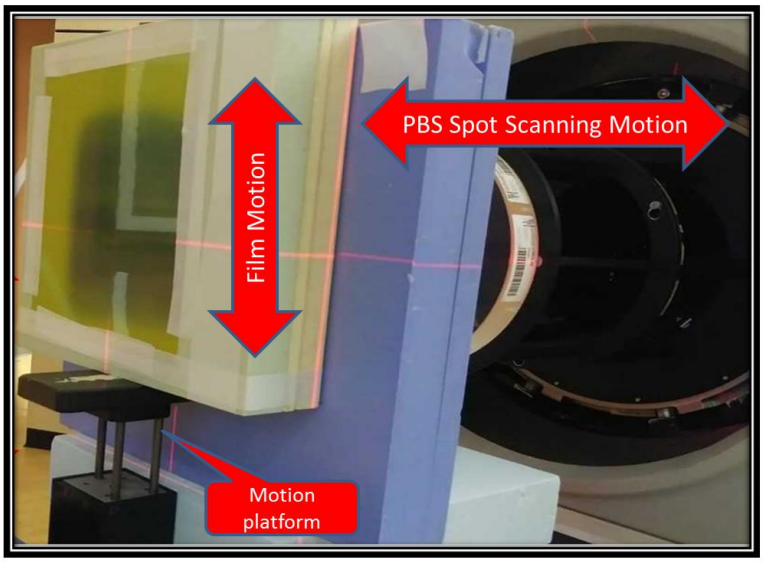

Figure 0-2: CIRS thorax motion phantom Model: 008A

To ensure the accuracy of the actuator motors, quality assurance of the thoracic phantom was performed prior to the initiation of this study. Two motion curves were generated, the first curve was Cos(x^4) and the second was Sin(x). Motion amplitude was verified in mm increments from 1 to 25 mm (peak-to-peak =50 mm). The physical motion of the rod and the surrogate platform were measured with a calibrated ruler.

Gafchromic EBT3 film was used for each objective. Gafchromic is designed to measure absorbed dose of ionizing radiation. The active layer of the film is sandwiched in between two of the polyester base surfaces. The dynamic range of the film used was 0.1 to 20 Gy with its optimal being 0.2 Gy to 10 Gy. EPSON Expression 10000XL flatbed color scanner was utilized to scan each film. To reduce inconsistencies in lateral scan artifacts (Schoenfeldt, Poppinga, Harder, Doerner, & PoppeB, 2014) due to Beer-Lambert Law, each (8"x10") film was placed in the same location on the flatbed scanner. All films were analyzed with

the steepest saturation color for the dose delivered using FilmQA-Pro software (Bridgewater, NJ).

IBA Proton Accelerator at Northwestern Medicine Proton Center (IBA, Inc Louvain-La-Neuve Country Belgium), in Warrenville, Illinois was used to irradiate all of the films in this study.

For the first aim, we placed Gafchromic film parallel to the surrogate platform and perpendicular to the pencil beam scanning proton therapy beam. A single energy (159MeV) Bragg peak plan was generated in RaySearch (RaySearch Laboratories, Inc. Stockholm, Sweden) with and without a 4 cm range shifter. Distinct PTV's were created in the plan as indicated in the beams eye view (BEV) in ***Figure 0-3:***. A total dose of 300 cGy was prescribed. The free and HFPV breathing curve for volunteer B was irradiated five times. Furthermore, ten of the breathing curves (free and HFPV) were irradiated once without shifter, and five of them (free and HFVP) were irradiated with shifter in place. Gamma analysis was calculated using Eq. (**8**) with a 3%/3 mm and 10 % threshold (TH) criteria (Low, Harms, Sasa, & Purdy, 1998), where DD is dose difference (%), DTA is the distance to agreement (mm), Tol is the dose threshold (%) and d is the distance to threshold (mm). Additionally, maximum and minimum intensities relative to the reference image were recorded using Eq (**9**) to identify hot and cold spots within the defined ROI (region of interest), where Dr is the reference dose from static film and Dc is the client dose from either free or HFPV film, depending on film evaluated.

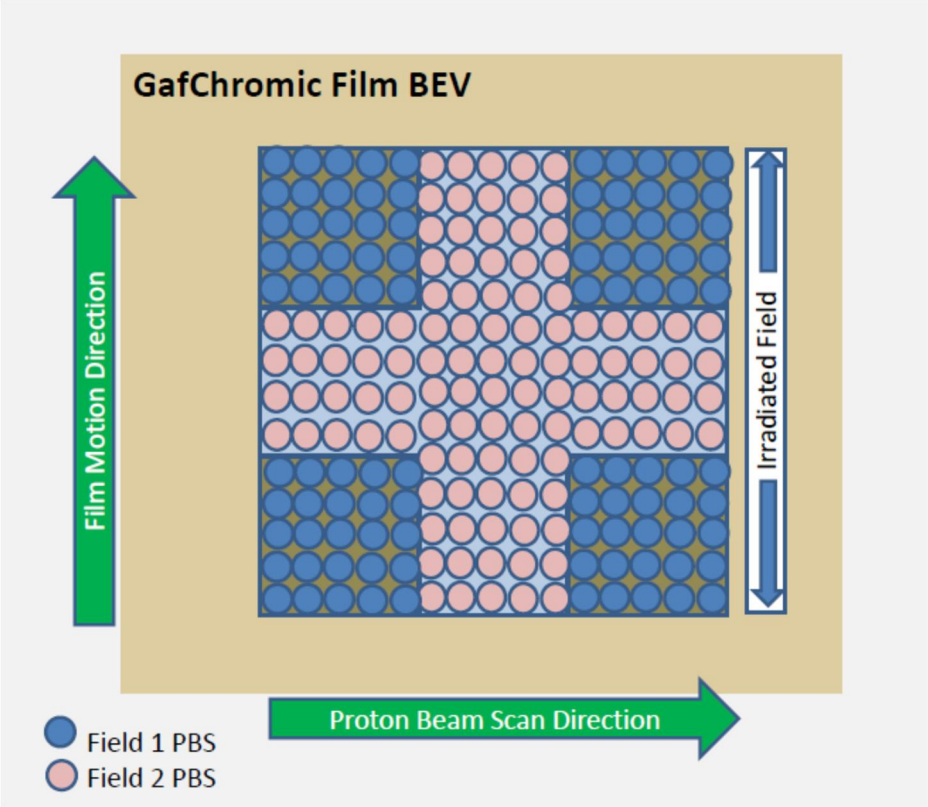

Figure 0-3: Example of plan created in RaySearch. Light beige background represents Gafchromic film. Solid green and striped pink represent PTV 1 and 2. Each grey circle represents a pencil beam of equal MU. Not to scale

$$\Gamma = \sqrt{\frac{DD^2}{Tol^2} + \frac{DTA^2}{d^2}} \quad \textbf{(8)}$$

$$\Delta = (D_r - D_c) \quad \textbf{(9)}$$

$$\%Error = \sqrt{(DD^2} + DTA^2 * Tol/d \quad \textbf{(10)}$$

Regarding the re-painting aim, we utilized the free and HFPV breathing curve from volunteer B. The same single energy Bragg peak plan from the previous aim with a 4 cm range shifter in place was used with the film positioned at iso-center. A dose of 300 cGy was delivered in 1, 2, 5, 7, 10, 20 and 50 re-

paintings. Relative % error, of the same ROI, was recorded for each film using Eq. (**10**) with 3%\3 mm and TH=10 criteria.

$$F = \frac{D_{max} - D_{min}}{D_{max} + D_{min}} \quad \textbf{(11)}$$

$$S = \frac{D_{left} - D_{right}}{D_{left} + D_{right}} \quad \textbf{(12)}$$

To further evaluate the effects of motion interplay, we calculated flatness and symmetry for all films irradiated above (with and without 4 cm shifter). Both flatness and symmetry were calculated using Eq. (**11**) and (**12**) as defined in TG Report 47 of AAPM were Dmax is the maximum dose, Dmin is the minimum dose, Dleft is the left side dose and Dright is the right side dose.

Lastly, we explored consistency of Γ passing rates for a spread-out Bragg peak for five free and five HFPV breathing curves relative to static ***Figure 0-4***. Three pieces of (8"x10") Gafchromic films were placed at the approximate distal (12 cm), mid (9 cm) and proximal (6 cm) depths of the SOBP (***Figure 0-5:***). All three films were placed on the surrogate platform moving with the same phase and analyzed with Γ criteria of 3%/3 mm and TH=10 utilizing the same pattern indicated in ***Figure 0-3:***.

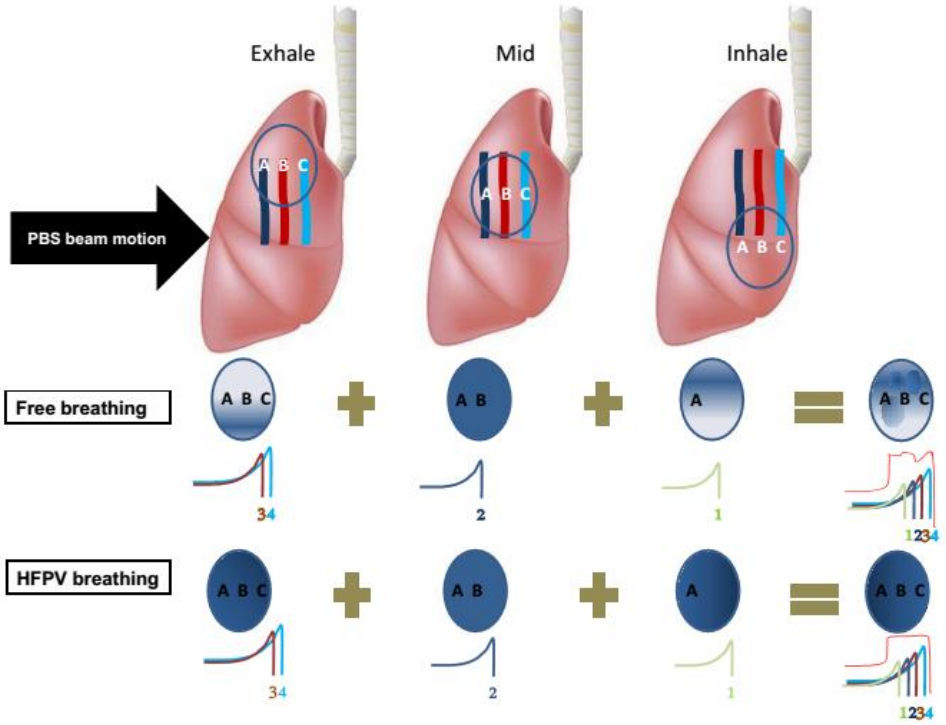

Figure 0-4: Heterogeneity consistency across SOBP. A, B, and C indicating 6, 9, and 12 cm depth of film placement.

Statistical analysis was performed for each aim. All analyses performed utilized a one sample t-Test

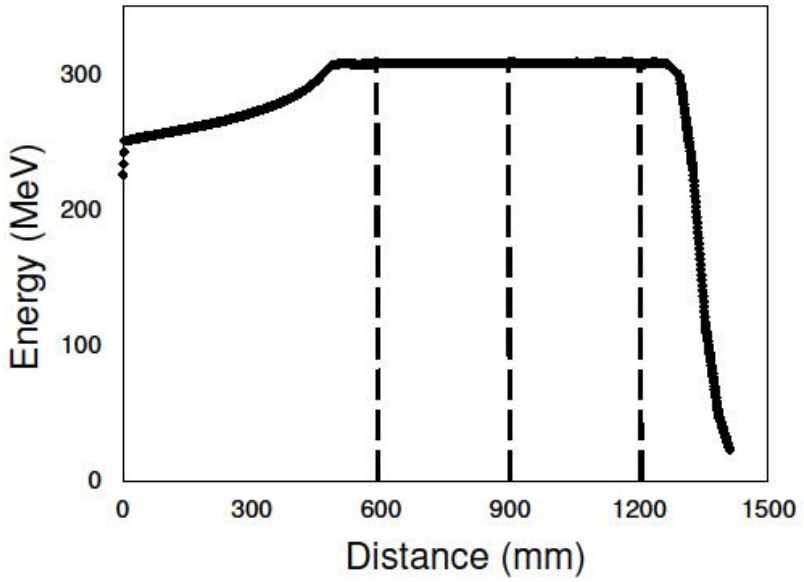

Figure 0-5: SOBP and the respective film placement at 6 cm, 9 cm and 12 cm

1.20.2 Photon

Five free and HFPV chest wall breathing curves of volunteers that previously underwent HFPV were utilized to drive the thoracic motion phantom that held high resolution GafChromic EBT3 film. Simultaneously, a predetermined static MLC (multi leaf collimator) defined photon (6MV) field was chosen to irradiate each film with a dose of 300 cGy. All films were placed on the motion platform at 100 cm SSD with 2 cm buildup. The mean peak-to-peak amplitude of the free and HFPV breathing curves were 19.20 mm (SD: 3.33) and 2.33 mm (SD: 0.82), respectively. We evaluated the dosimetric effects of

free and HFPV relative to static by measuring the Gamma Index, as defined by Low et al, with 3%/2 mm and 10 % threshold criteria. Furthermore, hot and cold spots, relative to static, for a set ROI (region of interest), were evaluated for each film.

1.21 Results

1.21.1 Proton

The motion accuracy of the surrogate platform was verified to be within the reported values of +/-0.1 mm from the vendor with R^2=0.9996 for the Cos(x^4) Eq. (**13**) wave and R^2=1.0000 for the Sin(x) wave Eq. (**14**).

$$y = 1.0018x - 0.007 \; and \; R^2 = 0.9999 \quad \textbf{(13)}$$

$$y = 0.9996x - 0.002 \; and \; R^2 = 1.0000 \quad \textbf{(14)}$$

The mean motion (peak-to-peak) of breathing curves imported into CIRS software was 17.12 mm (SD=4.38) and 2.31 mm (SD=1.10) for free and HFPV, respectively. For the ten films irradiated without the shifter, the mean Gamma passing rate for 3%/3 mm and TH=10 criteria was 77.03 % (SD=4.11, lower 95% CI of mean=74.09 %, upper 95 % CI of mean=79.98 % and median=78.21 %) and 99.20 % (SD=0.55, lower 95 % CI of mean=98.81 %, upper 95 % CI of mean=99.60 % and median=99.15 %) for free and HFPV respectively ***Figure 0-6***. The mean hot spot was +29.67 % and +9.33 % for free and HFPV, respectively. Likewise, the mean cold spot was -17.67 % and -1.66 % for free and HFPV, respectively ***Figure 0-7***.

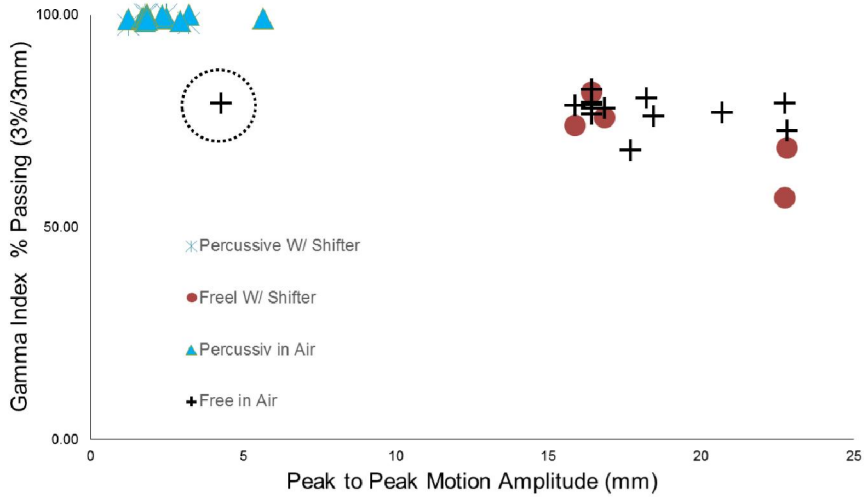

Figure 0-6: Peak-to-peak phantom motion versus Gamma passing at 3%/3 mm. Dash circle represents an outlier discussed further

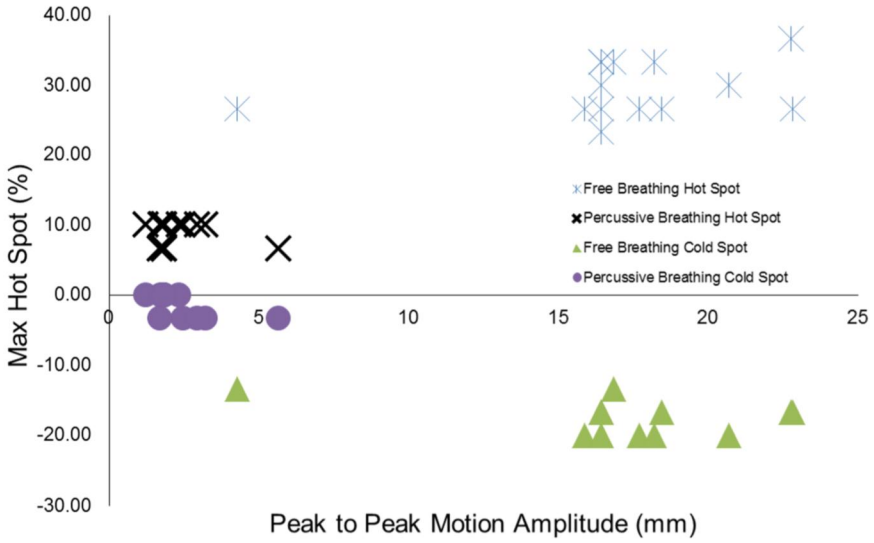

Figure 0-7: Peak-to-peak phantom motion (mm) versus (%) hot and cold spots for free and HFPV breathing

For the five films irradiated with the 4 cm range shifter, mean Gamma passing rate for 3%/3 mm and TH=10 criteria was 71.27 % (SD=9.35, lower 95

% CI of mean=59.66 %, upper 95 % CI of mean=82.88 % and median=73.72 %) and 99.10 % (SD=1.21, lower 95 % CI of mean=97.59 %, upper 95 % CI of mean=100.00% and median=99.94 %) for free and HFPV, respectively (***Figure 0-6:***). The mean hot spot was +24.00 % vs +7.34 % for free and HFPV, respectively; whereas, the mean cold spot was -20.26 % and -4.65 %. All statistically significant ($p < 0.0001$) from set mean of 5 %. Gamma passing rate was statistically significant from tested mean of 95% ($p < 0.00476$ for free and $p < 0.00163$ for HFPV).

Furthermore, the mean Gamma passing rate for 3%/3 mm and TH=10 criteria for volunteer B was 78.92 % (SD=2.12, lower 95 % CI of mean=76.29 %, upper 95% CI of mean=81.54 % and median=78.68 %) and 99.61% (SD=0.51, lower 95% CI of mean=98.97 %, upper 95% CI of mean=100.00 % and median=99.90 %) for free and HFPV, respectively. For the same data set, the mean hot spot was +29.33 % and +8.67 % for free and HFPV; whereas, the mean cold spot was -18.00 % and -0.00 % for free and HFPV, respectively. A one sample t-Test was performed showing statistical significance (< 0.007 and $p < 0.045$) for both free and HFPV, respectively. The peak-to-peak amplitude for volunteer B was 16.42 mm and 1.84 mm for free and HFPV, respectively.

The number of re-paintings to maintain a relatively consistent relative error (Eq. **10**) for free curve was 10, whereas for the HFPV curve was 1. ***Figure 0-8*** shows the number of paintings versus the mean relative error.

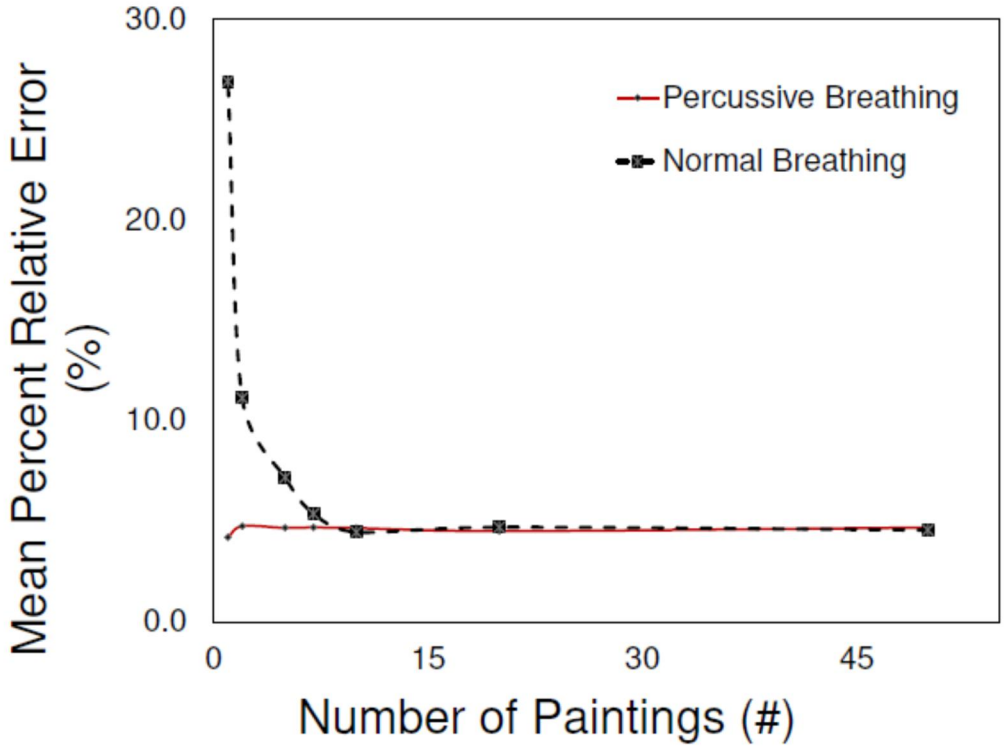

Figure 0-8: Number of re-paintings for free and HFPV vs. relative error (%)

For our next aim we investigated the effects that motion interplay has on flatness and symmetry. ***Table 3*** shows a distribution of flatness and symmetry for data measured with and without the 4 cm shifter. A one sample t-Test resulted in no significant difference from the test mean (5 %) for both static and HFPV. While showing great statistical significance for free breathing curve.

	Technique	**Flatness (Ave %)**	**Symmetry (Ave %)**
W/ Shifter	Static	5.76	2.66
	Percussive	3.78	1.40
	Free	32.46	20.62

	Static	6.97	1.78
In-Air	Percussive	5.89	2.10
	Free	31.50	13.00

Table 3: Flatness and Symmetry for In-Air and Range Shifter

Lastly, we investigated whether motion causes unintended dose distributions for proximal, mid and distal portion of a potential target when treated with a spread-out Bragg peak, because the most distal end of a target would only “see” the first peak (identified as 4 in ***Figure 0-9***), however the proximal end would “see” all. The dose distribution can therefore be distorted when the target is mobile.

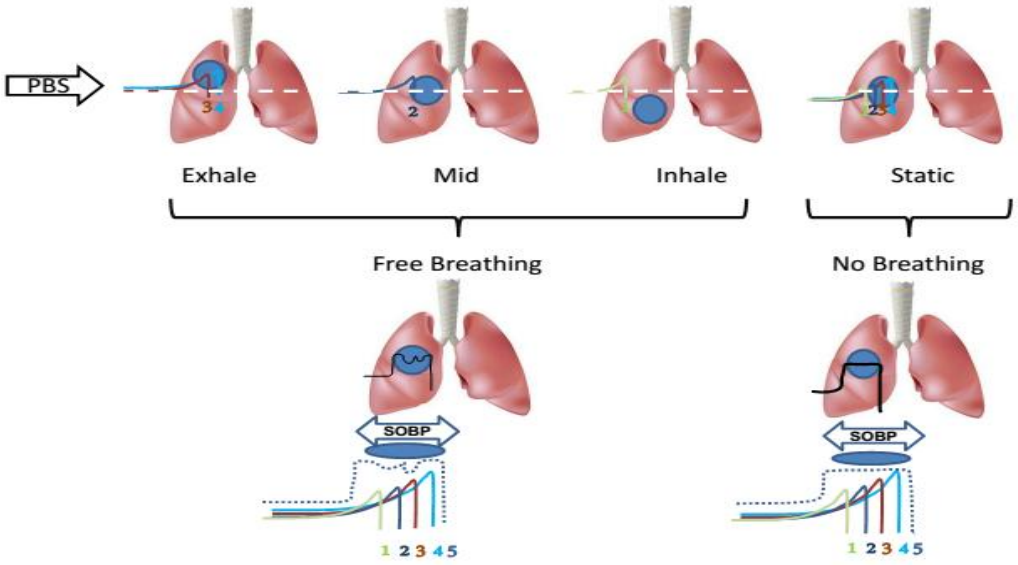

Figure 0-9: SOBP Consistency

Γ passing rates with criteria 3%/3 mm, 2%/3mm, 1%/1mm and TH=10 were used to analyze each film for HFPV, free and static. These results are represented in ***Figure 0-10*** and ***Table 4***.

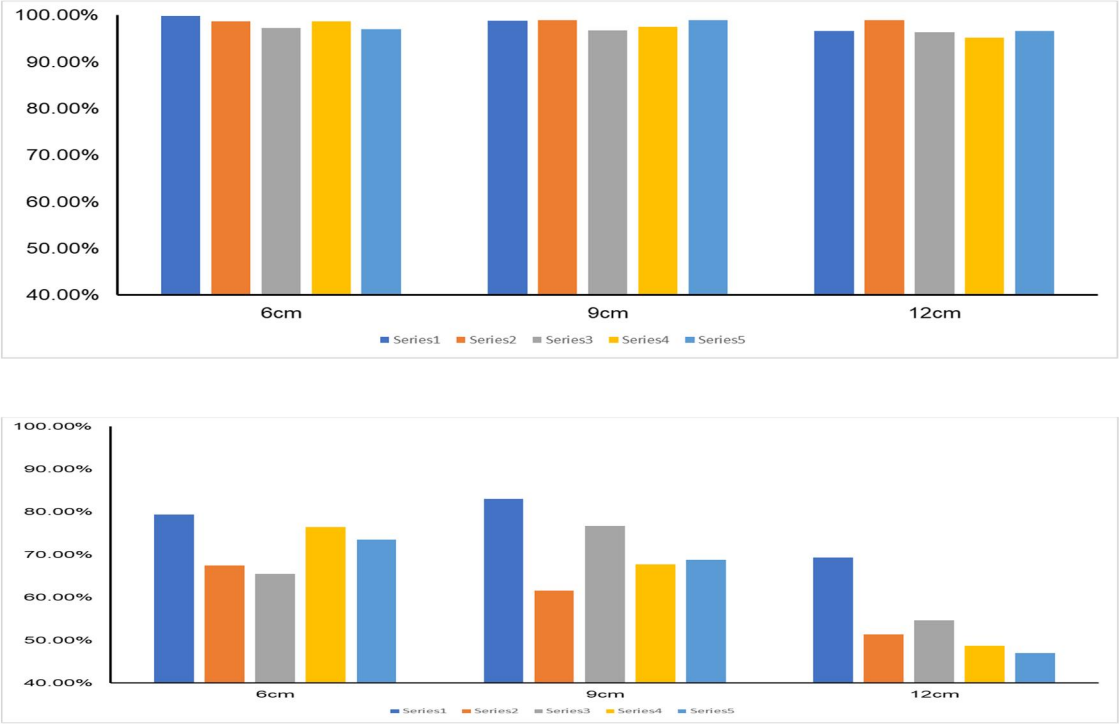

Figure 0-10: Gamma passing rate for all films relative to their respective static films. a) HFPV breathing b) Free Breathing

HFPV Depths 3%/3mm	1	2	3	4	5	Average	SD
6cm	99.9%	98.7%	97.2%	98.7%	97.0%	98.3%	1.2%
9cm	98.9%	99.0%	96.7%	97.6%	99.0%	98.2%	1.0%
12cm	96.7%	99.0%	96.3%	95.2%	96.7%	96.8%	1.4%

Free Depths 3%/3mm	1	2	3	4	5	Average	SD
6cm	79.4%	67.4%	65.5%	76.4%	73.6%	72.5%	5.9%
9cm	83.0%	61.6%	76.8%	67.7%	68.8%	71.6%	8.4%
12cm	69.4%	51.4%	54.6%	48.7%	47.0%	54.2%	8.9%

HFPV Depths 2%/2mm	1	2	3	4	5	Average	SD
6cm	96.4%	97.2%	95.1%	96.2%	96.12%	96.2%	0.7%
9cm	96.2%	96.1%	95.6%	96.1%	95.1%	95.8%	0.5%
12cm	94.2%	96.2%	94.1%	94.4%	94.2%	94.6%	0.9%

Free Depths 2%/2mm	1	2	3	4	5	Average	SD
6cm	70.2%	66.1%	60.0%	72.1%	69.2%	67.5%	4.7%
9cm	78.0%	58.2%	71.2%	62.1%	64.1%	66.7%	7.9%
12cm	60.1%	48.2%	50.0%	44.2%	43.3%	49.2%	6.7%

HFPV Depths 1%/1mm	1	2	3	4	5	Average	SD
6cm	92.2%	92.1%	90.0%	90.2%	91.0%	91.1%	1.0%
9cm	90.1%	90.0%	91.0%	90.4%	90.6%	90.4%	0.4%
12cm	91.0%	91.1%	90.1%	90.1%	89.2%	90.3%	0.8%

Free Depths 1%/1mm	1	2	3	4	5	Average	SD
6cm	66.1%	60.0%	59.2%	67.2%	61.1%	62.7%	3.7%
9cm	70.0%	50.0%	64.6%	57.2%	60.2%	60.4%	7.6%
12cm	54.0%	41.4%	46.7%	40.4%	38.4%	44.2%	6.3%

Table 4: Gamma passing rates for SOBP heterogeneity 3%/3mm, 2%/2mm and 1%/1mm

1.21.2 Photon

All films were scanned using EPSON 1000CL scanner and analyzed with FilmQA Pro (Ashland Inc, Bridgewater, NJ) film software. The average Gamma Index for free breathing vs. HFPV was 79.29 % (SD: 4.65) and 99.70 % (SD:0.35) respectively ***Figure 0-11*** . The median cold spots for HFPV was -2.86 % and -20.00 % for free breathing. Similarly, the median hot spots for HFPV was 17.14 % and 5.71 % for free breathing.

Patient	Free Breathing Gamma Index (%)	HFPV Gamma Index (%)
A	74.30	99.98
B	82.17	99.33
C	84.70	99.30
D	84.60	99.90
E	80.66	99.98
Average	**79.29**	**99.70**
SD	**4.65**	**0.35**

Figure 0-11: Gamma Passing Rates for Photon Gradient Effects

	Hot Spot		Cold Spot	
	Normal	HFVP	Normal	HFPV
Median (%)	+17.14	+5.71	-20.00	-2.86
Range (%)	17.14 - 20.00	5.71 - 8.57	19.61 - 20.00	2.81 - 5.71

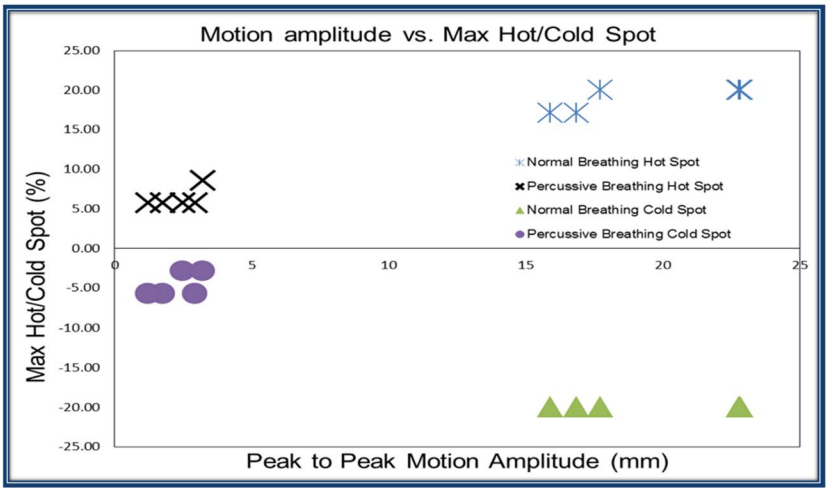

Figure 0-12: Hot and Cold Spots for Photon Beam Gradient Effects

A typical gradient effect of the relative dose difference on the GAFChromic film is denoted in **Figure 0-13**.

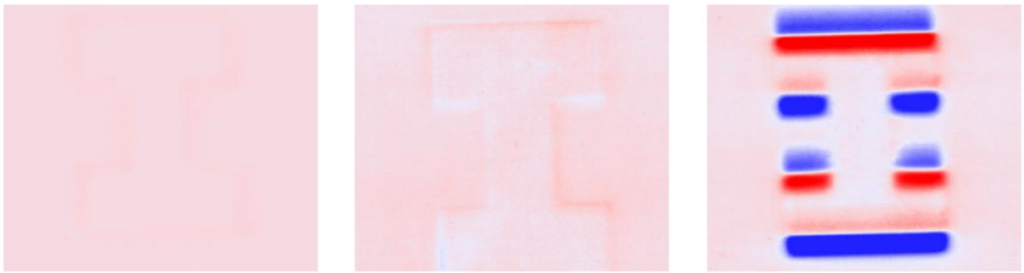

Figure 0-13: Typical Gradient Effect for GAFChromic photon test

1.22 Discussion

1.22.1 Proton

The results found in this study validate the importance of motion management in radiotherapy, particularly for PBS radiotherapy. HFPV provides significant dosimetric advantages relative to free breathing. This is well supported by ***Figure 0-1:***, which shows static, HFPV and free breathing for two randomly selected curves.

EBT Gafchromic film was selected for this study due to its high spatial resolution of < 25μm. Reference dosimetry performed by (Girard, Hugo, & LacroixF, 2012) has shown considerable errors in film response of the active layer due to the influence of humidity, temperature, and non-catalytic development which can introduce error response as high as 2 % (1-sigma) (Girard, Hugo, & LacroixF, 2012). Therefore, in this study, we ensured that all films were kept in the same environment. Additionally, EBT film has shown to under respond in the presence of proton spread out Bragg Peak (Fiorini, et al., 2014) and discrepancies (up to 10 %) in dose have been reported at depth due to the uncertainties of the processor (yeo, Teran, Ghebremedhin, Johnson, & Patyal, 2015), thus all films processed in this study were placed in the same location on the EPSON scanner.

While not investigated in this study, the direction of motion parallel to the pencil beam scanning may yield different results (Dowdell, Grassberger, Sharp, & Paganetti, 2013) (Lambert, Suchowerska, McKenzie, & Jackson, 2005). Additionally, it is assumed that the chest wall motion curves obtained from each volunteer are similar to that of a typical thoracic tumor.

It was observed that the phase and amplitude for free and HFPV breathing curves differed widely among all volunteers. Although we elected to irradiate one film per respiratory curve, at a random phase, it is important to note that other respiratory phase locations may yield different results. Such dosimetric variability could be even more significant for large breathing amplitudes. To estimate the dosimetric outcome of dose delivery at a random respiratory phase, we irradiated the free and HFPV breathing curves of volunteer B five times. The free breathing curves resulted in a broader range (SD=2.12) that trended toward statistical significance, contrary to the narrow range of HFPV (SD=0.51). This result is particularly important for proton stereotactic body radiotherapy (SBRT) where the number of fractions delivered is limited (often < 5), potentially resulting in drastic under- or over-dosage. On the other hand, PBS with HFPV resulted in high conformity and appears to be unaffected by the difference in intra-fractional starting phase variably. Therefore, HFPV does not appear to possess limitations that other motion mitigation techniques exhibit.

Furthermore, we explored if HFPV motion mitigation technique would result in higher Gamma passing rates and under- or over-dosage. It is evident that HFPV results in significantly lower percent differences when compared to static (***Figure 0-6:***). Similarly, the large range of Gamma and hot/cold spots for the same free breathing curve is significant and further reinforces the need for motion management. We do believe that motion reduction by HFPV can provide satisfactory tumor motion control without requiring any other mitigation strategies or algorithms previously mentioned by Chang et al. (Chang, et al.,

Consensus Guidelines for Implementing Pencil-Beam Scanning Proton Therapy for Thoracic Malignancies on Behalf of the PTCOG Thoracic and LYmphoma Subcommittee, 2017). One breathing curve circled in ***Figure 0-7*** was an outlier. This particular volunteer was a non-diaphragmatic breather resulting in almost the same peak-to-peak chest wall motion for both free and HFPV.

Additionally, several studies have been performed on the effects of spot size broadening due to the use of range shifters (Shen, et al., 2015) and in this study we explored the Gamma passing rate for free vs. HFPV curves with and without a 4 cm range shifter. Although, the broadening of dose smearing was more evident for the free breathing curves, no statistical difference was observed.

Re-painting has been extensively discussed in literature as a technique to mitigate motion artifacts, although a single Bragg peak was used, our data is consistent with (Seco, Robertson, & Trofimov , 2009). The suggested number of re-paintings per field to obtain a relative error below 5 % is 10 and 1 for free and HFPV, respectively. The minimum relative error for free breathing was 4.46 % and 4.21 % for HFPV. We attribute this to the energy dependence of the film (<5 %), its sensitivity (< 5%), uniformity (< 3 %) and EPSON scanner. Nonetheless, the drastic reduction in repainting from free breathing to HFPV is significant and enforces the positive impact of HFPV.

For our last aim, we explored the consistency of Gamma index for three films placed at three different depths of the SOBP (***Figure 0-5:***). We elected to have all of them move with the same phase in order to eliminate any errors that could have been introduced from the phase differences (Bernatowicz, Lomax, &

Knopf, 2013). It is evident from the results that the Gamma passing rates for the proximal, mid and distal end of a typical target can be different depending on the motion amplitude, however HFPV resulted in uniform Gamma, different from free breathing (***Table 4***) and (***Figure 0-10***). This can be explained from the way each Bragg peak is delivered. The distal end of a typical moving target can potentially only "see" one peak whereas the proximal end will "see" all of them ***Figure 0-9***.

We previously noted that approximately 50% of the early stage tumors move > 0.5 cm and about 40% for locally advanced NSCLC required some type of motion mitigation technique. However, those techniques had significant limitations and uncertainties that may not apply to some patients, therefore we believe that HFPV can be superior in consistently addressing all tumor stages and motion amplitudes.

1.22.2 Photon

As previously noted, photon beams are not delivered with a pencil beam technique like proton therapy, therefore the outcome of gradient and interplay effects can be different. In this study we only measured the gradient effects (MLC Static) and as anticipated the edges of the field are drastically either over- or under-dosed, therefore motion mitigation is greatly recommended and the application of large enough margins, that would encompass the entire trajectory of a target, is necessary. HFPV can drastically reduce motion and consequently have acceptable Gamma passing rates for photon radiotherapy.

1.23 Conclusion

High frequency percussive ventilation can result in significant dosimetric advantages for PBS radiotherapy. It drastically mitigates the interplay effects and significantly lowers the hot/cold spots relative to free breathing. Additionally, it allows for highly homogeneous and consistent dose distribution across several depths. HFPV may be able to address and treat all motion amplitudes and potentially lead to revenue increase while consistently maintaining high target conformity and OAR sparing.

CHAPTER 5: DETERMINATION OF DIRECT TUMOR AND DIAPHRAGM MOTION WITH HFPV: PROSPECTIVE STUDY

1.24 Determination of Direct Tumor Motion using Fluoroscopy

1.24.1 Abstract

Purpose: The purpose of this prospective study is to investigate HFPV as a respiratory motion technique to directly immobilize thoracic tumors.

Methods: A total of 105 lung patients with conspicuous tumor were prospectively screened to enroll in an IRB approved study. Only 27 had tumors that moved greater than 10 mm as part of the inclusion criteria for the study. Seventeen of them declined participation and 9 were excluded due to their age and COPD FEV1 scores < 50% as indicated in the exclusion criteria of the protocol. Only one patient accepted and underwent fluoroscopy imaging while in free and HFPV breathing. Patient was setup supine with arms above her head in the treatment couch of the Elekta (Elekta, Stockholm, Sweden) Linear Accelerator. The kV arms of the Linear Accelerators were used to obtain 1D

images every 5.5 seconds. A total of 147 1D frames in the AP direction were obtained during HFPV breathing mode and 92 in free breathing. Each frame was acquired continuously with gantry at 270 degrees and kV=120, mA=25, ms=40 and SFOV (Small Field of View). The size of the images was 512x512x16bit with a Horizontal and Vertical resolution of 0.518 mm/pixel. Two different points within the tumor were traced along each fluoroscopy frame for both free and HFPV breathing.

Results: Patient tolerated the procedure well. She had previous COPD history, therefore total peak pressure applied was 12cmH2O. The mean peak-to-peak motion of the tumor during free breathing was 6.20 cm, lower than that recorded during 4DCT, while peak-to-peak motion of the tumor during HFPV was 2.675 cm, resulting in 57% reduction of motion.

Conclusions: This is the first study to ever report direct tumor motion with HFPV. It is evident that despite the lower peak pressure that the patient tolerated, motion was significantly reduced, making HFPV a viable technique for respiratory motion.

1.24.2 Introduction

High frequency percussive ventilation (HFPV) is a novel immobilization technique that has gained little attention in radiotherapy. It utilizes high frequency low tidal volume ventilation to produce endotracheal percussion (Salim A. a., 2005) (Allan, Osborn, Chung, & Wanek, 2010). It deliverers 100 to 400 bursts of oxygen per minute into the patients' trachea while simultaneously

allowing for passive O_2/CO_2 exchange. HFPV improves oxygenation versus conventional ventilation, with no barotrauma, in patients with acute respiratory distress syndrome (Spapen, 2014) (Gallagher, 1989).

Previously, in an IRB approved study (IRB# 2017-046), we evaluated HFPV for chest wall motion immobilization (Sala I. , Maurer, Nair, & Guerrero, 2019). We found volunteers tolerated the HFPV for varying lengths of time – from a few to tens of minutes. In that study, we reported significant reduction in chest wall motion after initiation of percussive ventilation (mean: > 60%) as well as high duty cycle (mean: > 80%).

Recently, high frequency percussive ventilation (HFPV) was reported for immobilization of thoracic tumors for imaging (Prior J. e., 2016) and stereotactic body radiotherapy (SBRT) (Peguret N. e., 2016). In Peguret's SBRT study, thoracic tumor respiratory motion was inferred from changes in the chest diameter measured by an Anzai respiratory belt (ANZAI Medical Co, Tokyo, Japan). There were patients who could not tolerate percussive ventilation assisted breath-holds for greater than 10 to 15 seconds. That preliminary study provided no direct evidence of tumor motion reduction. Filling this gap in knowledge is an important consideration before moving HFPV into clinical practice for tumor immobilization.

In this first-in-man clinical case study, we combined HFPV and fluoroscopy to directly visualize and quantify tumor motion.

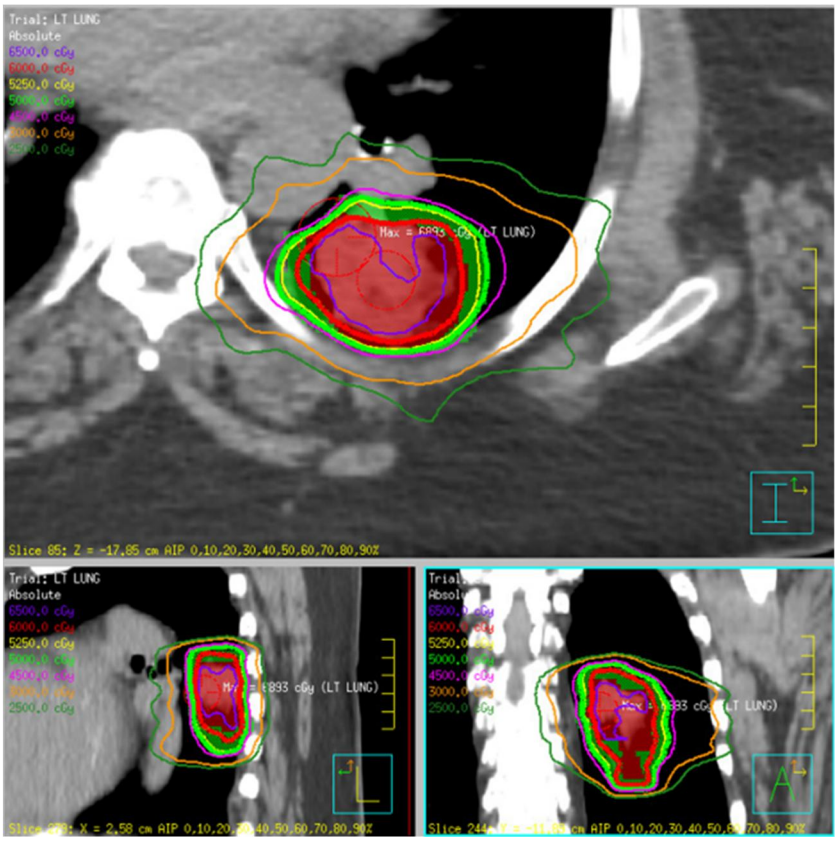

Figure 0-1: Cohort II Patient Tumor Location

1.24.3 Methods and Material

1.24.3.1 Patient Selection

Any patient with conspicuous (visible on projection x-ray, e.g. CT scout AP projection) lung tumors that exhibited ≥ 10 mm motion on their standard of care treatment planning 4DCT was recruited for this study. Between December 2018 and July 2019, we screened a total of 105 lung patients. Of which 27 had conspicuous tumors that moved >10 mm. Of the twenty-seven, seven had COPD FEV1 (Forced Expiratory Volume) score <50 percentile which automatically excluded them from the study. One was under the age of 18, which also excluded them from the study. Eighteen declined for personal

reasons. Only one patient accepted and underwent fluoroscopy with HFPV. The patient was a 69-year-old female with Stage IB (cT2a, cN0, cM0) adenocarcinoma of the LLL (left lower lobe) with lepidic and acinar growth pattern ***Figure 0-1***.

1.24.3.2 Procedural Workflow

The patient was connected to the intrapulmonary percussive ventilation (IPV-2C) device (Percussionaire Corp., Sagle, Idaho) through the Phasitron and the Fischer & Paykel Oracle 452 CPAP (Fischer and Paykel Healthcare, Auckland, New Zealand) interface. The patient was then transferred to the treatment room where she was setup supine using her three-point isocenter tattoos with both arms above her head. We acquired two sets of consecutive fluoroscopy frames during multiple breathing cycles. One set was acquired while the patient was freely breathing and the other approximately 10 seconds post HFPV initiation. The settings of the Percussionaire IPV-2C (pressure, frequency, CPAP, inspiration time) were set by a certified respiratory therapist, but at the direction and comfort of the patient.

All fluoroscopy images were acquired in the AP (Anterior Posterior) direction with the gantry positioned at 270 degrees. Images were acquired with kV=120, mA=25, ms=40 and SFOV (Small Field of View) and a frame rate of 5.5 frames/second. The size of the images was 512x512x16bit with a Horizontal and Vertical resolution of 0.518 mm/pixel.

Two points were selected in the target and traced along each fluoroscopy frame as indicated in ***Figure 0-3***.

Prior to initiation of Cohort II quality assurance was performed on the fluoroscopy unit to ensure that it would identify tumor location correctly. A predetermined motion curve was imported into the CIRS motion phantom (CIRS, Inc Norfolk, Virginia) with a BB (high density material) attached at the end of the mobile rod. The phantom underwent fluoroscopy imaging while in motion ***Figure 0-2*** using the kV (motionview) arms of the Elekta Linear Accelerator (Elekta, Inc, Stockholm, Sweden). A python-based algorithm was designed to trace the BB across all of the frames acquired.

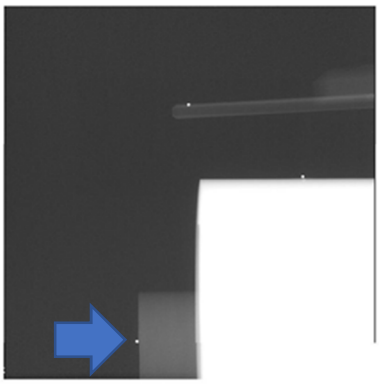

Figure 0-2: Motion Phantom with BB at the end of the mobile rod (Blue arrow)

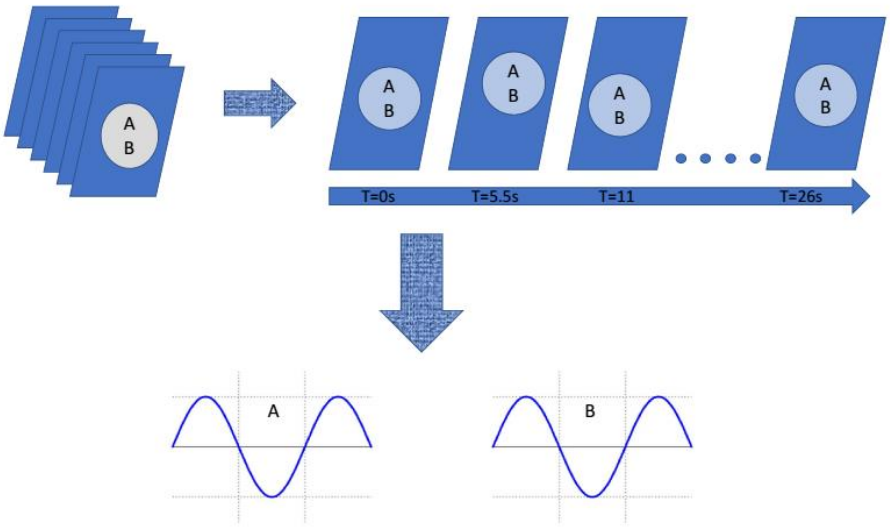

Figure 0-3: Point Motion Tracing Along Fluoroscopy Frames

1.24.3.3 Study Oversight

Patient was enrolled in the study following IRB approval (#2017_046) and verification of the inclusion criteria. Informed consent and authorization document specific to the study were provided to the patient. The patient was informed about the rationale of the study, logistics, risks and how the data would be used.

1.24.4 Results

The pre-determined signal imported into the motion phantom was within 0.2 mm accuracy to the traced signal from the fluoroscopic images obtained. The red line represents the expected target motion and the black line represents the BB motion acquired from each fluoroscopy frame.

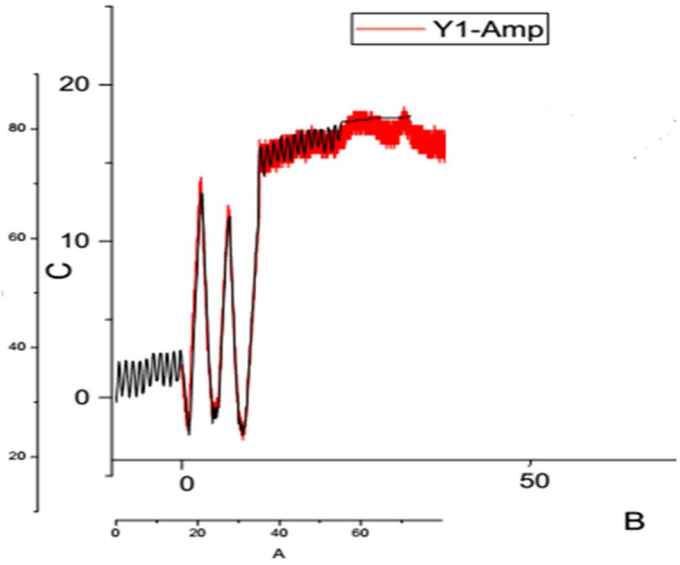

Figure 0-4: Quality Assurance of Fluoroscopy Imaging. Red indicating the imported pattern and black indicating the bb tracing along each fluoro imaging obtained.

A total of 92 fluoroscopy frames were acquired while the patient was in free breathing and 147 in HFPV. Patient had prior history of COPD and was unable to tolerate a peak pressure higher than 12 cmH2O, whereas the healthy volunteers in Cohort I were between 20-22 cmH2O. A few of the fluoroscopy frames with contours of the tumor visualized tumor motion during free- and HFPV breathing is shown in ***Figure 0-5***.

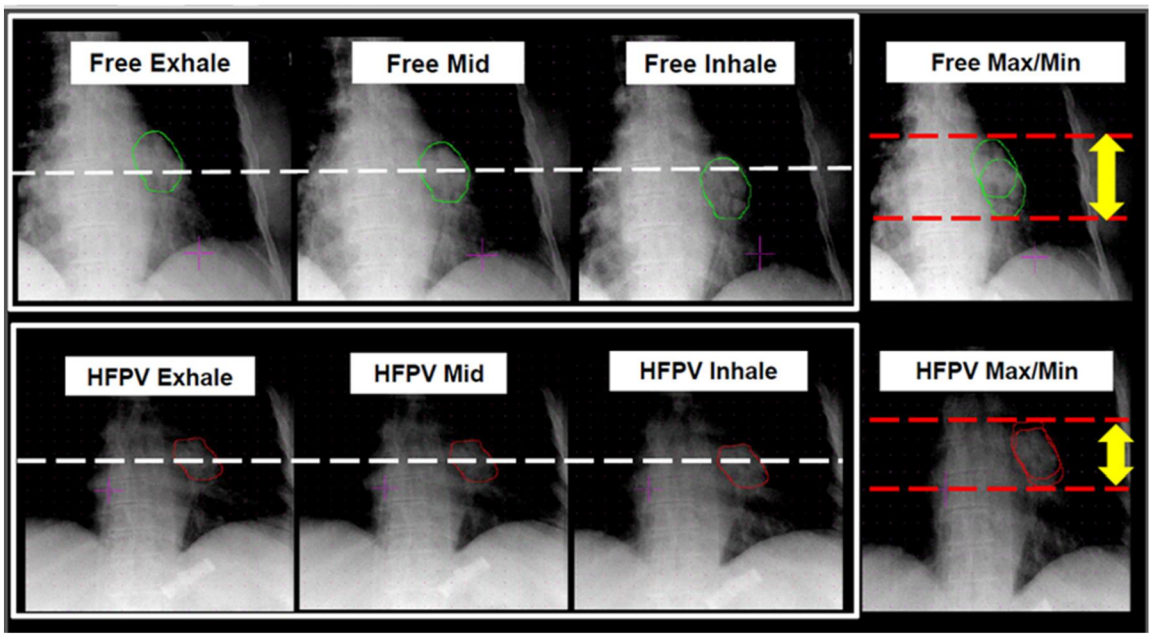

Figure 0-5: Direct tumor motion measurement with HFPV

The two points that were traced along each frame are represented in ***Figure 0-6***

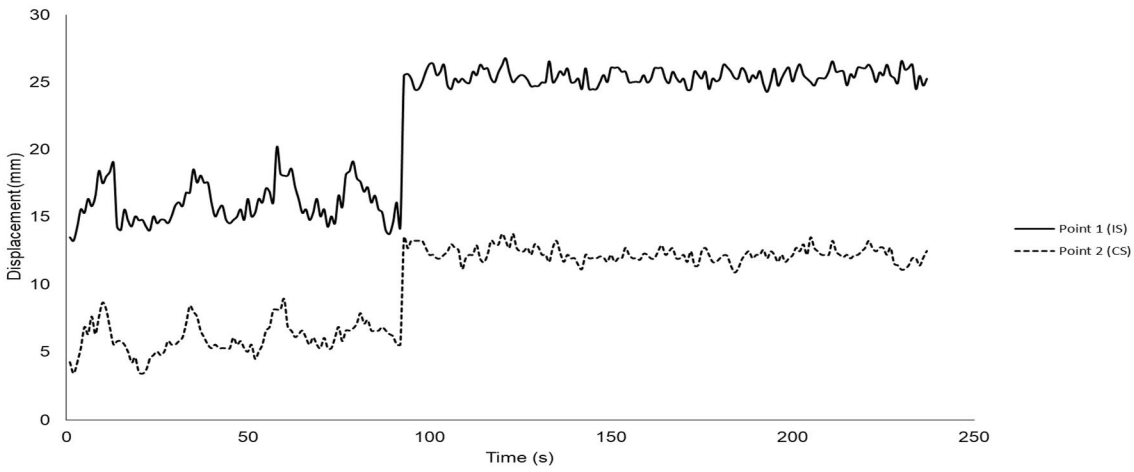

Figure 0-6: Direct Tumor Motion Graph. Point 1 and 2 represent two different points within the tumor

The mean peak-to-peak motion for free breathing for both points was 6.2 mm (slightly lower than 10 mm measured during 4DCT). The mean peak-to-peak motion for HFPV breathing for both points was 2.7 mm. Therefore, the

mean reduction in tumor motion while in HFPV, for both selected points, was at 57%. Although the correlation of tumor motion as it relates to chest-wall motion was not investigated for this patient, due to the length of time and discomfort that patient was on the table, the relative % reduction is comparable to the results of Cohort I.

1.24.5 Discussion

Target respiratory motion and control continues to be of importance in radiotherapy. More recently, in a landmark study by Cuculich et al (Cuculich, et al., 2017) in the New England Journal treated five patients, with a single dose of 25 Gray to the area of heart responsible for generating ventricular tachycardia. 6 weeks following treatment, patients were observed and found to have a 99.9% decrease in the frequency of ventricular tachycardia episodes. They detected 6,577 total episodes during 3 months before therapy, compared to only 4 episodes for 46 patient-months following SBRT and a 6-week wash-out period. Despite the good clinical outcomes of the study, no respiratory management techniques were applied, and this remains a concern.

Providing consistent and direct tumor motion control is critical in escalating radiation doses, while maintaining good sparing of the healthy tissue. In this study we show direct tumor motion management that is consistent and maintained for longer periods of time than a typical breath-hold. Although the patients' last reported FEV1 score was in the normal range (>50 %), the patient had previous history of COPD which might have hampered our ability to maintain a pressure of 20 cmH2O, like that seen in the volunteer cohort.

However, even with the low peak pressure of 12 cmH2O motion was drastically reduced relative to patients free breathing.

Additionally, tumor motion recorded during the 4DCT simulation was about 11 mm, however free breathing motion during fluoroscopy was approximately 6.2 mm. Although, the motion was slightly different, we attribute this to the 4x10Gy fractions that the patient had already received prior to her fluoroscopy study. We believe that tumor size/motion might have changed from what was initially recorded in 4DCT.

In this study we did not evaluate prolonged HFPV times that the patient could've tolerated, but rather acquired several hundred fluoroscopic frames that would allow us to calculate direct tumor motion. Patient was however comfortable with the device and the length of time that she was in HFPV (<5 mins). We were unable to setup the external Anzai laser system on the patient's chest wall due to the setup time and her discomfort on the hard table top, but we aim to do so for subsequent patients.

To our knowledge, this is the first study to ever show direct tumor motion using such a novel technique for radiotherapy. Its drastic reduction of tumor motion, prolonged time, and other parameters measured in the Cohort I, make HFPV a promising technique for respiratory motion management in radiotherapy, particularly for high risk cases like SBRT and cardiac arrythmias like the study by Cuculich et al (Cuculich, et al., 2017).

1.24.6 Conclusions

HFPV is a viable and novel technique that can be used for direct tumor immobilization. In this first ever study, we showed significant tumor reduction relative to free breathing.

1.25 Determination of Direct Diaphragm Motion using MRI

1.25.1 Introduction

Magnetic Resonance Imaging (MRI) in the thorax is complicated by the low proton density of lung parenchyma (Mulkern, et al., 2014))and motion due to breathing or the beating heart (Schultz, Alfidi, Nelson, Kopiwoda, & Clampitt, 1984). Motion causes image artifacts that appear as blurring, ghosting or image harmonics, and misregistration. Images corrupted by motion are often uninterpretable. Respiratory motion can be suspended for < 30 seconds by breath holding in healthy cooperative patients. This time can by lengthened using supplemental oxygen and hyperventilation by up to 40%. The effect of respiratory motion is illustrated in ***Figure 0-11***, where a thoracic MRI image volume was acquired while breathing versus during a breath hold. The yellow arrows demonstrate the motion of the diaphragm and consequently the elongation of the heart.

The MRI signal-to-noise ratio is proportional to the voxel size and to the square root of the number of averaged measurements. High spatial resolution therefore requires long data acquisitions; up to 10 mins of data acquisition. For these longer acquisitions, respiratory and cardiac gating may be employed. However, dual gating introduces a lower acquisition duty cycle prolonging the

total acquisition times. A method to reliably suspend respiratory motion for ≥ 10 minutes is needed.

MRI has high soft-tissue contrast allowing the differentiation of malignant versus benign processes, such as tumor and atelectasis. This has the potential for more accurate targeting of the malignancy while sparing normal tissue has lead the interest in using MRI for radiation therapy treatment planning simulation (Schmidt & Payne, 2015) and for image-guided delivery (Raaymakers, et al., 2017) (Lagendijk, et al., 2014) .

Combined MRI and radiotherapy machines are being introduced to provided image-guidance during treatment delivery. The radiation oncology department currently has a 3T Philips Ingenia MR simulator. An Elekta Unity MR-Linac utilizing a Philips 1.5 Tesla MRI machine is scheduled for installation late-2019 at Beaumont Hospital, Royal Oak. Motion remains an issue both for thoracic MRI imaging and for radiotherapy delivery for MR-Linac machines. The motivation behind this study is to use HFPV as a method to reproducibly suspend respiratory motion during MR imaging and directly measure diagraph motion.

1.25.2 Methods and Materials

One volunteer was recruited to prospectively undergo MRI imaging while in HFPV, free and breath-hold for two consecutive days. The Fischer and Paykel mask, that was used during Cohort I, was utilized for this study. Due to the ferromagnetic material in the Percussionaire unit, the custom designed 20-foot

tubing, described in ***Figure 0-5*** D), was utilized to connect the Phasitron (MR compatible) to the Percussionator which was located by the treatment console, outside of the MR field (***Figure 0-7***). The Sentec or the Anzai laser system were not utilized for this study due to their MR incompatibility. The volunteer was in HFPV during the entire imaging acquisition process (> 25 minutes).

Figure 0-7: MRI Setup with HFPV

MRI data was acquired on the Department of Radiation Oncology's 3T Philips Ingenia MR simulator, equipped with 32 channel torso coils. The subject was setup in a supine position, head first, on the flat table top, with the torso coil placed on the coil bridge (***Figure 0-7***). We acquired three, 3D T1 TFE weighted imaging data with fat suppression radially using Enhanced T1 High Resolution Isotropic Volume Excitation (e-THRIVE), performed using breath-hold, free-breathing, and HFPV acquisitions.

The pressure and frequency at the end of the 15 and 20- feet long tubing was tested prior to initiation of this study. Each tube was connected individually to a custom designed Phasitron which held an inflated balloon. The Anzai laser

system was projected on the balloon. Frequency and pressure changes were incrementally changed following the same procedure as described in Section 1.28.1.

1.25.3 Results

The 15 and 20-feet tubing decreased the balloon volume much more rapidly (***Figure 0-8***) than the standard 4-foot tubing clinically used when only the frequency dial was changed (from highest to lowest frequency). However, this was only noticed towards the end of the dialing range (8-12).

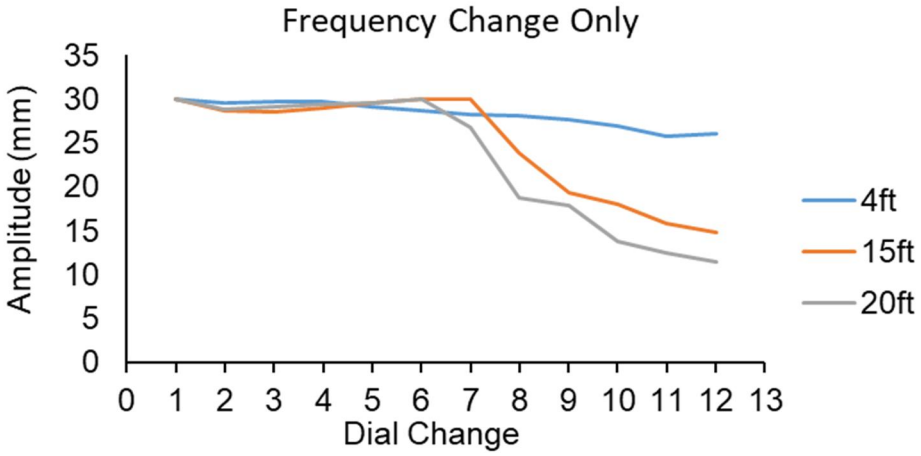

Figure 0-8: Changes in Frequency for 4, 15 and 20ft Phasitron tubing.

Similarly, as the pressure decreased, the balloon was drastically affected. The 4-foot tubing provided slightly higher pressure at the balloon than the 15ft or the 20ft, however a reversal was noticed towards the 6-11 dial range.

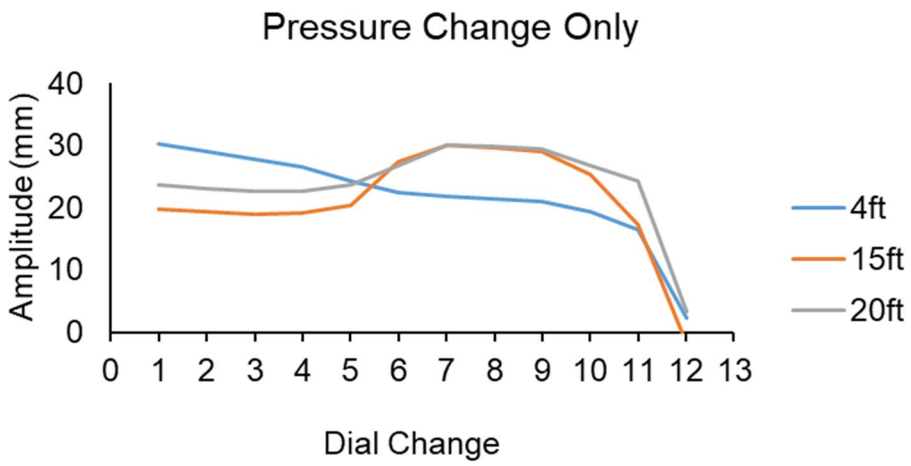

Figure 0-9: Changes in Pressure for 4, 15 and 20ft Phasitron tubing

Incremental changes for frequency and pressure resulted in similar outcomes for the clinically sued dials (3-9).

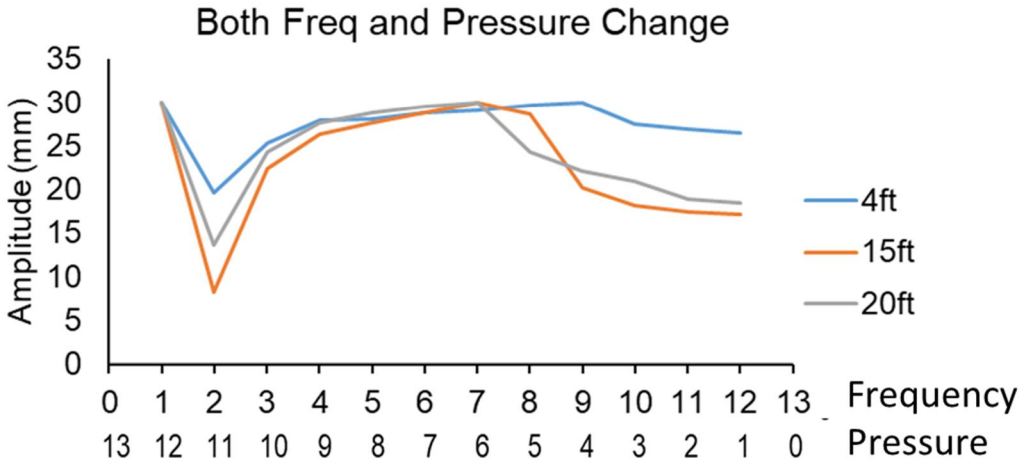

Figure 0-10: Changes in Frequency and Pressure for 4, 15 and 20ft Phasitron tubing

The volunteer was setup in the MRI unit with arms above his head and 20-foot tubing. Like the other cohorts, a peak pressure between 19-20cmH2O and frequency of approximately 300-350 bursts/min were achieved without any significant loses in ventilation.

For day 1, diaphragm peak-to peak motion relative to breath hold was 5.25 cm for free- breathing and 0.18 for HFPV. Similarly, for day 2, diaphragm motion relative to breath-hold was 5.13 cm for free-breathing and 0.12 cm for

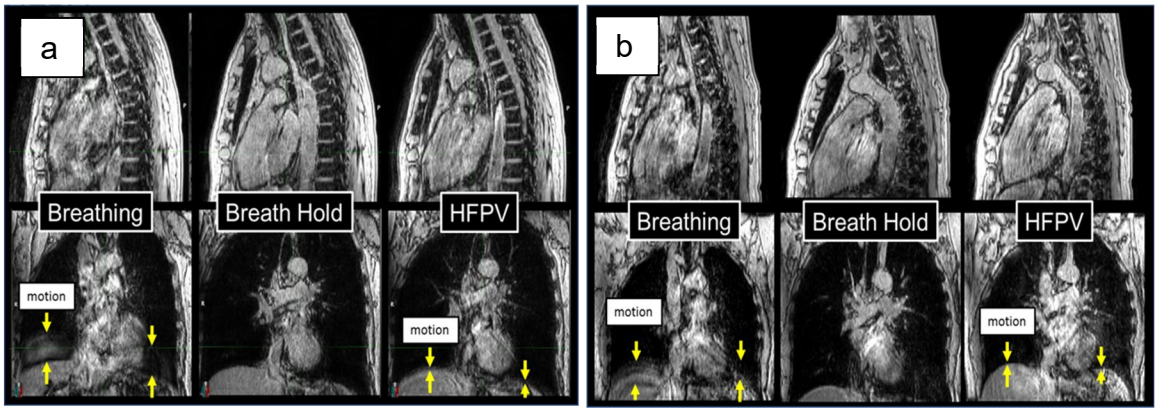

Figure 0-11: MRI with HFPV a) indicates images acquired in day 1 and b) those acquired in day 2. Yellow arrows indicate the extent of motion for free, breath hold and HFPV breathing.

1.25.4 Discussion

It is evident from the results that within the clinical operating limits between 3 to 8, the Percussionator can deliver adequate pressure and frequency for both 15- and 20-feet tubing. Similarly, the peak pressure and frequency achieved during the prospective volunteer study was easily achieved and matched the Cohort I and II parameters of about 20cmH2O and 350 bursts/min frequency.

The volunteer was able to tolerate the entire image acquisition process of >25 minutes without interruption of HFPV. The drastic reduction in diaphragm motion is further indication that HFPV is a novel technique in reducing motion for long periods of time (>25 mins) and comparable to that of breath-hold. This is

significant when compared to conventional kV imaging because MRI has high soft tissue contrast. Additionally, HFPV greatly reduced image artifacts that are caused due to motion. These artifacts are prominent around the heart and liver in ***Figure 0-11***.

1.25.5 Conclusions

We have demonstrated that HFPV can be utilized in an MRI setting for long periods of time (>25 mins) and drastically reduces diaphragm motion (>90%) as well as motion artifacts noticed during imaging.

CHAPTER 6: A RETROSPECTIVE PLAN STUDY OF THE DOSIMETRIC IMPACT OF HFPV

1.25.6 Abstract

Purpose: The purpose of this retrospective study is to investigate and quantify: 1) PTV volume reduction and 2) OAR sparing for HFPV as a tumor immobilization technique.

Methods: In an IRB approved study we previously recruited volunteers to undergo HFPV. Their chest wall motion was recorded using a laser system that was projected 10 cm inferior to the xyphoid process. A total of 3 HFPV and 3 free-breathing chest wall motion curves were imported into a motion lung phantom. The phantom underwent 4DCT while the 2cm target imbedded inside the phantom moved as determined by each imported curve. Varian RPM was utilized to bin each CT slice into 10 phases (10-100 %). An average and MIP were created from each 4DCT. The target was contoured on the MIP and the OARs on the average. A uniform 5 mm margin was applied to all ITVs. OARs

and target were contoured on each scan by qualified professionals. A total of 6 (3 free and 3 HFPV) RapidArc treatment plans were created using 10FFF, with two partial beams and 30-degree collimator rotation. Each plan was designed to deliver 50 Gy in 5 fractions.

Results: The PTV volume was reduced by > 7cc for HFPV. V5 and V20 were also scientifically reduced by >5 Gy and >3 Gy, respectively. Similarly mean heart dose was reduced by as much as 3.56 Gy

Conclusion: We have shown that HFPV dosimetry is greatly improved relative to free-breathing. Relative to free breathing, HFPV plans were superior in reducing V20, V5, Heart doses as well as PTV volumes.

1.25.7 Introduction

The goal of radiotherapy planning is the accurate delivery of radiation to the target while limiting the dose to nearby healthy tissues. Improvements in radiation delivery techniques (Armstrong, 1993) enable clinicians to achieve these goals. The International Commission on Radiation Units and measurements (ICRU) Report 50 (ICRU 50, 1993) and the Supplement Report 62 (ICRU 60, 1999) describe the current recommendation for incorporation of tumor motion into radiation therapy planning. In the thorax, targeting is complicated by respiratory motion, which can cause tumor displacements as large as 2 cm during treatment (Seppenwoolde, et al., 2002) (Shimizu, et al., 2001) (Seppenwoolde Y. e., 0094-2405). Accurate targeting is critical, particularly for SBRT, in which high doses of radiation are delivered in just 1 to 5

fractions. The American Association of Physicists in Medicine (AAPM) Task Group 76a report on the management of respiratory motion in radiation oncology (Keall, et al., 2006), recommends margins around the treatment target be sufficient to ensure coverage of the target.

In a landmark SBRT trial for early stage inoperable lung cancer, Timmerman, et al. used planning target volume (PTV) expansions from the gross tumor volume (GTV) of up to 5 mm in the axial dimension and 10 mm in the cranial-caudal (CC) direction (Timmerman, et al., 2010). This relatively large PTV expansion in the CC direction results in a larger volume of healthy tissue being irradiated. Four-dimensional computed tomography (4DCT) provides a snapshot of respiratory-induced tumor motion and is used to individualize the internal target volume (ITV) [10], yielding smaller treatment margins than fluoroscopy. As 4DCT scanning and image-guided radiotherapy (IGRT) became more readily available, recent studies have reduced the PTV margins to a 5 mm uniform expansion around an ITV that accounts for respiratory motion (Liang) (Li X. e.) (Kilburn, 2016).

In the SABR-COMET trial there was a 4.5% death rate due to radiation pneumonitis, GI bleed, and lung abscess. Similarly, In RTOG 0617, increasing the dose from 60 to 74 Gy killed more patients than it saved. Therefore, reducing margins while still maintaining high therapeutic doses is critical. In this retrospective simulated study we evaluate whether HFPV motion has an impact on 1) PTV margin reduction (volume), 2) spearing of healthy organs.

1.25.8 Methods and Material

In this study we randomly selected a total of six breathing curves from Cohort I data, three HFPV and three free breathing. Their peak to peak amplitude for free-breathing was 22.8 mm, 22.8 mm and 16.415 mm and 3.2 mm, 2. mm and 1.8 mm for HFPV. Each pattern was imported into the CIRS lung phantom. The RPM (Real Time Position Management by Varian Medical Systems, Palo Alto, California) cube with the fluorescence reflectors was position on the platform and the infrared camera projected on (***Figure 0-1***).

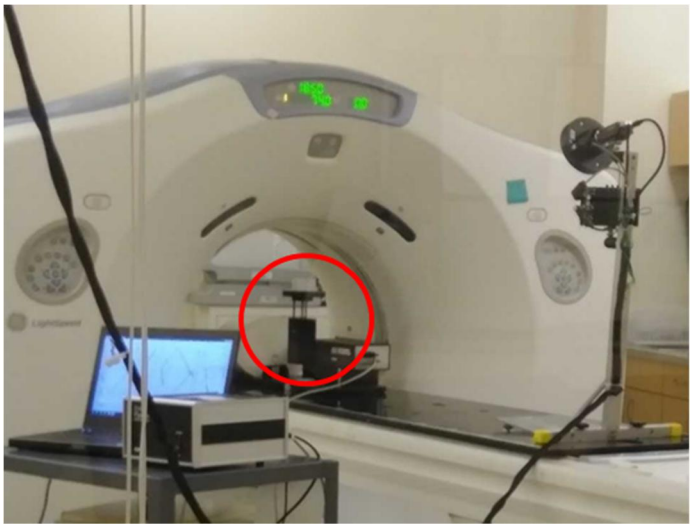

Figure 0-1: 4DCT of Lung Thoracic Motion Phantom using RPM

A 4DCT of the body of the phantom, with a 2 cm target in the mobile rod, was acquired for each of the breathing curves utilizing a 16 slice GE scanner (GE Healthcare, Chicago, IL). All scans were performed using 1.25 mm slice thickness and 120kVp. GE Advantage Sim MD was utilized to bin each slice into the appropriate phase bin. Average and MIP (Maximum Intensity Projection) reconstructions were automatically performed for each of the six scans. The 2

cm target in the mobile rod was contoured on the MIP, however the computerized treatment plan was done on the average CT.

A total of 6 plans were designed. Three with the average 4DCT acquired from free breathing patterns and three with the average 4DCT acquired from HFPV breathing patterns. We utilized a 10FFF (Flattening Filter Free) beam with HDMLC RapidArc for creating all computerized plans using Eclipse (Varian Medical Systems, Palo Alto, CA) treatment software. Jaws were conformed to the target with 0.5 cm uniform margin. Two partial arcs were utilized, one going clockwise and the other counter-clockwise (345 to 180 degrees). The collimator was rotated at 30 and 330 respectively for each arc. A standard Flattening Filter Free dose rate of 2400MU/min was used. Heterogeneity was turned on for all plans.

Target was contoured by a board-certified radiation oncologist, whereas the OARs by a board-certified radiation physicist. A standard SBRT prescription of 50 Gy in 5 fractions was used. All plans were normalized to deliver at least 95% of the dose to 100% of the target. OARs contoured: Chest-wall, Heart, L/R Lung, Lungs-PTV, Spinal Cord, Spinal Cord+5 mm, Spinal Cord +3 mm. The PTV was identified by contouring the ITV (target along each of the 10 phases identified) plus a uniform 5 mm margin.

The acceptable plan criteria were based on RTOG 0813 protocol for 50 Gy in 5 fractions as noted in ***Table 5:*** *RTOG 0813 Criteria for 50Gy in 5 fractions* ***Table 5***.

	Volume	Dose	Max Point
Heart:	< 15cc	> 32 Gy	< 52.5 Gy
Spinal Cord	<0.25 cc	> 22.5 Gy	< 30 Gy
	< 0.5 cc	> 13.5 Gy	
Lung-GTV	<1500 cc	> 12.5 Gy	
	< 1000 cc	> 13.5 Gy	
Skin	< 10 cc	> 30 Gy	

Table 5: *RTOG 0813 Criteria for 50Gy in 5 fractions*

1.25.9 Results

A summary of the results are represented in ***Table 6***. To be noted that the average PTV volume defined during free breathing was 12.067cc vs. 4.7cc. Similarly, V20 and V5 of the lung was drastically reduced from a mean of 5.44 Gy (Range: 3.3 -7.97Gy) to 1.94 Gy (Range: 1.68 – 2.46 Gy) for V20 and 16.49 Gy (Range: 14.3 – 20.24 Gy) to 10.74 Gy (Range: 8.84 – 13.31 Gy), for V5 for Free vs. HFPV breathing respectively.

Maximum hot spot distribution was statistically non-significant between the two breathing patterns. The 15cc criteria for the heart dose was significantly different from 16.64 Gy (Free Breathing) to 13.08 Gy (HFPV).

An iso-dose color wash sample of the plans is represented in ***Figure 0-2***. It is evident that the drastic motion reduction allows for a conformal dose

distribution around the 2 cm target.

	OARs								TARGET	
	Lung - PTV									
10X FFF, 2 Partial Fields RapidArc , 30/330 Collimator	< 1000cc receives > 13.5Gy (Gy)	< 1500cc receives > 12.5Gy (Gy)	Max Lung (%)	V20 (Gy)	V5 (Gy)	SpinalCord < 0.25cc receives > 22.5 Gy (Gy)	SpinalCord <0.5cc receives > 13.5 (Gy)	Heart <15cc receives >32Gy (Gy)	PTV Volume (cc)	PTV 2cc (Gy)
Free Breathing 1	2.296	1.089	110.2	5.06	20.24	6.854	5.6	18.22	16.4	57.43
Free Breathing 2	1.45	0.539	108.6	3.302	14.94	6.29	5.93	15.39	9.6	55.89
Free Breathing 3	0.35	-	110.4	7.97	14.3	6.69	6.44	16.31	10.2	57.71
HFPV Breathing 1	0.6153	0.2637	107.4	1.6864	8.843	5.77	6.37	13.84	5	54.31
HFPV Breathing 2	0.66	0.27	105.9	1.68	10.06	5.62	5.22	13.34	4.4	53.89
HFPV Breathing 3	0.58	0.18	107.1	2.46	13.31	5.74	5.43	12.06	4.7	55.65
Δ1	1.6807	0.8253	2.8	3.3736	11.397	1.084	-0.77	4.38	11.4	3.12
Δ2	0.79	0.269	2.7	1.622	4.88	0.67	0.71	2.05	5.2	2
Δ3	-0.23	#VALUE!	3.3	5.51	0.99	0.95	1.01	4.25	5.5	2.06
Average Δ	0.75	0.55	2.93	3.50	5.76	0.90	0.32	3.56	7.37	2.39

Table 6: Dose Volume Histogram for Photon Plans

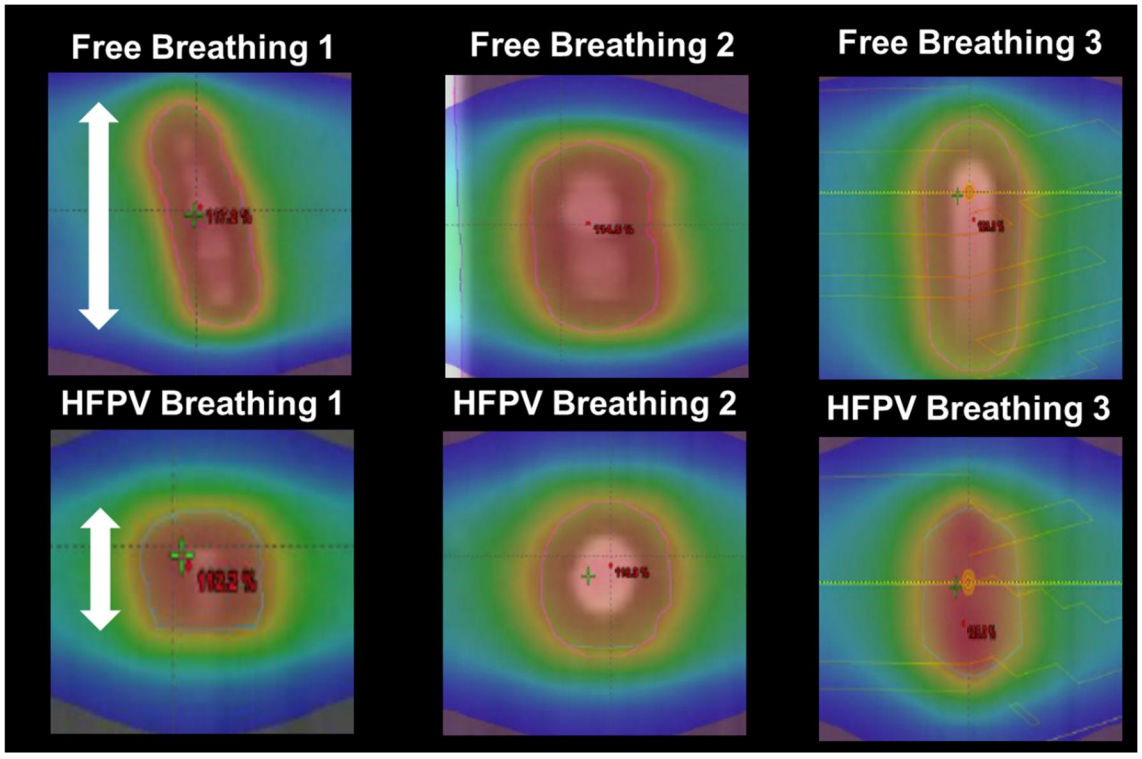

Figure 0-2: Dose Colorwash and motion distribution of Free vs. HFPV plans

1.25.10 Discussion

It is apparent from previous studies and trials like SABR-COMET and RTOG 0617 that reducing margins is critical in sparing organs at risk which consequently result in fewer side effects.

In this simulated retrospective phantom study, we evaluated whether motion reduction by HFPV is dosimetrically beneficial. We assumed that chest wall motion acquired from the volunteers undergoing free- and HFPV- breathing was the same as tumor motion. It was elected to use the smaller slice thickness due to the small size of the target. The 95 % normalization was used as a baseline for comparison. Motion of the rod was >10 mm for free breathing and <5 mm for HFPV-breathing.

As the results indicate, the volume of the PTV was drastically reduced from free to HFPV breathing. The expansion margin from ITV to PTV was kept at 5 mm for all plan. In one of the scans, the lung volume was < 1500 cc, therefore no data was reported. V5 and V20 of the lung experienced the greatest dosimetric benefits from HFPV by reducing the dose by > 5Gy and >3 Gy, respectively.

1.25.11 Conclusions

HFPV can drastically improve the dosimetric parameters for SBRT plans when compared to free-breathing. V20 improved from 5.44Gy to 1.94Gy and V5 from 16.49Gy to 10.75Gy.

CHAPTER 7: NEW MASK DESIGN AND REPRODUCIBILITY

1.26 Mask Design

Upon review of the subjective scores, analysis of data from Anzai system and SenTec monitoring system from all 15 volunteers enrolled in Cohort I, we concluded that to optimize the comfort of HFPV for patients undergoing radiotherapy a custom mask is important. In the new designed mask, we aimed at resolving some of the shortcomings that the commercial masks exhibited during Cohort I.

1.26.1 Commercial Design Shortcomings

Fischer & Paykel Oracle 452 interface resulted in the longest times under HFPV. However, air leakage through the side of the patient's mouth resulted in loss of percussive bursts and drift in amplitude. Although, it had a strap around the mask, volunteers indicated it was difficult to hold in place with their teeth. Additionally, it introduced the highest dry throat and the nasal prongs continually fell off. The above issues make this interface less optimal for radiotherapy.

Amici Tru-Fit was the most difficult to hold in place due to lack of straps. Therefore, it was held in place by hand. Similarly, to the above device, the nasal prongs continually fell off. CO_2 level increased faster with Amici Tru-Fit than the other two devices. Holding this device by hand would not be optimal for patients undergoing radiotherapy due to gantry rotation around the patient and other inconsistent placements.

Phillips Respironics Oro-Nasal mask was the most comfortable based on the subjective scores. All volunteers indicated that it rested comfortably on their face, however they did not feel well ventilated. It was noted that the high frequency bursts would “puff up” the patients’ cheeks, resulting in the delivery of pressurized pulses within the buccal space and oral cavity rather than their oropharynx. Delivery of pulses in buccal space and low duty cycle for this interface would create inconsistent results in target immobilization

During clinical radiotherapy treatments, patients are accompanied into the radiotherapy treatment room by the Radiotherapy Technician (RTT). The radiotherapy room is a large vault that is shielded by several feet of concrete on all sides; in addition to the multi thousand-pound steel door that provides protection to the outside staff while the linac is on. After the patient is setup on the treatment couch, the therapists will exit the vault. Once outside, they will take preliminary imaging to verify isocenter and then deliver the treatment. The patient is in the treatment room by themselves (audio and visual is mandatory). As a result, our current three masks and Phasitron tubing have major limitations in radiotherapy. To address them we proposed:

- Design a custom mask with a valve that would allow the patients to switch between the ventilator and room air.
- Design custom nasal prongs that are either part of the mask or don’t fall off during radiotherapy treatment (usually 15 to 30 minutes).

- Design a custom mask that would allow the delivery of the pressure wave pulses to the oropharynx, beyond the buccal space and oral cavity while maintain mandible comfort.

Additionally, during our Cohort I measurements, the volunteers were setup in a research room where the Oxygen supply, Phasitron and Phasitron tubing was within three to five feet from the patient. Therefore, long tubing to connect the patient to the high frequency air bursts was not necessary. Such setup would not be possible in a clinical radiotherapy room since the patient is in a room by him or herself. The Percussionaire (IPV Control System) will be positioned outside of the room to protect the technician operating it from high doses of radiation while the patient receives treatment. To overcome such matter, we propose:

- Custom design of longer tubing that would allow for the same mechanical impedance.
- Development and Design Partners

1.26.2 Beaumont HFPV Mask Design

1.26.2.1 Introduction

To improve the shortcomings from the commercial masks, a new HFPV mask was designed and prototyped to accommodate for: 1) air leakage around the mouth, 2) direct delivery of the bursts into patients' oropharynx (less puffy cheeks), 3) patients' ability to control between room air and HFPV, 4) longer Phasitron tubing for MRI imaging.

1.26.2.2 Methods

Beaumont HFPV design and prototype, with some commercially available components, are shown in ***Figure 0-1*** through **Figure 0-2**. We recruited five volunteers to undergo four HFPV sessions with the new prototype. They were positioned flat on the treatment table with their arms above their head. Their chest-wall motion was monitored using the Anzai system. A total of 20 free- and 20 HFPV-breathing patterns were analyzed. For each breathing pattern we calculated the absolute difference between the max (peak) to min to min (peak) value. The % reduction in motion for HFPV was relative to the free breathing for each individual session.

1.26.2.3 Results

Figure 0-1 is an overview of the initial design. The straps would allow the mask to fit tightly around the patient, while the mouthpiece with the adjustable length allows for additional fine tuning of the interface. The ability to adjust the mouthpiece would allow the bursts of air to be delivered directly into the patients' oropharynx without creating "puffy cheeks".

Figure 0-1: Overview of Beaumont Mask Design with some AF451 Commercially available integration-ECRLab Design

Figure 0-2 shows how each component fits together whereas ***Figure 0-3*** shows the positioning and design of the diverter valve that would allow the patient to switch between room air and HFPV. The placement of the diverter valve was investigated (***Figure 0-5***). We decided to place it as close to the Phasitron as possible to eliminate introducing dead space between the Phasitron and diverter (recommended < 50 mL), which would consequently introduce drop in pressure and discomfort to the patient.

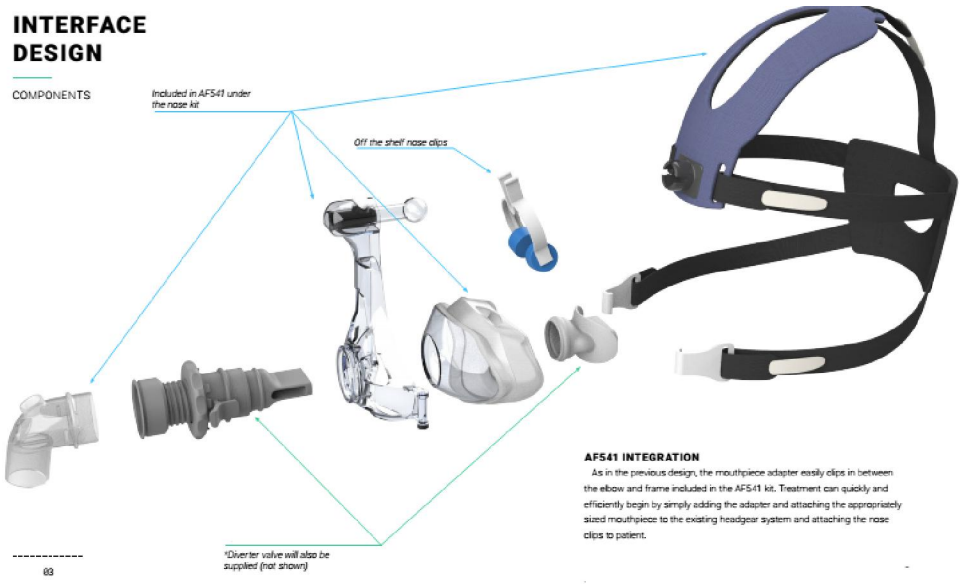

Figure 0-2: *Components of the mask: Commercially available AF451 integrated with a fabricated 3D printed adjustable mouthpiece-ECRLabs Design*

A diverter valve that slides in and out was designed to allow the patient to

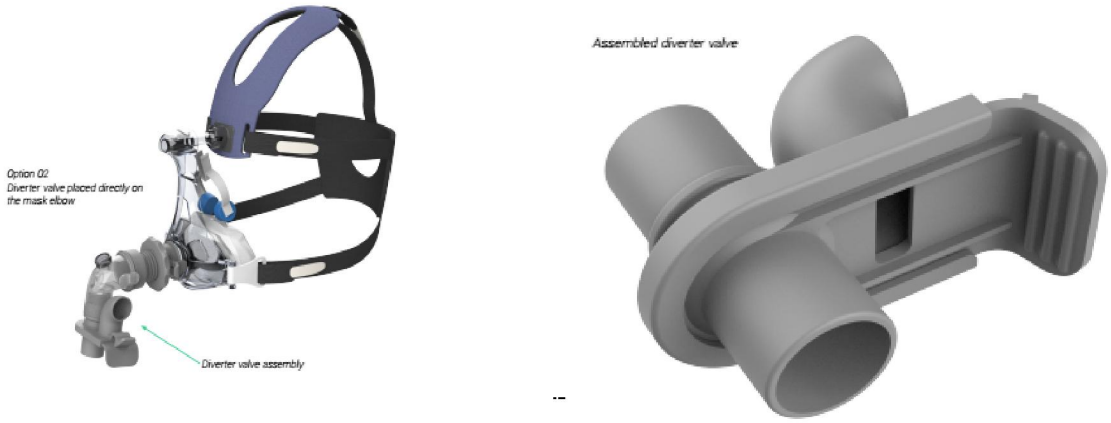

Figure 0-3: Diverter Valve placement

switch between room air and HFPV in the event of an emergency. This design allows for the HFPV bursts to be escaping outside of the patient if it is in the ON position and back into the patient if it is in the OFF.

Figure 0-4: Close-up of the mouthpiece assembly

Several options were also investigated and tested on volunteers in and effort to further revising the prototype. One such option is shown in ***Figure 0-5*** E. A new mouthpiece was introduced to investigate comfort around the patient for future prototyping.

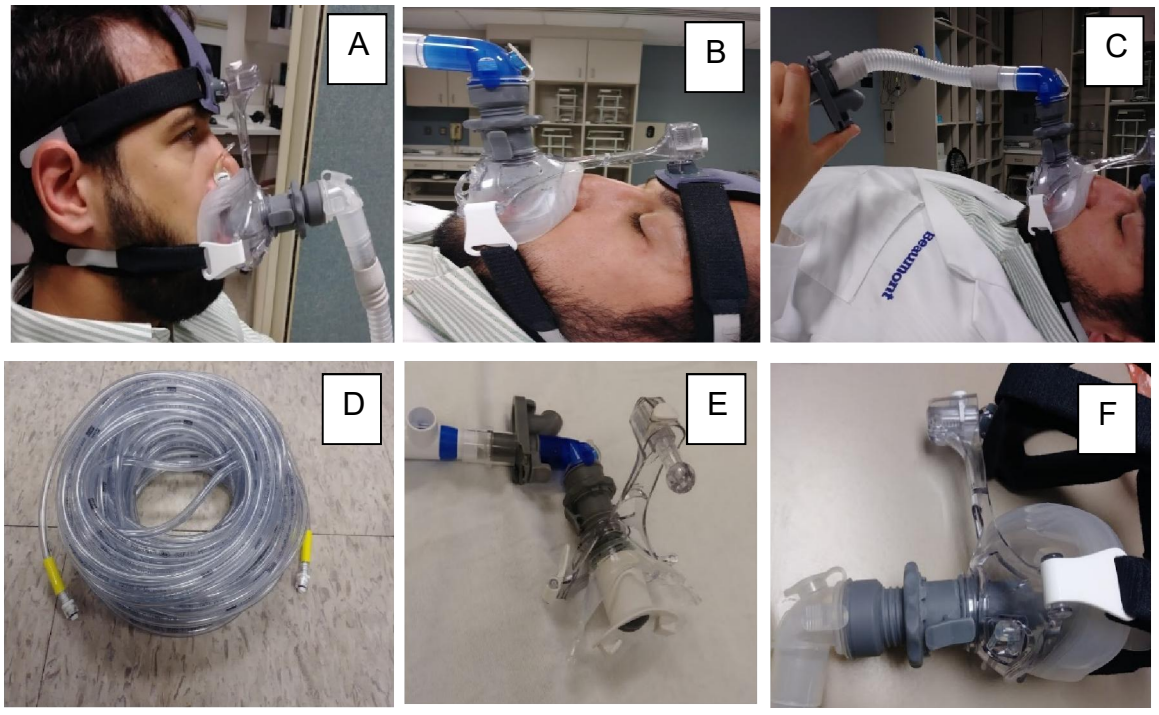

Figure 0-5: The prototype of the mask is shown in A, B, C, E and F. A and B shows a good fit on the volunteer. C shows diverter placement away from the Phasitron. D is the custom tubing (15 and 20 feet), E) shows a slight modification of the mouthpiece for further testing

All volunteers recruited for this study, successfully completed each HFPV session using the setup demonstrated in ***Figure 0-5***B. A total of 20 free- and HFPV- sessions were analyzed. The mean peak-to-peak chest wall motion for free breathing was 12.91 cm (SD: 4.15) and the mean peak to peak for HFPV breathing was 2.88 cm (SD: 1.33).

1.26.2.4 Discussion

Data acquired with the first Beaumont HFPV mask provided promising results. HFPV peak-to-peak motion improved compared to the commercial Fischer Paykal, 2.88 cm (SD: 1.33) vs. 3.8 cm (SD: 0.96). We believe the improvement was due to the adjustable mouthpiece (***Figure 0-4***) which allowed the bursts of oxygen to be delivered directly to the oropharynx as opposed to the buccal space. We also noticed that all volunteers experienced less “puffy cheeks” which is a subjective validation that the percussions were being delivered into the oropharynx

The silicone 3D printed oral part of the mask (depicted as the portion closest to the headgear in **Figure 0-2**), was not as comfortable as the commercially available devices. The volunteers indicated that lack of prongs for teeth to rest on (like the Amici Trufit) is essential. Additionally, with the new diverter valve and adjustable components, the assembly became heavy and harder to hold by hand for long periods of time. Therefore, for this initial version

of the prototype, we did not investigate the amount of time at which each volunteer could be under HFPV. Further improvements to our initial prototype will be made to account for teeth resting prongs, like that depicted in ***Figure 0-5***E, as well as providing support for the entire assembly to be hands free. All volunteers felt well ventilated and minor changes in CO2 levels were noted.

The diverter valve was functioning as designed, however some force was required to slide it ON and OFF. We aim to further improve the initial prototype to accommodate for patients with minimal strength.

1.26.2.5 Conclusions

Our initial prototype provided great improvements to the air delivery into the oropharynx. Our second version of the prototype will be adjusted to accommodate for teeth resting prongs, to prolong patient comfort, as well as providing support for the entire assembly to stay fixed on the patient.

1.27 Reproducibility of HFPV

1.27.1 Abstract

Purpose: The purpose of this study is to identify the chest-wall reproducibility of HFPV as a method for mitigation thoracic motion.

Methods: Five volunteers underwent HFPV in three different days. Each day, they underwent five separate sessions and each session entailed of two 1-minute long HFPV sessions with free breathing in between. Chest wall motion was monitored using the Anzai (Anzai Medical Co., Tokyo, Japan) laser system

which was projected 10 cm inferior to the xyphoid process. Intra-session reproducibility was calculated by obtaining the difference (Δ) between 2 HFPV sub-session means for each the 5 sessions. Inter-session reproducibility was calculated by taking the maximum-minimum difference of the mean daily (Δ).

Results:

A total of 75 sessions were analyzed for all 5 volunteers. Intra- session reproducibility for HFPV was calculated at 1.50 mm (SD: 0.82 and 1.56 mm (SD: 0.56) for free breathing. Inter-session reproducibility was 1.10 mm (SD: 1.27) and 0.80 mm (SD: 0.6) for free- and HFPV- breathing, respectively.

Conclusions: HFPV can be a reproducible technique for thoracic immobilization to within 2 mm, however initial lung volume at on-set of HFPV plays an important role in consistency.

1.27.2 Introduction

Due to biological effectiveness, in almost all thoracic radiotherapy tumors, the dose is delivered in multiple fractions which entails each patient being imaged and treated daily. The fractionation varies between 3 to 5 for SBRT and as high as 30 or more for conventional radiotherapy. Each patient is setup daily on the treatment couch, by the radiological technologist, the same way they were setup during their initial CT-Sim, which is the CT that the computerized treatment plan was designed from.

Because of the daily setups or even multiple setups in one day, it is critical that HFPV inter- and intra- fraction reproducibility is quantified. This would allow clinicians to have confidence (and comfort to the patient) that, if the treatment should be halted for any reason, applying the same parameters (pressure, frequency etc.) as those set in the CT sim would bring the patient to the same initial setup. Similarly, applying the same initial parameters daily should produce the same results. Although, in slightly different circumstances, data has shown that lung function can change over time, therefore it is possible that over a 6-week (Magnussen, et al., 2016) radiotherapy course, patients' ability to tolerate the same pressure and frequency may change. In that event, a new HFPV baseline can be set followed by imaging and other departmental protocols.

Additionally, during Cohort II study, we noticed a slight baseline drift, which we attributed to the increase in CO_2 of the patient which triggered them to gradually stop HFPV. In this study we aim to evaluate intra- and inter fraction reproducibility as well our ability to adjust the baseline shift by altering the dials on the Percussionaire IPV-2C unit.

1.27.3 Methods

We recruited 5 healthy volunteers to undergo HFPV with the Beaumont designed prototype. Each volunteer underwent five sessions (N_s=5) of percussive ventilation in three sperate days (N_d=3). Each session (N_s) consisted of two individual sub-sessions of HFPV (N_{ss}=2) of 1 minute long with re-

breathing in between (***Figure 0-6***). A total of N_s=75 sessions and N_{ss}=150 sub-sessions were acquired for all volunteers ***Figure 0-7*** in three different days.

Volunteers were positioned on a flat table with the Anzai laser system projected approximately 10 cm inferior to the xiphoid process. Like Cohort I, their CO_2 was monitored using the Sentec monitoring system. Each volunteer underwent an initial training session of approximately 30 minutes prior to the initiation of the study. The baseline parameters of the Percussionaire (pressure, frequency, cpap and inspiration time) were also set during the initial training session.

The data acquired from the sessions in the first day followed right after the initial training session, therefore the baseline parameters were used. During the consecutive days, the volunteers were set with the same parameters as the previous day, but minor adjustments were made if the volunteer felt uncomfortable from lack of pressure, frequency etc. The Percussionaire settings were kept unchanged within each daily session.

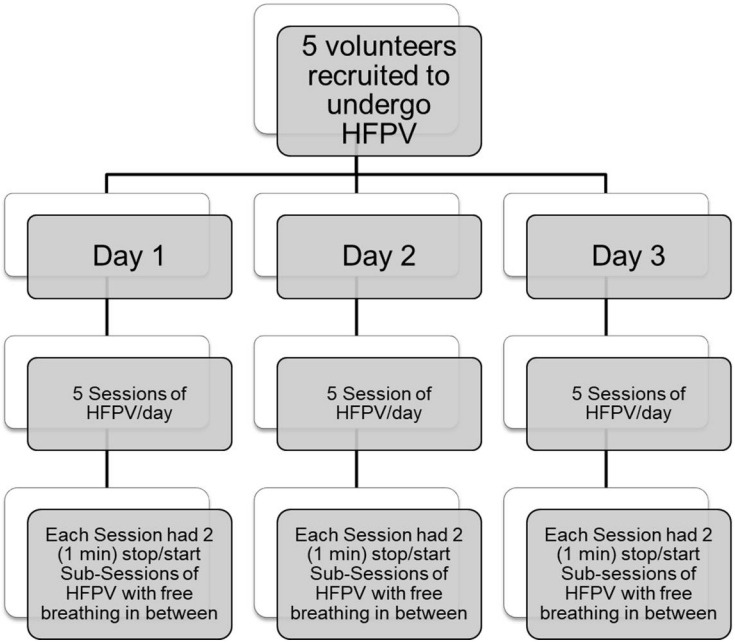

Figure 0-6: *Reproducibility study methods*

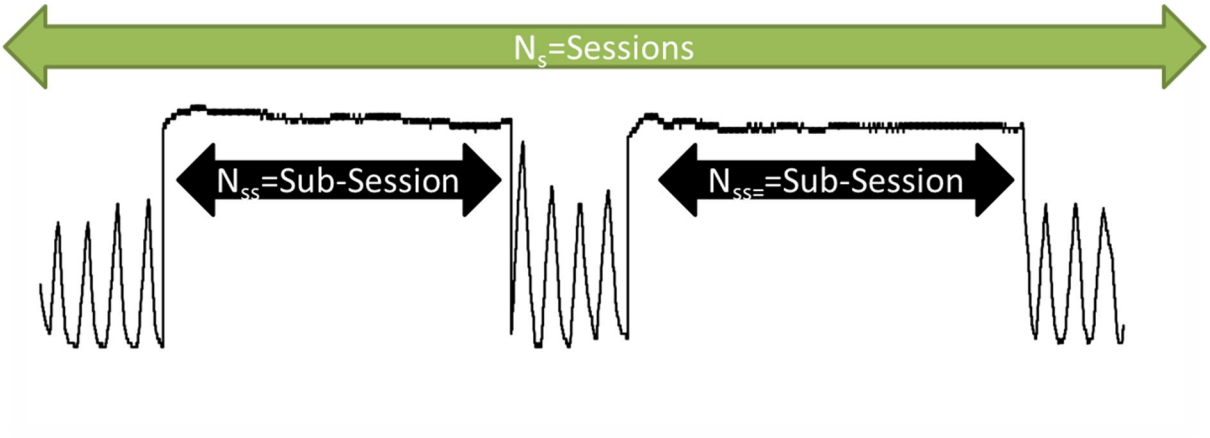

Figure 0-7: Definition of Session, Sub-Session. Each volunteer underwent 5 sessions a day for three days and each session consisted of 2 sub-sessions with free breathing in between.

Intra-session reproducibility was calculated for all of the N_s=75 sessions. For each of the sessions, the mean location (Y-Axis (mm)) of the sub-sessions (indicated by red and green in ***Figure 0-8***) was calculated and the absolute Δ

difference (mm) was calculated. The same methodology was also followed for free breathing.

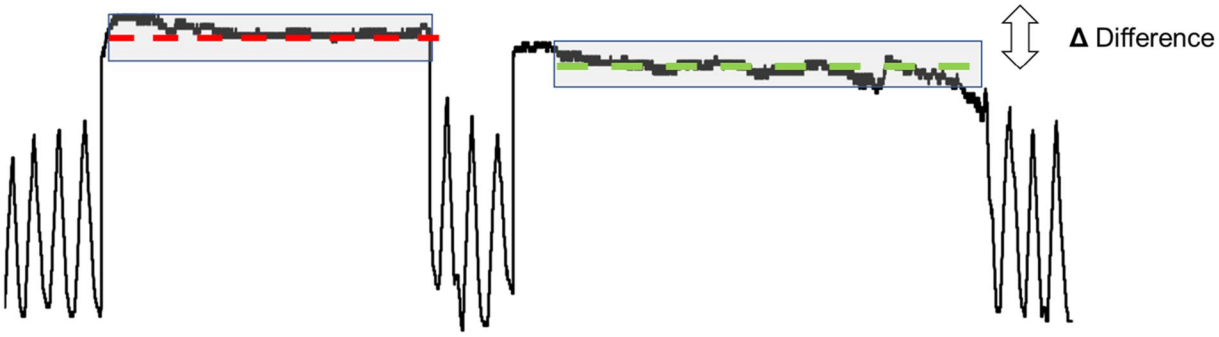

Figure 0-8: Method of calculating reproducibility

Inter-session reproducibility was calculated by taking the maximum to minimum difference in mean delta for all three days. Additionally, the percent change in pressure, cpap, frequency and inspiration time were recorded for each day.

1.27.4 Results

All volunteers that were recruited successfully completed all three days of HFPV. All reached a total peak volume of approximately 18-20 cmH2O and frequency between 300-350 bursts/min.

1.27.4.1 Intra-Session Reproducibility

Intra- session reproducibility for free breathing was calculated to be 1.56 mm (SD: 0.56). The results are represented in ***Table 7***.

Free Breathing Intra-Session Reproducibility (mm)						
		V#1	V#2	V#3	V#4	V#5
Day 1	Session 1	2.39	2.02	1.30	1.77	0.27
	Session 2	1.49	0.02	1.00	1.34	2.54
	Session 3	2.41	2.84	2.66	0.01	0.61
	Session 4	0.04	1.37	0.64	2.45	0.42
	Session 5	3.69	1.66	0.23	0.51	2.25
Day 2	Session 1	1.51	0.32	1.06	4.96	0.18
	Session 2	3.00	1.54	0.78	1.98	0.70
	Session 3	0.08	0.64	0.91	4.16	1.48
	Session 4	1.07	0.67	2.63	4.86	1.08
	Session 5	2.16	1.33	0.02	6.48	0.71
Day 3	Session 1	1.73	1.72	1.16	0.64	0.61
	Session 2	1.56	1.33	2.26	0.80	0.27
	Session 3	1.97	2.13	0.86	2.79	2.12
	Session 4	1.48	2.17	1.28	2.31	0.57
	Session 5	2.61	3.01	0.67	0.17	0.15
	Average (mm)	1.81	1.52	1.16	2.35	0.93
	SD (mm)	0.98	0.86	0.79	1.96	0.79

Total Average (mm)	1.56	Total SD (mm)	0.56

Table 7: Free breathing intra-session reproducibility

Intra- session reproducibility for HFPV breathing was calculated to be 1.50 mm (SD: 0.82). The results are represented in ***Table 8***.

HFPV Intra-Session Reproducibility (mm)						
		V#1	V#2	V#3	V#4	V#5
Day 1	Session 1	1.35	4.87	1.17	2.99	0.42
	Session 2	1.23	0.30	1.10	0.77	0.13
	Session 3	2.38	3.27	0.96	1.86	0.17
	Session 4	0.64	0.01	1.44	0.22	0.28
	Session 5	3.35	0.18	0.40	0.18	0.09
Day 2	Session 1	0.59	2.89	2.36	1.12	0.56
	Session 2	4.05	7.53	0.63	2.15	0.30
	Session 3	2.30	1.55	0.65	0.78	0.10
	Session 4	0.49	4.76	1.99	3.00	1.36
	Session 5	4.24	0.69	0.86	1.79	0.68
Day 3	Session 1	4.55	2.15	2.11	1.75	0.16
	Session 2	1.81	6.05	0.58	0.16	0.63
	Session 3	2.71	2.33	1.87	0.46	0.09
	Session 4	1.64	0.22	0.94	0.06	0.43
	Session 5	1.09	0.10	0.95	1.41	1.04
	Average (mm)	2.16	2.46	1.20	1.25	0.43
	SD (mm)	1.36	2.41	0.61	0.99	0.38
	Total Average (mm)	1.50		Total SD (mm)	0.82	

Table 8: HFPV intra-session reproducibility

1.27.4.2 I nter-Session Reproducibility

For free breathing inter-session reproducibility was 1.10 mm (SD: 1.27)

Free Breathing Inter-Session Reproducibility

	Day 1	Day 2	Day 3	Largest Delta (mm)
V#1	2.00	1.57	1.87	0.44
V#2	1.58	0.90	2.07	1.17
V#3	1.17	1.08	1.25	0.17
V#4	1.21	4.49	1.34	3.27
V#5	1.22	0.83	0.74	0.47
			Average (mm)	1.10
			SD (mm)	1.27

Table 9: Free-breathing inter-session reproducibility

For HFPV breathing inter-session reproducibility was 0.80 mm (SD: 0.6)

HFPV Breathing Inter-Session Reproducibility

	Day 1	Day 2	Day 3	Largest Delta (mm)
V#1	1.79	2.33	2.36	0.57
V#2	1.73	3.48	2.17	1.76
V#3	1.02	1.30	1.29	0.28
V#4	1.21	1.77	0.77	1.00
V#5	0.22	0.60	0.47	0.38
			Average (mm)	0.80
			SD (mm)	0.60

Table 10: HFPV-breathing inter-session reproducibility

On average the changes made to the settings of the Percussionaire device from day-to-day for all volunteers were 3.27, 0.36, 6.91, and 0.73% for inspiration time, frequency, pressure and CPAP, respectivally (***Table 11***). Range of change for each dial varies between increments of 1 (0%) to 12 (100%).

	Average Change(%)
A Insp Time	3.27
B Frequency	0.36
C Flow Pressure	6.91
D CPAP	0.73

*1 incremental dial introduces ~ 9% change

Table 11: Daily adjustments of the Percussionaire parameters

1.27.5 Discussion

The aim of this study was to calculate our ability to reproduce position. All measurements were calculated based on chest wall motion, therefore reproducibility of the tumor may or may not be the same as that of the chest-wall.

The total average intra- session reproducibility for free breathing was 1.56 mm +/- 0.56 mm and for HFPV 1.50 mm +/- 0.82 mm. Although, these results are promising in our abilities to position the patient at the desired location in the event that the treatment was interrupted, the main factor that can alter the results is the amount of initial volume of air that the patient inhales at onset of HFPV. It was noted that HFPV maintained consistent volume delivery, however taking the voluntary mid- or full- inhale breath at onset of HFPV allowed for the slight variations in chest-wall positioning. Therefore, it is recommended that the patients are provided with adequate HFPV training (approximately 1 hour) to establish good familiarity with the device as well as their ability to take the consistent *initial* volume at onset of HFPV.

The total maximum inter-session variability was calculated to be 1.10 mm +/- 1.27 mm for free breathing and 0.80 mm =+/- 0.6 mm for HFPV breathing. Recalling that although each day the volunteer was setup with the same percussionare settings as the day prior, slight adjustments were made per volunteer's request. These adjustments were on an average +/-1 increment (***Table 11***) where each increment introduced >10 % change. Therefore, we believe that patients can be consistently setup from day to day, but minor adjustments of the pressure, cpap, inspiration time and frequency maybe needed (+/- 5%).

Consistency in free-breathing was simply calculated for comparison. It was noted that almost all volunteers increased their inhale air volume for the first 10 seconds after HFPV was turned off (deeper free-breathing). We attribute this to our natural receptors and probably CO_2 level increase (Section 1.28). Additionally, chest-wall position for some volunteers experienced and spike of about 6 to 10 seconds before leveling off. We believe that this is due to the CO_2 levels (Section 7.4).

Volunteers noted that the weight of the new Beaumont prototype would cause the mouthpiece to move, therefore causing loss of pressing. Further fixation changes will be made to the prototype to ensure stability of the device on the patient while prolonging their comfort and percussions. Therefore, this study only looked at the reproducibility of HFPV sessions with the 1-minute window. Therefore, reproducibility for longer than 1-minute intervals maybe different.

1.27.6 Conclusions

The reproducibility of HFPV is <2 mm, however it could vary depending on the initial lung volume at onset of HFPV. Up to +/- 10 % adjustments for some of the Percussionaire parameters maybe needed daily.

1.28 CO_2 and Amplitude Drifts during HFPV

During initial measurements it was noted that, at onset of HFPV, chest-wall motion experienced an initial peak before it leveled off approximately 6 to 10 seconds later ***Figure 0-9***. Additionally, the consistency and peak-to-peak motion of HFPV began to deteriorate after a few minutes under HFPV (> 3 to 5 minutes). This was further investigated and concluded that CO_2 levels play a direct role in baseline drift.

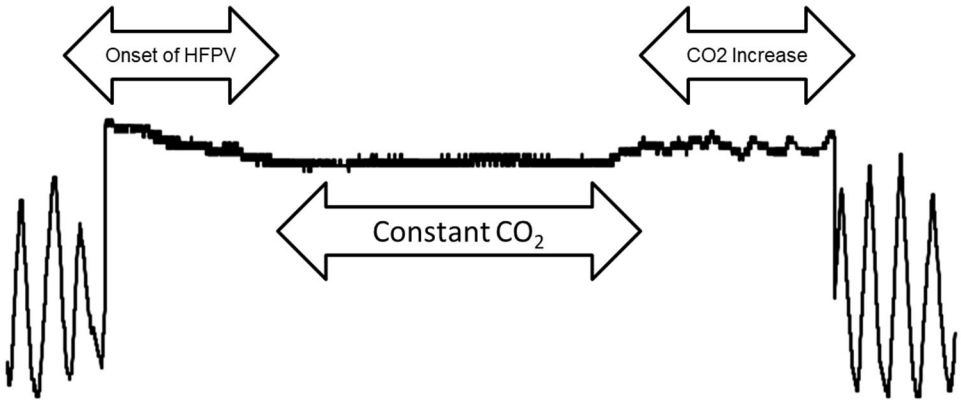

Figure 0-9: First arrow indicates the initial peak of chest-wall motion during onset of HFPV and the second arrow represents the increase in CO_2

The CO_2 levels were recorded throughout the HFPV session and it was noted that at onset of HFPV the CO_2 level begins to drop due to the initial continuous positive air pressure ***Figure 0-10***. This decrease in CO_2 directly

correlates with the initial chest-wall motion of HFPV that was noted on most volunteers. There is a leveling off window of the CO_2 which is an indication of good ratio of O_2 to CO_2 exchange in the patient, therefore having a specifically designed oral mask that would provide equal exchange is critical in maintaining reproducibility and consistency.

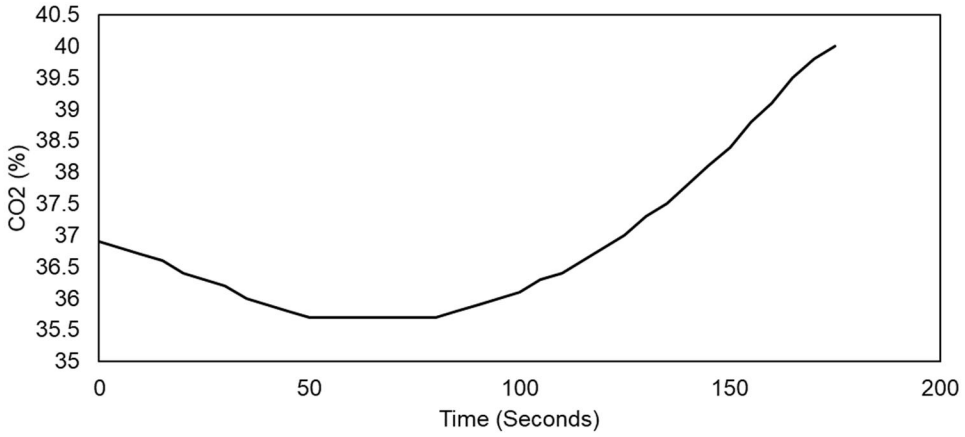

Figure 0-10: CO_2 level during HFPV

Similarly, as the CO_2 level increased the HFPV became less consistent. This data is overlaid with the HFPV curve of the same patient/time in **Figure 0-11**. It is evident that as CO_2 decreases at onset of HFPV the chest wall motion experiences an initial decrease. While the CO_2 is maintained constant, the HFPV is consistent and therefore desirable. Subsequently, as CO_2 beings to increase, HFPV becomes less consistent which results in patient's desire to terminate the session.

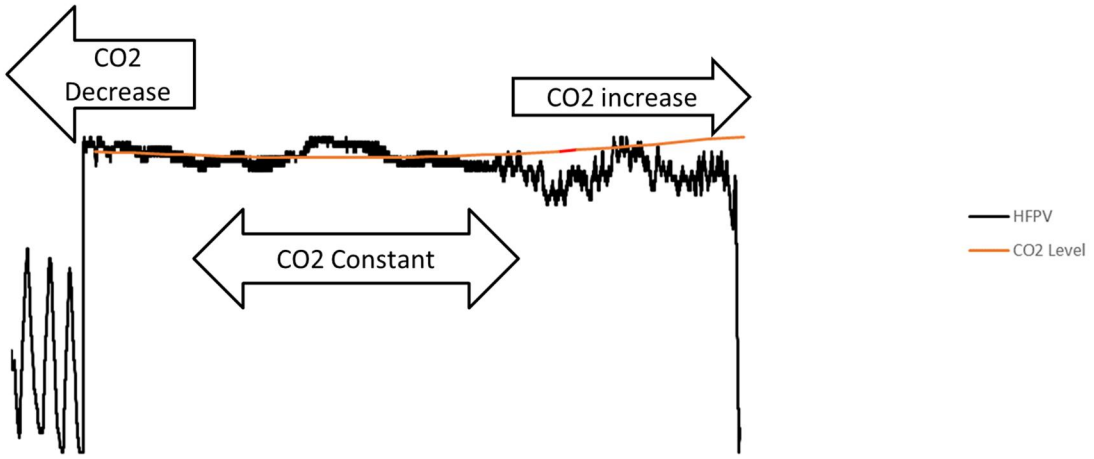

Figure 0-11: Correlation of CO_2 and *HFPV Chest wall Motion*

Furthermore, we investigated whether CO_2 is linearly correlated to peak-to-peak amplitude drift of HFPV. The upward drift of CO_2 in the top right section of graph in **Figure 0-11** had a slope of 3.9 mm (Max – Min), for the same corresponding HFPV curve the downward drift had a slope of 4.2 mm. These results were further tested with a balloon experiment.

1.28.1 Methods

A plastic balloon was inflated to maximum capacity and the Anzai laser system was projected as in all prospective studies (***Figure 0-12***). In the first experiment, inspiration time, CPAP and pressure dial were kept constant while the frequency was incrementally changed from the highest dial (1) to the lowest (12), while simultaneously acquiring motion amplitude of the balloon with the Anzai system.

For the second experiment, the inspiration time, CPAP, and frequency dial were kept constant, while pressure dial was incrementally changed from the highest (1) to lowest (12).

Lastly, for the third experiment, inspiration time and CPAP dial were kept constant while simultaneously changing both the flow and the frequency. The pressure increased incrementally from the lowest (12) to the highest (1) dial, while the frequency decreased by the same amount.

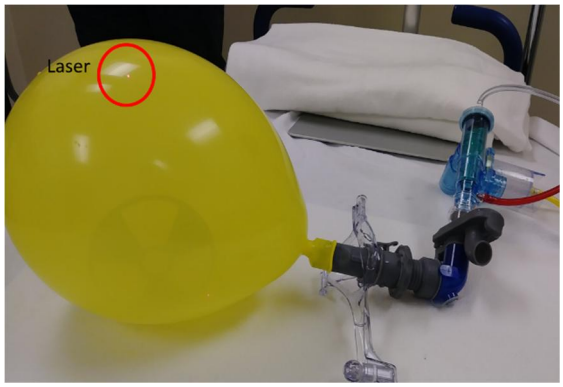

Figure 0-12: Setup of the Balloon measurements

The manual dial of 12 (~8 %) indicated the lowest and 1 (100 %) indicated the highest. The mean distance from the laser to the balloon was used for each change in frequency, pressure or both.

1.28.2 Results

Each increment on the frequency dial, from 3 to 9, resulted in a slope of 0.4 mm (***Figure 0-13***), indicating that every incremental dial on the frequency knob may introduce an upward or downward (depending on direction) drift of about 0.4 mm for each turn.

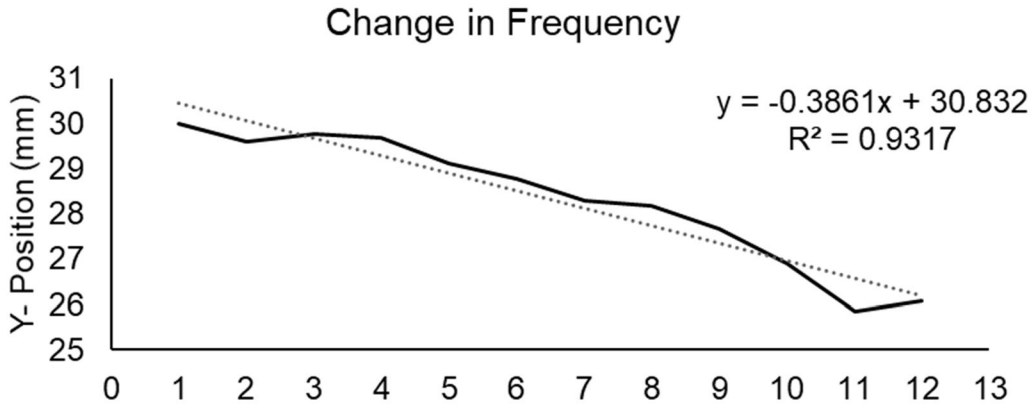

Figure 0-13: Incremental Change in Frequency. Frequency went from highest (1) dial to lowest (12).

Similarly, incremental changes on the pressure dial between the range of 3 to 9, resulted in an average slope decrease of 1.21 mm (***Figure 0-14***). Indicating that decreasing the pressure dial by one increment would subsequently decrease the baseline drift slope by 1.21 mm.

Changing both frequency and pressure resulted in a slope of 0.3 mm (***Figure 0-15***). A composite of all data is given in ***Figure 0-16***.

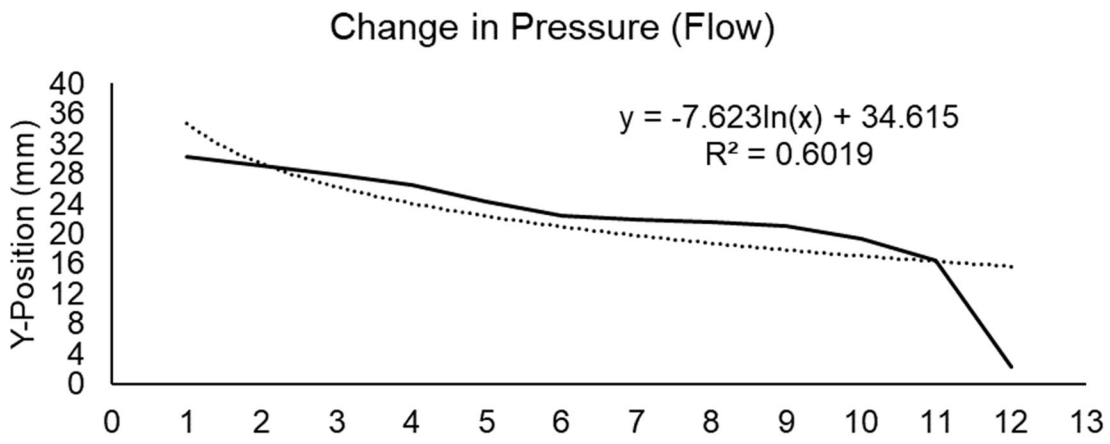

Figure 0-14: Incremental Change in Pressure. Pressure went from highest (1) dial to lowest (12).

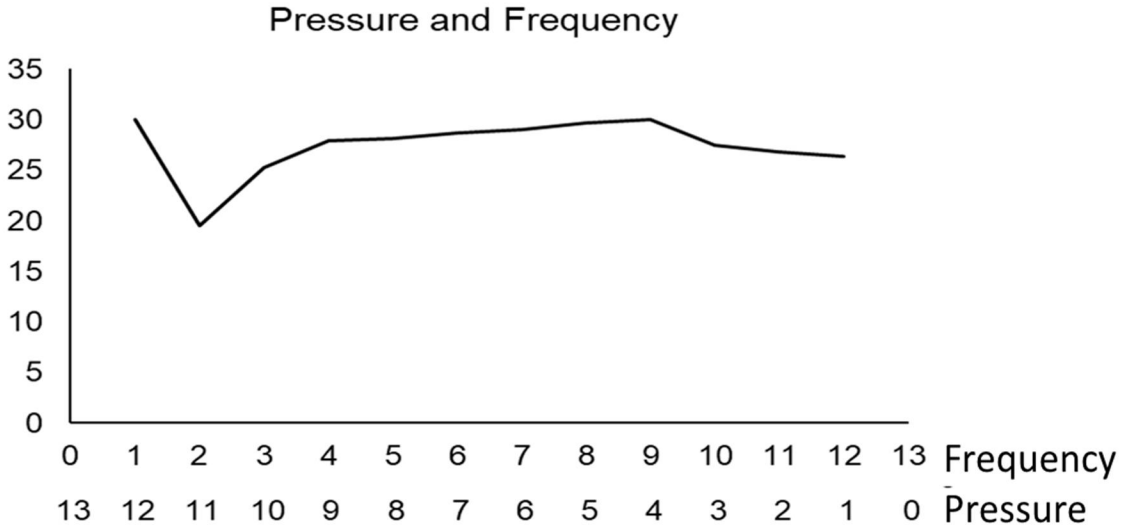

Figure 0-15: Incremental both Pressure and Frequency. Frequency went from highest (1) dial to lowest (12) and Pressure in the opposite direction

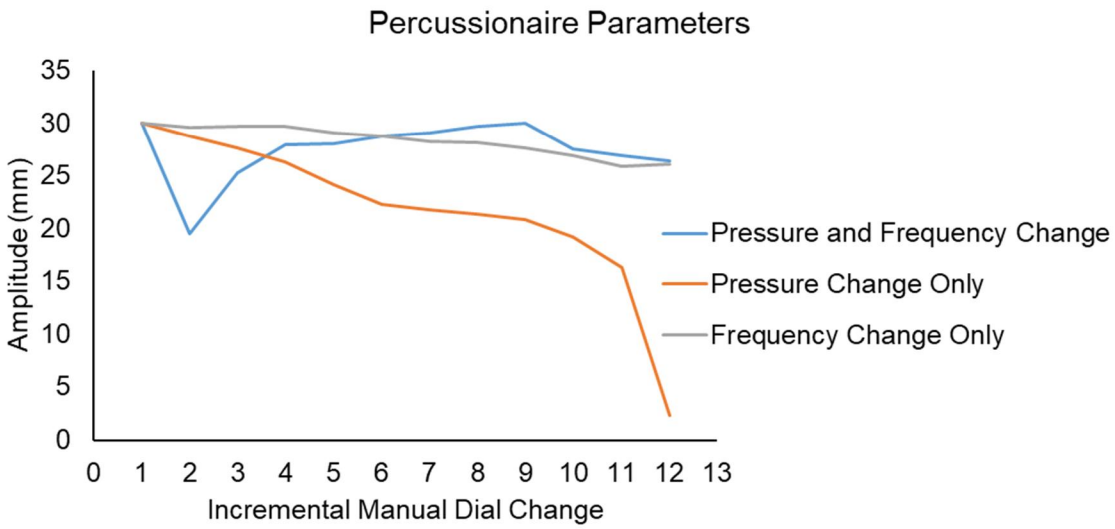

Figure 0-16: Composite data

1.28.3 Discussion

It is evident from the results that the initial decrease in CO_2 level plays an important role in the initial spike at onset of HFPV. As a result, if HFPV is used for imaging or radiotherapy, it is important to do so 6 to 10 seconds post HFPV initiation. It would allow for the CO_2 to O_2 ratio to become constant.

Change in frequency behaved in a linear fashion with an R^2 value of 0.9317, but the average slope between each dial was higher for the pressure knob. Indicating that changing the pressure has a higher effect on the ability of the lungs to stay inflated than the frequency. However, the high frequency rate is necessary to maintain the appropriate CO_2 and O_2 gas exchange. Therefore, results in ***Figure 0-15*** are promising. Likewise, changes in pressure behaved linearly between the dials of 3 and 9 with an R^2 value of 0.9192 and slope of 1.18 mm.

Adjustments between pressure and frequency made in the third experiment, resulted in a slope of 0.3 mm, however it maybe the desired method as it would allow the user to slowly adjust for amplitude drifts while maintaining good pressure and frequency without introducing discomfort to the patient.

In Section 1.27, the mean intra- and inter- fraction reproducibility was 1.50 mm (SD: 0.82) and 0.80 mm (SD: 0.6), respectively which is within the range of our ability to adjust the pressure and frequency dial while the patient is in HFPV, which would correct for any amplitude drifts or CO_2 increase. These changes would allow the clinicians to comfortably keep the patient in HFPV for the entire duration of their treatment.

Lastly, it is critical that a balance between pressure and frequency is maintained during HFPV. The pressure would allow for the lungs to stay inflated while the frequency allows for good exchange of CO_2 to O_2. Ideally the rate of exchange should be $^{CO_2}/_{O_2} = 1$, an indication that the oxygen bursts are entering the lungs just as fast as CO_2 is leaving. If the $^{CO_2}/_{O_2}$ ratio is >1 the CO_2 will continue to rise, triggering the patient to stop HFPV. Conversely a $^{CO_2}/_{O_2}$ ratio of <1 can result in alkalosis.

1.28.4 Conclusions

Maintaining a unity ratio of CO_2/ O_2 is critical in prolonging HFPV times as well as reproducibility. Incremental changes in the frequency and pressure dial of the Percussionaire could allow for adjustments in amplitude drifts during treatment or daily positioning.

CHAPTER 8: CONCLUSIONS OF DISSERTATION

1.29 Hypothesis Restatement

It was hypothesized that HFPV:

1. HFPV provides direct tumor immobilization of <5 mm for all targets exhibiting respiratory motion >10 mm
2. HFPV reproducible thoracic immobilization with <5 mm residual motion, over 1-minutes intervals with rebreathing between each instance.
3. Significantly reduces the interplay effects noticed in pencil beam scanning proton radiotherapy.
4. HFPV can significantly reduce the PTV margin for thoracic targets and subsequently healthy tissue toxicity

1.30 Set Aims

1.30.1 Set Aim I

The primary objective of this study is to test if HFPV can be a viable method for thoracic immobilization

1.30.2 Set Aim II

A second primary objective is to evaluate if HFPV can reduce lung tumor motion from ≥ 10 mm to < 5 mm. This will be the ***first*** study to directly measure tumor motion reduction using HFPV.

1.30.3 Set Aim III

A second objective is to evaluate the reproducibility of HFPV immobilization. Will the target return to the same location after re-breathing then repeat HFPV?

1.30.4 Set Aim IV

Another secondary objective is to evaluate the interplay effects of HFPV motion.

1.31 Hypothesis Response

1. In Chapter 1.24 we were the first to directly measure tumor motion with HFPV. Despite patients' history of COPD and a peak pressure less than desired (12cmH2O vs 20cmH2O), tumor motion was reduced from 10 mm in 4DCT to 2.67 mm
2. This is the first study to directly measure reproducibility of HFPV as a technique for thoracic immobilization. In Chapter 1.27.4 mean intra-fraction reproducibly (N_{ss}=75) was calculated at 1.50 mm (SD: 0.82) and inter-fraction at 0.80 mm (SD: 0.6).
3. The interplay effects for proton PBS were significantly reduced. In Chapter 1.21.1 it was concluded that Gamma passing rate, with 3%/3mm and 10% threshold criteria, improved from 77.03 % during free-breathing to 99.20 % during HFPV breathing. Similarly, hot and cold spots were drastically reduced from 10-30% to 5-10% during HFPV.

4. In Chapter 1.25.9 it was concluded that although the margin applied from ITV to PTV was kept at 5 mm, the PTV volume was drastically reduced during HFPV. In free-breathing PTV volume was 12.037 cc vs. 4.7 cc for HFPV. Similarly, V20 and V5 of the lung was drastically reduced from a mean of 5.44 Gy (Range: 3.3 -7.97Gy) to 1.94 Gy (Range: 1.68 – 2.46 Gy) for V20 and 16.49 Gy (Range: 14.3 – 20.24 Gy) to 10.74 Gy (Range: 8.84 – 13.31 Gy), for V5 for Free vs. HFPV breathing respectively.

1.32 Long Term Goal and Future Work

Future use of HFPV will entail multiple aspects of radiotherapy as indicated in ***Figure 0-1***.

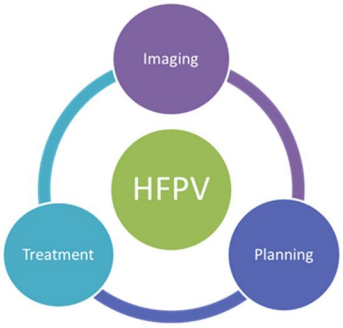

Figure 0-1: Long term goals of HFPV

1.32.1 Imaging:

Further work will be performed in determining the benefits of HFPV for reducing motion artifacts in a multi-modality setting like MR, CT and PET. Prior work by (Beigelman-Aubry, et al., 2017) reported a drastic increase in spatial resolution of chest MRI for volunteers undergoing pulsatile flow, similarly (Prior

J. a., 2016) reported an increase in legion SUV for patients undergoing pulsatile flow. Utilizing HFPV for all image modalities in radiotherapy is feasible and further work will be performed to validate them. An MRI protocol with HFPV has already been written and submitted to the IRB for approval.

1.32.2 Planning:

We have shown that HFPV can drastically reduce dose to the OARs while still maintaining high target dose. Our future directions include application of HFPV to proton radiotherapy as well as heart ventricular tachycardia. A recent publication (Cuculich, et al., 2017) validates the importance of radiotherapy for ventricular tachycardia, however no respiratory motion was used in the study. Therefore, future work entails using HFPV for ventricular tachycardia due to its prolonged time as well as reproducibility.

1.32.3 Treatment:

In this study we have shown great benefits of using HFPV in PBS, photon and MR setting. Our future direction entails the use of HFPV for treating lung cancer with MR-Linac as well as conventional photon or proton accelerators.

ABBREVIATIONS

BIBLIOGRAPHY

{Keall, P. a. (2007). Respiratory regularity gated 4DCT acquisition: concepts and proof of principle. *Australasian Physical and Engineering Sciences in Medicine, 30*(3).

Allan, P. e. (2010). High-frequency percussive ventilation revisited. *Journal Burn Care Res, 30*(1), 510-20.

Allan, P., Osborn, E., Chung, K., & Wanek, S. (2010). High Frequency percussive ventilation revisted. *J Burn Care Res*, 510-20.

Allen A, Pawlicki, T., Dong, L., Fourkal, E., Buyyounouski, M., CengelK, . . . Konski, A. (2012). An evidence based review of proton beam therapy: The report of ASTRO's emerging technology committee. *Radiotherapy and Oncology, 103*, 8-11.

Armstrong, J. e. (1993). Three-dimensional conformal radiation therpay may improve the therapeutic ratio of high dose radiation therapy for lung cancer. . *International Journal of radiation oncology, Biology, Physics, 26*(4), 685-9.

Attix, F. H. (1986). Charged Particles Interactions in Matter. In *Introduction to Radiological Physics and Dosimetry* (p. 160). Madison, Wisconsin: John Wiley and Sons, Inc.

Baues, C., Marnitez, S., Engert, A., Baus, W., Jablosnka, K., Fogliata, A., . . . cozzi, L. (2018). "A planning comparison of deep inspiration breath hold

intensity modulation radiotherapy and intensity modulated proton therapy. *Radiation Oncology, 13*, 122.

Beigelman-Aubry, C., Peguret, N., Stuber, M., Delacoste, J., Belmondo, B., Lovis, A., . . . Bourhis, J. (2017). Chest-MRI under pulsatile flow ventilation: A new promising technique. *PloS One*, 12(6): e0178807.

Berman, A., James, S., & Rengan, R. (2015). Proton beam Therapy for Non-Small Cell Lung Cancer: current clinical evidence and future directions. *cancers, 7*, 1178-1190.

Bernatowicz, K., Lomax, A., & Knopf, A. (2013). Comperative study of layered and volumetric rescanning for different scanning speeds of proton beam in liver patients. *Physics Medicine and Biology, 58*(22), 7905-20.

Bert, C. a. (2008). Quantification of interplay effects of scanned particle beams and moving targets. *hysics in Medicine and Biology, 53*, 2253-2265.

Bert, C. a. (2008). Quantification of interplay effects of scanned particle beams and moving targets. *Physics in Medicine and Biology, 53*, 2253-2265.

Boda-Heggemann, J. e. (2016). Deep Inspiration breath Hold-Based Radiation Therapy: a clinical review. *International journal of Radiation Oncology Biology Physics, 94*(3), 478-492.

Bouilhol, G. a. (2013). Is abdominal compression useful in lung stereotactic body radiation therapy? A 4DCT and dosimetric lobe-dependent study. *European Journal of Medical Physics*, 333-340.

Bouilhol, G., Ayadi, M., Rit, S., Thengumpallil, S., Schaerer, J., Vandemeulebroucke, J., . . . Sarrut, D. (2013). Is abdominal compression useful in lung stereotactic body radiation therapy? A 4DCT and dosimetric lobe-dependent study. *European Journal of Medical Physics*, 333-340.

Castriconi, R., Ciocca, M., Mirandola, A., Sini, C., Broggi, S., Schwartz, M., . . . Arico, G. (2017). ose-response of EBT3 radiochormic films to proton and carbon ion clinical beams. *Physics in Medicine and Biology, 62*, 377-393.

Chang, J., Jabbour, S., DeRuysscher, D., Schild, S., Simone, C., RenganR, . . . Hoppe, B. (2016). Consensus statement on proton therapy in early-stage and locally advanced non-small cell lung cancer. *International Journal of Radiation Oncology Biology Physics, 95*(1), 505-516.

Chang, J., Zhang, X., Knopf, A., Li, H., Mori, S., Dong, L., . . . Zhu, X. (2017). Consensus Guidelines for Implementing Pencil-Beam Scanning Proton therapy for Thoracic Malignancies on Behalf of the PTCOG Thoracic and Lymphoma Subcommittee. *International Journal of Radiation Oncology, 99*(1), 41-50.

Chang, J., Zhang, X., Knopf, A., Li, H., Mori, S., Dong, L., . . . Zhu, X. (2017). Consensus Guidelines for Implementing Pencil-Beam Scanning Proton Therapy for Thoracic Malignancies on Behalf of the PTCOG Thoracic and LYmphoma Subcommittee. *International Journal of Radiation Oncology Biology Physics, 99*(1), 41-50.

Chang, J., Zhang, X., Wang, X., Kang, Y., Riley, B., Bilton, S., . . . Cox, J. (2006). Significant reduction of normal tissue dose by proton radiotherapy compared with three-dimensional conformal or intensity-modulated radiation therapy in Stage I or Stage III non–small-cell lung cancer. *International Journal of Radiation Oncology Biology Physics, 65*, 1087-1096.

Chung, K. e. (2010). High-frequency percussive ventilation and low tidal volume ventilation in burns: A randomized controlled trial. *Critical Care Medicine, 38*(10).

Ciocca, M., Mirandola, A., Molinelli, S., Russo, S., Mastella, E., Vai , A., . . . Baroni, G. (2016). Commissioning of the 4-D treatment delivery system for organ motion management in synchrotron-based scanning ion beams. *Physica Medica, 32*, 1667-1671.

Cole, A., Hanna, G., Jain, S., & O'Sullivan, J. (2014). Motion Management for Radical Radiotherapy in NOn-small cell Lung Cancer. *"Clinical Oncology, 26*, 67-80.

Cuculich, P., Schill, M., Kashani, R., Mutic, S., Lang, A., Cooper, D., . . . Robinson, C. (2017). Noninvasive Cardiac Radiation for Ablation of Ventricular Tachycardia. *New England Journal of Medicine, 377*(24).

Curie, M. (1967). Nobel Lectures, Physics 1901-1921. *Elsevier Publishing Company*.

Das, I., Cheng, C.-W., Watts, R., Ahnesjo, A., Gibbons, J., Li, X., . . . Zhu, T. (2008). *Accelerator beam data commissioning equipment and procedures: Report of the TG-106 of the Therapy Physics Committee of the AAPM.* AAPM Medical Physics.

Dasu, A., Flejmer, A., Edvardsson, A., & Nystrom, P. (2018). Normal tissue sparing potential of scanned proton beams with and without respiratory gating for the treatment of internal mammary nodes in breast cancer radiotherapy. *Physica Medica, 52*, 81-85.

De Ruysscher, D., Sterpin, E., Haustermans, K., & Depuydt, T. (2015). Tumour Movement in Proton Therapy: Solutions and Remaining Questions: A Review. *Cancers*, 1143-53.

Dou, T., Thomas, D., O'connell, D., Bradley, J., lamb, J., & Low, D. (2015). Technical Note: Simulation of 4DCT tumor motion measurements errors. *Medical Physics, 42*(10), 6084-6089.

Dowdell, S., Grassberger, C., Sharp, G., & Paganetti, H. (2013). Interplay effects in proton scanning for lung: a 4D Monte Carlo study assessing the impact of tumor and beam delivery parameters. *Physics in Medicine and Biology, 58*, 4137-4156.

Espana, S., & Paganetti, H. (2011). Uncertainties in planned dose due to the limited voxel size of the planning CT when treating lung tumors with proton therapy. *Physics in Medicine and Biology, 56*, 3843-3856.

Evans, P., Coolens, C., & nioutsikou, E. (2006). Effects of averaging over motion and the resulting systematic errors in radiation therapy. *Medical Physics and Biology, 51*, N1-7.

Evans, P., Coolens, C., & Nioutsikou, E. (2006). Effects of averaging over motion and the resulting systematic errors in radiation therapy. *Physics in Medicine and Biology, 51*, N1-N7.

Faiz Khan, P. (2003). Clinical radiation Generators. In *The Physics of Radiation Therapy* (p. 43). Philladelphia, PA: Lippincott Williams & Wilkins.

Faiz Khan, P. (2003). Structure of Matter. In *The Physics of Radiation Therapy* (p. 9). Philadelphia, PA: Lippincott Williams & Wilkins.

Fiorini, f., Kirby, D., Thompson, J., green, S., Parker, D., Jones, B., & Hill, M. (2014). Under-response correction for EBT3 Films in the presence of proton spread out Bragg Peaks. *Physica Medica, 30*, 454-461.

Frank Herbert Attix, P. (1986). Charged-Particle Interactions in Matter. In *Introduction to Radiological Physics and Radiation Dosimetry* (p. 160). Madison, Wisconsin: Wiley-VCH Verlag GmBh & Co. KgaA.

Frank Herbert Attix, P. (1986). Charged-Particle Interactions in Matter. In *Introduction to Radiological Physics and Radiation Dosimetry* (p. 162). Madison, Wisconsin: Wiley-VCH Verlag GmbH & Co, KGaA.

Fritz, P., Kraus, H., Muhlnickel, W., Sassmann, V., Hering, W., & Strauch, K. (2010). High-Frequency jet ventilation for complete target immobilization

and reduction of planning target volume in stereotactic high single dose irradiation of stage I non-small cell lung cancer and lung metastases. *International Journal of Radiation Oncology Biology Physics, 78*(1), 136-142.

Gallagher, T. e. (1989). High-frequency percussive ventilation compared with conventional mechanical ventilation. *Critical Care med, 17*(4), 364-6.

Gatani, T. e. (2010). Management of Localized Pneumothoraces After Pulmonary Resection With Intrapulmonary Percussive Ventilation. *The Annals of Thoracic surgery, 90*(5), 1658-1661.

Girard, f., Hugo, B., & LacroixF. (2012). References dosimetry using radiochromic film. *Journal of Applied clinical medical Physics, 13*(6).

Glide-Hurst, C., Gopan, E., & Hugo, G. (2010). Anatomic and Pathologic Variability during Radiotherapy for a Hybrid Active Breath-Hold Gating Technique. *International Journal of Radiation Oncology*, 910-917.

Gomez, D., Gillin, M., Liao, Z., Wei, c., Lin, S., Swanick, C., . . . Chang, J. (2013). Phase 1 Study of Dose Escalation in Hypofractinated Proton Beam Therapy for Non-Small Cell Lung Cancer. *International Journal of Radiation Oncology Biology Physics, 85*(4), 665-670.

Grassberger, C., Daartz, J., Dowdell, S., Ruggieri, T., Sharp, G., & Paganetti, H. (2014). Quantification of proton dose calculation accuracy in the lung. *International Journal of Radiation Oncology Biology and Physics, 89*(2), 424-430.

Guang-wen, L. a.-w.-y.-z.-f. (2011). Investigation on the impact to beam characteristics of a linear accelerator related to duty cycle of respiratory gating. *Radiation Measurements, 46*, 1996-1999.

H, P. (2002). Nuclear interactions in proton therapy: dose and relative biological effect distributions originating fromprimary and secondary particles. *Physics of Medicine and Biology, 47*, 747-764.

Harada, K., Katoh, N., Suzuki, R., Ito, Y., Shimizu, S., Onimaru, R., . . . Shirato, H. (2016). Evaluation of motion of lung tumors during stereotactic body radiation therapy (SBRT) with four-dimensional computed tomoghrapy (4DCT) using real-time tumor tracking radiotherapy system (RTRT). *Physica Medica, 32*, 306-311.

Heinz, C. a. (2015). Technical evaluation of different respiratory monitoring systems used for 4DCT acquisition under free breathing. *Journal of Applied Clinical Medical Physics, 16*(2).

Herfarth, K. e. (2000). Extracranial stereotactic conformal radiation treatment of tumors in the liver and the lung. . *International Journal of Radiation Oncology Biology Physics, 41*(1S), 214.

Hospital, R. U. (2015). *Lung cancer radiotherapy using realtime dynamic Multileaf Collimator Adapation and radiofrequency tracking.* Retrieved from https://Clinicaltrials.gov/show/NCT02514512

Huang, S., Kang , M., Souris, K., & Ainsley, C. (2018). Validation and clinical implementation of an accurate Monte Carlo code for pencil beam

scanning proton therapy. *Journal of Applied Clinical Medical Physics, 19*(5), 558-572.

Hui, Z., Zhang, X., Starkschall, G., Li, Y., Mohan, R., Komaki , R., . . . Chang, J. (2008). Effects of interfractional motion and anatomic changes on proton therapy dose distribution in lung cancer. *International Journal of Radiation Oncology Biology Physics, 72*(5), 1385-1395.

ICRU 50, R. (1993). *ICRU Report 50: Prescribing, Recording, and Reporting Photon Beam Therapy.* Washington, D.C: Internal Commission on Radiation Units and Measurements:.

ICRU 60, R. (1999). *ICRU Report 62: Prescribing, Recording and Reporting Photon Beam Therapy (Supplement to ICRU Report 50).* Washington, D.C.: International Commission on Radiation Units and Measurements.

Ionascu, D. a. (2007). Internal and external correlation investigations of respiratory induced motion of lung tumors. *{Medical Physics, 34*, 3893-3903.

Jakobi, A., Perrin, R., Knopf, A., & Richter, C. (2018). Feasibility of proton pencil beam scanning treatment of free-breathing cancer patients. *Acta Oncologica, 57*(2), 203-210.

Jiang, S. (2006). Technical aspects of image-guided respiratoion-gated radiation therapy. *Medical Dosimetry, 31*(2), 141-151.

Kang, M., Huang, S., Solberg, T., Mayer, R., Thomas, A., Teo, B., . . . Lin , L. (2017). A study of the beam-specific interplay effect in proton pencil beam scanning delivery in lung cancer. *Acta Oncology, 56*(4), 531-540.

Kardar, L., Li, Y., & Li, X. (2014). Evaluation and mitigation of the interplay effects of intensity modulated proton therapy for lung cancer in a clinical setting. *Medical Physics, 4*, e259-e267.

Kazerooni, E. e. (1996). Risk of pneumothorax in CT-guided transthoracic needle aspiration biopsy of the lung. *Radiology, 198*(2), 371-375.

Keall , P., Kini, V., Vedam , S., & Mohan, R. (2002). Potential radiotherapy improvements with respiratory gating. *Australaian Phyical & Engineering Sciences in Medicine*, 1-6.

Keall, e. a. (2006). Geometric accuracy of a real-time target tracking system with dynamic multileaf collimator tracking system. . *International Journal of Radiation Oncology Biology Physics, 65*(5), 1579-1584.

Keall, P., Mageras, G., Balter, J., Emery, R., Forster, K., Jiang, S., . . . Yorke, E. (2006). The management of respiratory motion in radiation oncology report of AAPM Task Group 76a. *Medical Physics*, 3874-3900.

Khan, F. (2003). The Physics of Radition Therapy. In F. Khan, *The Physics of Radiation Therapy* (pp. 38-58). Philadelphia, PA: Lippincott Williams & Wilkins.

Kilburn, J. e. (2016). Is a clinical target volume CTV necessary in the treatment of Lung cancer in the Modern Era Combining 4-D Imaging and Image-guided Radiotherapy (IGRT)? *Cureus, 8*(1), e466.

Kogel, M. J. (2009). Irradiation-induced damage and the DNA damage response. In *Basic Clinical Radiobiology* (pp. 11-12). Detroit, MI: CRC Press taylor & Francis Group.

Korreman, S. (2015). Image-guided radiotherapy and motion management in lung cancer. *British Institute of Radiology, 88*.

Kubo, H. a. (1996). Respiration gated radiotherapy treatment: a technical study. . *Physics in Medicine & Biology, 41*(1), 83-91.

Lagendijk, J., Raaymakers, B., Van Den Berg, C., Moerland, M., Philippens, M., & van Bulpen , M. (2014). MR guidance in radiotherapy. . *Physics of Medicine and Biology*, 59(21): R349-69.

Lambert, J., Suchowerska, N., McKenzie, D., & Jackson, M. (2005). Intrafractional motion during proton beam scanning. *Physics Medical Biology, 50*(20), 4853-4862.

Langen, K. a. (2001). Organ motion and its management. *International Journal of Radiation Oncology Biology and Physics, 50*, 265-78.

Langen, K., & Zhu, M. (2018). Concepts of PTV and Robustness in Passively Scattered and Pencil Beam Scanning Proton Therapy. *Seminars in Radiation Oncology, 28*, 248-255.

Laurent, F. e. (1999). Pneumothoraces and chest tube placement after CT-guided transthoracic lung biopsy using a coaxial technique: incidence and risk factors. *American journal of Roentgenology, 172*(4), 1049-1053.

Li, X. e. (n.d.). Margin reduction from image guided radiation therapy for soft tissue sarcoma: Secondary analysis of Radiation therapy Oncology Group 0630 results. *Electronic*, 1879-8519.

Li, Y., kardar, L., Li, X., Li, h., Cao, W., Chang, J., . . . Zhang, X. (2014). On the interplay effects with proton scanning beams in stage III lung cancer. *Medical Physics, 41*(2), 021721.

Liang, J. e. (n.d.). The effect of image-guided radiation therapy on the margin between the clinical target volume and planning target volume in lung cancer. *Print*, 2051-3895.

Liao, Z., Gandhi, S., Lin, S., & Bradley, J. (2018). Does Proton Therapy Offer Demonstrable Clinical Advantages for Treating Thoracic Tumors? *Seminars in Radiation Oncology, 28*, 114-124.

Lin, L., kang, M., Sheng, H., & MayerR. (2015). Beam-specific planning target volumes incorporating 4DCT for pencil beam scanning proton therapy of thoracic tumors. *Journal of Applied Clinical Medical Physics, 6*, 16.

Liu, H., Balter, P., Tutt, T., Choi, B., Zhang, J., Wang, C., . . . Dong, L. (2007). Assessing Respiration-induced tumor motion and internal target volume using four-dimensional computed tomography for radiotherapy of lung

cancer. *International Journal of Radiation oncology Biology and Physics, 68*(2), 531-540.

Lomax, A. (2008). Intensity modulated proton therapy and its sensitivity to treatment uncertainties 2: the potential effects of inter-fraction and inter-field motions. *Physics in Medicine and Biology, 53*, 1043-1056.

Low, D., Harms, W., Sasa, M., & Purdy, J. (1998). A technique for the quantitative evaluation of dose distributions. *Medical Physics, 25*(5), 656-661.

Lujan, A., BalterJ, & Ten Haken. (2003). A method for incorporating organ motion due to breathing into 3D dose calculations in the liver: Sensitivity to variations in motion. *American Association of Physicists in Medicine, 10*, 30.

Magnussen, H., Tetzlaff, K., Bateman, E., Watz, H., Kirsten, A., Wouters, E., . . . Calverley, P. (2016). Lung function changes over time following withdrawl of inhaled corticosteroids in patients with severe COPD. *European Respiratory Jounral , 47*, 651-654.

McNamara, J. (2008). Investigation of two respiratory monitoring systems used for 4DCT and respiratory gating.

Mohan, R., & Grosshans, D. (2017). Proton therapy - Present and Future. *Advanced Drug Delivery Reviews, 109*, 26-44.

mori, S., Kanematsu, N., Asakura, H., Sharp, G., Kumagai, M., Dobashi, S., . . . Baba, M. (2011). Four dimensional lung treatment planning in layer-stacking carbon ion beam treatment: comparison of layer-stacking and conventional ungated/gated irradiation. *Physics in Medicine and Biology, 40*(2), 597-607.

Mulkern, R., Haker, S., Mamata, H., Lee, E., Mitsouras , D., Oshio, K., . . . Hatabu, H. (2014). Lung Parenchymal Signal Intensity in MRI: A Technical Review with Educational Aspirations Regarding Reversible Versus Irreversible Transverse Relaxation Effects in Common Pulse Sequence Concepts in Magenetic Resoncance, Part A, Bridging Education and Rese. *PubMed 25228852*, 43(A) 2 29-53.

Murphy, M. J. (2004). Tracking Moving Organs in Real Time. *Seminars in Radiation Oncology, 91*.

Murphy, M. J. (2004). Tracking Moving Organs in Real Time. *Seminars in Radiation Oncology, 91*.

Murphy, M. J. (2004, January). Tracking MOving Organs in Real Time. *Seminars in Radiation ONcology*, 91.

Mutaf, Y., Scicutella, C., Michalski, D., Fallon, K., Brandner, E., Bednarz, G., & Huq, M. (2011). A simulation studyof irregular respiratory motion and its dosimetric impact on lung tumors. *Physics in Medicine and Biology, 56*, 845-859.

Nath, R., Biggs, P., Bova, F., Ling, C., Purdy, J., Geijn, J., & WeinhousM. (1994). AAPM Report NO 47. *American Association of Physicists in Medicine by the AIP, 21*.

Newhauser, W. a. (2015). The physics of proton therapy. *Institute of Physics and Engineering in Medicine, 60*, R155-209.

Nino, G. e. (2009). Use of intrapulmonary percussive ventilation (IPV) in the management of pulmonary complications of an infant with osteogenesis imperfecta. *Pediatric Pulmonology, 44*(11), 1151-1154.

Onishi, H., Shirato, H., & Nagata, Y. (2007). Hypofractionated stereotactic radiotherapy (HypoFXSRT) for stage I non-small cell lung cancer: updated results for 257 patients in a Japanese multi-institutional study. *Journal of Thoracic Oncology, 2*, S94-S100.

Paganetti, H. (2014). Relative Biological Effectiveness RBE values for proton beam therapy. Variations as a function of biological endpoint, dose and linear energy transfer. *Physics of Medicine and Biology, 59*, R419-R472.

Paganetti, H., Jiang, H., & Trofimov, A. (2005). 4D Monte Carlo simulation of proton beam scanning: modeling of variations in time and space to study the interplay between scanning pattern and time-dependent patient geometry. *Physics in Medicine and Biology, 50*, 983-990.

Pan, T. e. (2004). 4D-CT imaging of a volume influenced by respiratory motion on multi-slice CT. *Medical Physics, 31*(2), 333-40.

Park, , P., Zhu, R., Lee, A., Sahoo, N., Melancon, A., Zhang, L., & Dong, L. (2011). A beam-specific planning target volume (PTV) design for proton therapy to account for setup and range uncertainties. *Physics in Medicine and Biology, 82*(2), e329-e336.

Peguret, N. a.-d. (2016). Apnea like suppression of respiratory motion First evaluation in radiotherapy. *Radiotherapy and Oncology*, 220-226.

Peguret, N. e. (2016). Apnea-like supression of respiratory motion: First evaluation in radiotherapy. . *Radiotherapy and Oncology*, 220-226.

Perri, D., Colot, A., Delor, A., Ghoul, R., Janssens, G., Lacroix, V., . . . Geets, X. (2018). Effect of contiguous positive airway pressure administration during lung stereotactic ablative radiotherapy: a comparative planning study. *Strahlenther Onkologica, 194*, 591-599.

Persson, G., Nygaard, D., Brink, C., Jahn, J., Rosenschold, P., Specht, L., & Korreman, S. (2010). Deviations in delineated GTV caused by artefacts in 4DCT. *Radiotherapy and Oncology, 96*, 61-66.

Poulsen, P., Eley, J., LangnerU, Simone, C., & Langen, K. (2018). Efficient Interplay Effect Mitigation for proton pencil beam scanning by spot-adapted layered repainting evenly spread out over the full breathing cycle. *International Journal of Radiation Oncology Biology Physics, 100*(1), 226-234.

Prior, J. a. (2016). Reduction of Respiratory Motion During PETCT by Pulsatile Flow Ventilation A First Clinical Evaluation. *Journal of Nuclear Medicine*, 416-419.

Prior, J. e. (2016). Reduction of Respiratory Motion During PET/CT by Pulsatile-Flow Ventilation: A First Clinical Evaluation. *Journal of Nuclear Medicine*, 416-19.

PTCOG, P. T.-O. (2019, June). *Particle Therapy Co-Operative Group*. Retrieved from ptcog.ch: https://www.ptcog.ch/index.php/facilities-in-operation

Purdie, T., Moseley, D., Bissonnette, J., Sharpe, M., Franks, K., Bezjak, A., & Jaffrey, D. (2006). Respiration correlated cone-beam computed tomography and 4DCT for evaluating target motion in Stereotactic Lung Radiation Therapy. *Acta Oncologica, 45*, 915-922.

Raaymakers, B., Jurgenliemk-Schulz, I., Bol, G., Glitzner, M., Kotte , A., van Asselen , B., . . . Lagendijk, J. (2017). First patients treated with a 1.5T MRI-Linac: Clinical proof of concept of a high-precision, high-field MRI guidded radiotherapy treatment. *Physics of Medicine and Biology*, 62(23)L L41-I150.

Reardon, C. e. (2005). Intrapulmonary percussive ventilation vs incentive spirometry for children with neuromuscular diseas. *Arch pediatric Adolescent medicine, 159*(6), 526-31.

Reed, A., & Pa, H. (2011). The hisotry of radiation use in medicine. *Journal of Vascular Surgery, 53*, 3S-5S.

Register, S., Zhang, X., Mohan, R., & Chang, J. (2011). Proton stereotactic body radiation therapy for clinically challenging cases of centrally and superiorly located stage I non-small-cell lung cance. *International Journal of Radiation Oncology Biology and Physics, 80*(4), 1015-1022.

Sala, I., Maurer, B., Myziuk, N., Stevens, C., & Guerrero, T. (2018). High Frequency Percussive Ventilation for Chest Wall Motion Immobilization. *International Journal of Radiation Oncology Biology and Physics, 102*(35), S206-S207.

Sala, I., Maurer, B., Nair, G., & Guerrero, T. (2019). High frequency percussive ventilation for respiratory immobilization in radiotherapy. *Technical Innovations & Patient Support in radiation Oncology, 9*, 8-12.

Salim, A. a. (2005). High-frequency percussive ventlation. *Critical Care Med, 33*(3(suppl)), S241-5.

Salim, A., & Martin, M. (2005). High-Frequency percussive ventilation. *Critical Care Medicine*, S241-5.

Santiago, A., Jelen, U., Ammazzalorso, F., Engenhart-Cabillic, R., Fritz, P., Muhlnickel, W., . . . Witting, A. (2013). Reproducibility of target coverage in stereotactic spot scanning proton lung irradiation under high frequency jet ventilation. *Radiotherapy and Oncology, 109*, 45-50.

Santiago, A., Urszula, J., Ammazzalorso, F., Engenhart-cabillic, R., Fritz, P., Muhlnickel, W., . . . Witting, A. (2013). Reproducibility of target coverage

in stereotactic spot scanning proton lung irradiation under high frequency jet ventilation. *Radiotherapy and Oncology, 109*, 45-50.

Sarudis, S., Karlsson-Hauer, A., Nyman, J., & Back, A. (2017). Systematic evaluationof lung tumor motion using four-dimensional computed tomography. *Acta Oncologica, 56*(4), 525-560.

Schmidt, M., & Payne, G. (2015). Radiotherapy planninng using MRi. *Physics of Medicine and Biology*, 60(22): R323-61.

Schoenfeldt, A., Poppinga, D., Harder, D., Doerner, K., & PoppeB. (2014). The artefacts of radiochromic film dosimetry with flatbed scanners and their causation by light scattering from radiation-induced polymers. *Physics of medicine and Biology, 59*, 3575-3597.

Schultz, C., Alfidi, R., Nelson, A., Kopiwoda, S., & Clampitt, M. (1984). The effect of motion on two-dimensional Fourier transformation magenetic resonance images. . *Radiology*, 152(1): 117-21.

Schweikard, A. e. (n.d.). Robotic motion compensation for respiratory movement during radiosurgery. *Print*, 1092-9088.

Seco, J., Robertson, D., & Trofimov , A. (2009). Breathing interplay effects during proton beam scanning: simulation and statistical analysis. *Physics in Medicine and Biolog, 54*, N283-N294.

Seco, J., Robertson, D., Trofimov, A., & Paganetti H, H. (2009). Breathing interplay effects during proton beam scanning: simulation and statistical analysis. *Physics in Medicine and biology*.

Seppenwoolde, Y. e. (0094-2405). Accuracy of tumor motion compensation algorithm from a robotic respiratory tracking system: a simulation study. *Print*.

Seppenwoolde, Y., Shirato, H., Kitamura, K., Shimizu, S., Van Herk, M., Lebesque, J., & Miyasaka, K. (2002). Precise and real time measurement of 3D tumor motion in lung due to breathing and heartbeat, measured during radiotherapy. *International Journal of Radiation Oncology*, 822-34.

Shen, J., Liu, W., Anand, A., StokerJ, Ding , X., & Fatyga, M. (2015). Impact of range shifter material on proton pencil beam spot characteristics. *Medical PHysics, 42*(3), 1335-1340.

Shi, X., Chen, S., D'Souza, W., & Mistry, N. (2013). Margins Determined Using 4DCT Often Underestimate Tumor Motion in Thoracic Tumors. *Radiation Oncology Biology and Physics, 87*(2), S67-S69.

Shimizu, S. e., Shimizu, S., Shirato, H., Ogura, S., Akita-Dosaka, H., Kitamura, K., . . . Miyasaka, K. (2001). Detection of lung tumor movement in real-time tumor tracking radiotherapy. *International Journal of Radiation Oncology, Biology, Physics*, 304-310.

Shirato, H. e. (2000). Four-dimensional treatment planning and fluoroscopic real-time tumor tracking radiotherapy for moving tumor. . *International Journal of Radiation oncology Biology and Physics, 48*(2), 435-42.

Shirato, H. e. (n.d.). Real-time tumour-tracking radiotherapy. *The Lancet, 353*(9161), 1331-1332.

Siegel, R., MillerKD, & Jemal, A. (2015). Cancer Statistics. *Cancer Journal Clin, 65*, 5-29.

Spapen, H. e. (2014). High-Frequency percussive ventilation in sever acute respiratory distress syndrome: A single center expereience. . *Journal of Anaesthesiology Clinical Pharmacology*, 65-70.

Stuschke, M., Kaiser, A., Pottgen, C., Lubcke, W., & Farr, J. (2012). Potentials of robust intensity modulated scanning proton plans for locally advanced lung cancer in comparison to intensity modulated photon plans. *Radiotherapy and Oncology, 104*, 45-51.

Timmerman, R., McGarry, R., & Yiannoutsos, C. (2006). Excessive toxicity when treating central tumors in a phase II study of stereotactic body radiation therapy for medically inoperable early stage lung cancer. *Journal of clinical Oncology, 24*, 4833-4839.

Timmerman, R., Paulus, R., Galvin, J., Michalski, J., Straube, W., Bradley, J., . . . Choy, H. (2010). Stereotactic Body radiation Therapy for Inoperable Early Stage Lung Cancer. *JAMA, 303*(11), 1070-1076.

Tobias, C., Anger, H., & Lawrence, J. (1952). Radiological use of high energy deuterons and alpha particles. *American Journal Roetgenol Radium Therapy Nuclear Medicine, 67*, 1-27.

Torshabi, E. (2013). Investigation of tumor motion influence on applied dose distribution in conventional proton therapy vs. IMPT; a 4D Monte Carlo simulation study. *International Journal of Radiation Research, 11*(4).

Uematsu, M., Shoda, A., Tahara, K., Fukui, T., Yamamoto, F., & Tsumatori, G. (1998). Focal, high dose, and fractionated modified steretoactic radiation therapy for lung carcinoma patients: a preliminary experience. *Cancer, 82*, 1062-1070.

Vargas, F., Bui, H., Boyer, A., Rachid, L., Salmi, Gbikpi-Benissan, G., . . . Hilbert, G. (ISRCTN17802078). Intrapulmonary percussive ventilation in acute exacerbations of COPD patients with mild respiratory acidosis: a randomized controlled trial [ISRCTN17802078]. *Critical Care*, 1466-609X Electronic.

Verellen, D. a. (2010). Gating and tracking, 4D in thoracic tumors. *Radiotherapie*, 446-454.

Verstegen, N., Lagerwaard, F., & Hashemi, S. (2015). Patterns of disease recurrence after SABR for early stage non-small cell lung cancer: optimizing followup schedules for salvage therapy. *Journal of Thoracic Oncology, 10*, 1195-1200.

Vestbo, J. e. (2013). Global strategy for the Diagnosis, Management and Prevntion of Chronic Obstructive Pulmonary Disease. *American Journal of Respiratory and Critical Care Medicine, 187*(4), 347-365.

Westover, K., Seco, J., Adams, J., Lanuti, M., Choi, N., Engelsman, M., & Willers, H. (2012). proton SBRT for Medically inoperable Stage I NSCLC. *Journal of Thoracic Oncology, 76*, 1021-1025.

Williams, D. G. (1997). The Microwave System and its High-Voltage Supplies. In *Linear Accelerators for Radiation Therapy* (pp. 27-47). Manchaster, UK: Taylor & Francis Group.

Wong, J. W. (1999). The use of active breathing control (ABC) to reduce margin for breathing motion. . *International Journal of radiation Oncology, Biology, Physics, 44*(4), 911-9.

yeo, I., Teran, A., Ghebremedhin, A., Johnson, M., & Patyal, B. (2015). Radiographic film dosimetry of proton beams for depth-dose constancy check and beam profile measurement. *Journal of Applied Clinical Medical Physics, 16*(3).

yu, H., Lin, S., Balter, P., Zhang, L., & Dong , L. (2012). A comparison of tumor motion characteristics between early stage and locally advanced stage lung cancers. *Radiotherapy and Oncology, 104*, 33-38.

Zeng, C., Plastaras, J., Tochner, Z., White, B., Hill-Kayser, C., Hahn, S., & Both, S. (2015). Proton pencil beam scanning for mediastinal lymphoma: the

impact of interplay between target motion and beam scanning. *Institute of Physics and Engineering in Medicine, 60*, 3013-3029.

Zhan, L. R., Lixin, Z., Jiang, R., & Osei, E. (2012). Transformation, Beam Coordinate from DICOM to DOSXYZnrc. *Physics in Medicine and Biology*, N515.

ABSTRACT

HIGH FREQUENCY PERCUSSIVE VENTILATION (HFPV) FOR TUMOR MOTION IMMOBILIZATION

by

INA MARINA SALA

December 2019

Advisor: Dr. Thomas Guerrero, MD, PhD & Dr. Jay Burmeister, PhD

Major: Medical Physics

Degree: Doctor of Philosophy

This work investigates the use of High Frequency Percussive Ventilation as a technique for respiratory motion mitigation in radiotherapy. This technique was extensively investigated in several prospective and retrospective studies.

In an initial prospective study, we evaluated the feasibility of HFPV and chest-wall motion reduction, by recruiting 15 healthy volunteers to undergo HFPV with three commercially available interfaces. For direct tumor motion immobilization, a second prospective study was performed in which with ten lung cancer patients underwent HFPV while imaged with high frame rate fluoroscopy. Diaphragm motion and image artifacts were quantified in a prospective study of a healthy volunteer that underwent MRI while undergoing HFPV. Several retrospective studies were performed to quantify the interplay effects as well as gradient effects of HFPV vs. free breathing in photon and proton radiotherapy. Furthermore, a retrospective phantom study was performed for quantifying PTV volume reduction as well as doses to the organs at risk.

Reproducibility of the HFPV was evaluated in a prospective study of five volunteers who underwent five sessions of HFPV in three different days. Lastly, as part of this study, a HFPV mask was designed and prototyped for better comfort, prolonged percussive time, minimal baseline drifting, as well as patient-controlled valve.

HFPV provides prolonged breath-hold like apnea in awake patients that could last as long as 16 minutes. In this first ever study, direct tumor motion was drastically reduced from > 10 mm to < 3mm. Similarly, diaphragm motion was reduced by as much as > 90 %. HFPV proved significantly beneficial in reducing effects of interplay in proton radiotherapy and photon dose gradient measurements, increasing gamma index by as much as 20 to 30 % from free breathing to HFPV. Similarly, hot and cold spots were reduced by > 50 %. HFPV is reproducible within < 2 mm both intra- and inter- fraction, but it can be further improved by applying minor adjustments to the pressure and frequency of the Percussionaire unit. Although further modifications will be made, the newly designed prototype provided less leakage and better comfort as well as providing patients with the direct ability to switch between room air and HFPV. HFPV is novel and promising technique for tumor immobilization in a radiotherapy setting.

AUTOBIOGRAPHICAL STATEMENT

Ina graduated from Wayne State University with a bachelor's degree in physics and subsequently moved to North Chicago to pursue her master's degree in medical physics from Chicago Medical School. Upon completion of her master's degree, she began her clinical career as a Staff Clinical Physicist in and around Chicago metro area. Shortly after she became board certified by the American Board of Radiology and continued her clinical career as we well as community involvement with AAPM Midwest Chapter. After several years in the clinic, leadership roles as well as radiation safety, Ina began her journey towards her PhD and MBA.

Furthermore, as an affiliated Clinical Faculty for Grand Valley University School of Medical Dosimetry, Ina has been involved in mentoring our future CMDs for years. Specifically, her goal is to empower women around the country in working towards scientific and terminal degrees.